NASA/TM—2005-213795 GRC–DDV–FCF–2005–001

Fluids and Combustion Facility: Combustion Integrated Rack Modal Model Correlation

Mark E. McNelis and Vicente J. Suarez
Glenn Research Center, Cleveland, Ohio

Timothy L. Sullivan, Kim D. Otten, and James C. Akers
Analex Corporation, Brook Park, Ohio

May 2005

The NASA STI Program Office . . . in Profile

Since its founding, NASA has been dedicated to the advancement of aeronautics and space science. The NASA Scientific and Technical Information (STI) Program Office plays a key part in helping NASA maintain this important role.

The NASA STI Program Office is operated by Langley Research Center, the Lead Center for NASA's scientific and technical information. The NASA STI Program Office provides access to the NASA STI Database, the largest collection of aeronautical and space science STI in the world. The Program Office is also NASA's institutional mechanism for disseminating the results of its research and development activities. These results are published by NASA in the NASA STI Report Series, which includes the following report types:

- TECHNICAL PUBLICATION. Reports of completed research or a major significant phase of research that present the results of NASA programs and include extensive data or theoretical analysis. Includes compilations of significant scientific and technical data and information deemed to be of continuing reference value. NASA's counterpart of peer-reviewed formal professional papers but has less stringent limitations on manuscript length and extent of graphic presentations.

- TECHNICAL MEMORANDUM. Scientific and technical findings that are preliminary or of specialized interest, e.g., quick release reports, working papers, and bibliographies that contain minimal annotation. Does not contain extensive analysis.

- CONTRACTOR REPORT. Scientific and technical findings by NASA-sponsored contractors and grantees.

- CONFERENCE PUBLICATION. Collected papers from scientific and technical conferences, symposia, seminars, or other meetings sponsored or cosponsored by NASA.

- SPECIAL PUBLICATION. Scientific, technical, or historical information from NASA programs, projects, and missions, often concerned with subjects having substantial public interest.

- TECHNICAL TRANSLATION. English-language translations of foreign scientific and technical material pertinent to NASA's mission.

Specialized services that complement the STI Program Office's diverse offerings include creating custom thesauri, building customized databases, organizing and publishing research results . . . even providing videos.

For more information about the NASA STI Program Office, see the following:

- Access the NASA STI Program Home Page at ***http://www.sti.nasa.gov***

- E-mail your question via the Internet to help@sti.nasa.gov

- Fax your question to the NASA Access Help Desk at 301–621–0134

- Telephone the NASA Access Help Desk at 301–621–0390

- Write to:
  NASA Access Help Desk
  NASA Center for AeroSpace Information
  7121 Standard Drive
  Hanover, MD 21076

NASA/TM—2005-213795 GRC–DDV–FCF–2005–001

Fluids and Combustion Facility: Combustion Integrated Rack Modal Model Correlation

Mark E. McNelis and Vicente J. Suarez
Glenn Research Center, Cleveland, Ohio

Timothy L. Sullivan, Kim D. Otten, and James C. Akers
Analex Corporation, Brook Park, Ohio

National Aeronautics and
Space Administration

Glenn Research Center

May 2005

Trade names or manufacturers' names are used in this report for identification only. This usage does not constitute an official endorsement, either expressed or implied, by the National Aeronautics and Space Administration.

Available from

NASA Center for Aerospace Information
7121 Standard Drive
Hanover, MD 21076

National Technical Information Service
5285 Port Royal Road
Springfield, VA 22100

Available electronically at http://gltrs.grc.nasa.gov

TABLE OF CONTENTS

1. Introduction

1.1 Background

The Fluids and Combustion Facility (FCF – Figure 1) is a modular, multi-user, two-rack facility dedicated to combustion and fluids science in the US Laboratory Destiny on the International Space Station. FCF is a permanent facility that is capable of accommodating up to ten combustion and fluid science investigations per year. FCF research in combustion and fluid science supports NASA's Exploration of Space Initiative for on-orbit fire suppression, fire safety, and space system fluids management.

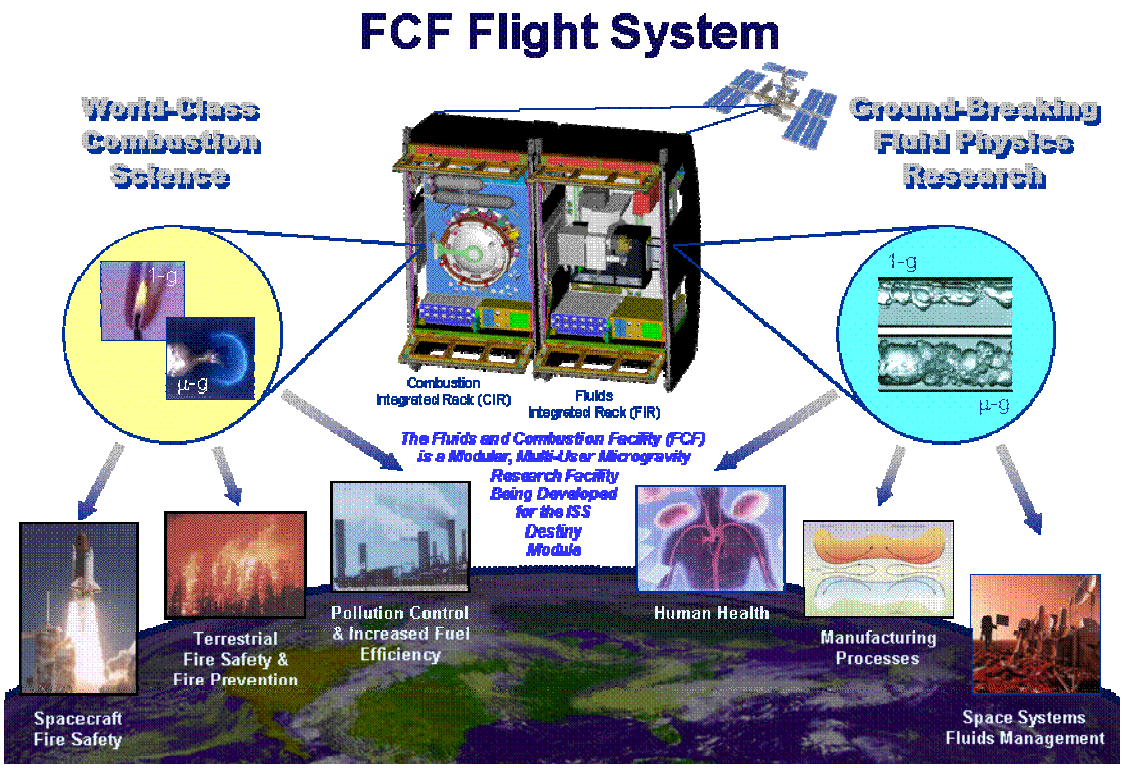

FIGURE 1 - FLUIDS AND COMBUSTION FACILITY

The Combustion Integrated Rack (CIR) is one of two racks in the FCF. The CIR major structural elements (Figure 2) include the International Standard Payload Rack (ISPR), Experiment Assembly (optics bench and combustion chamber), Air Thermal Control Unit (ATCU), Rack Door, and Lower Structure Assembly (Input/Output Processor and Electrical Power Control Unit). The load path through the rack structure is outlined in Figure 3.

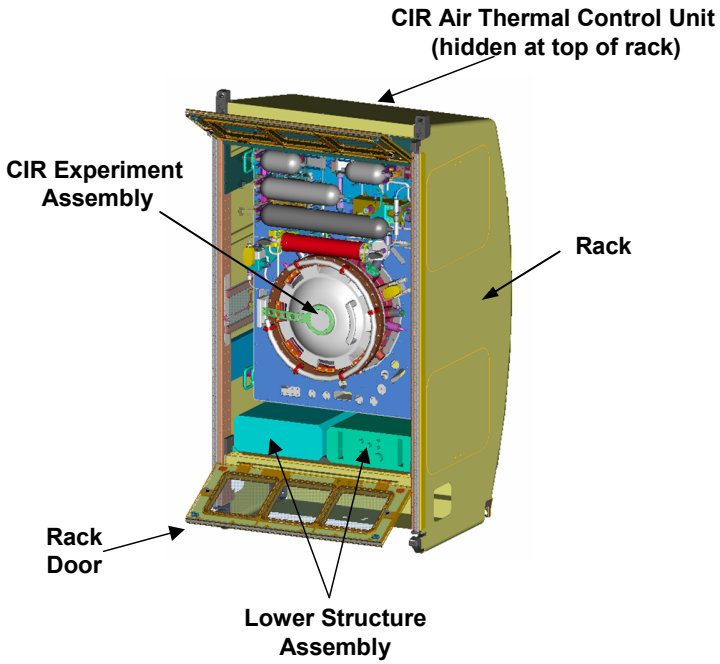

FIGURE 2 - COMBUSTION INTEGRATED RACK (CIR)

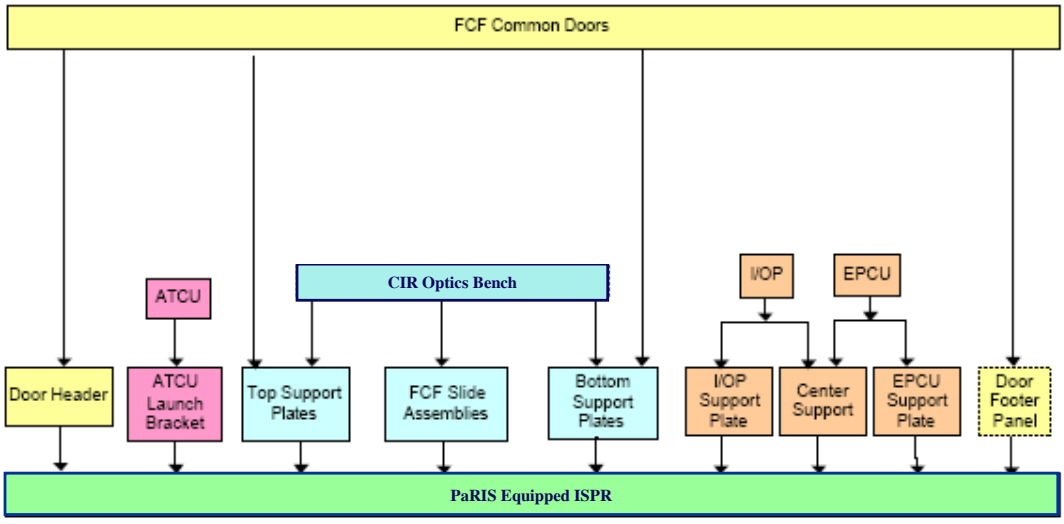

FIGURE 3 - LOAD PATH DIAGRAM

1.2 Purpose of CIR Model Correlation

The CIR modal survey was conducted to validate the load path predicted by the CIR finite element model (FEM). The modal survey is done by experimentally measuring the CIR frequencies and mode shapes. The CIR model was test correlated by updating the model to represent the test mode shapes. The correlated CIR model delivery is required by NASA JSC at Launch-10.5 months.

The test correlated CIR flight FEM is analytically integrated into the Shuttle for a coupled loads analysis of the launch configuration. The analysis frequency range of interest is 0-50 Hz.

A coupled loads analysis is the analytical integration of the Shuttle with its cargo element, the Mini Payload Logistics Module (MPLM), in the Shuttle cargo bay (Figure 4). For each Shuttle launch configuration, a verification coupled loads analysis is performed to determine the loads in the cargo bay as part of the structural certification process (Figure 5).

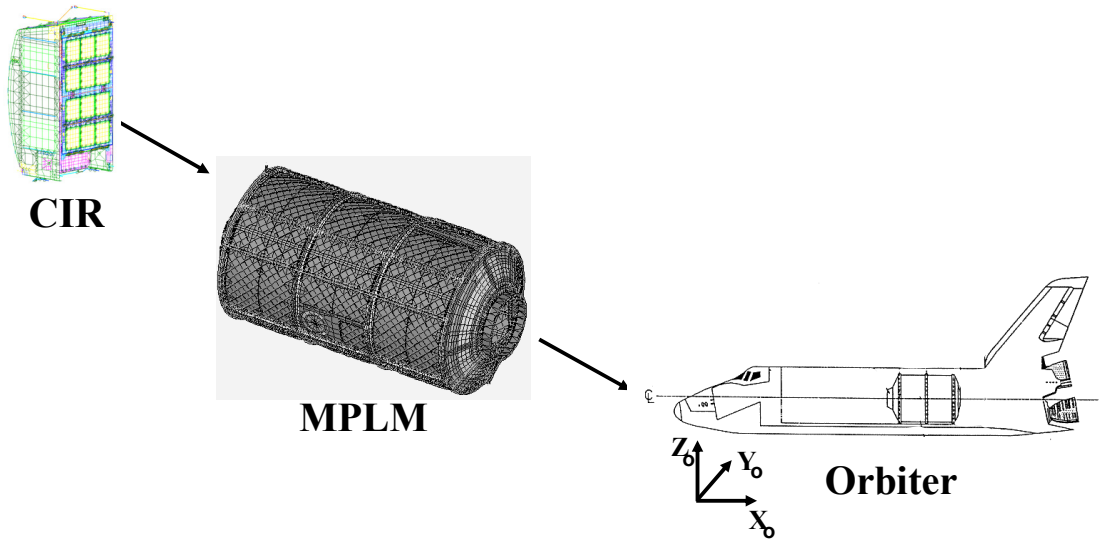

FIGURE 4 - ANALYTICAL INTEGRATION PROCESS FOR COUPLED LOADS ANALYSIS

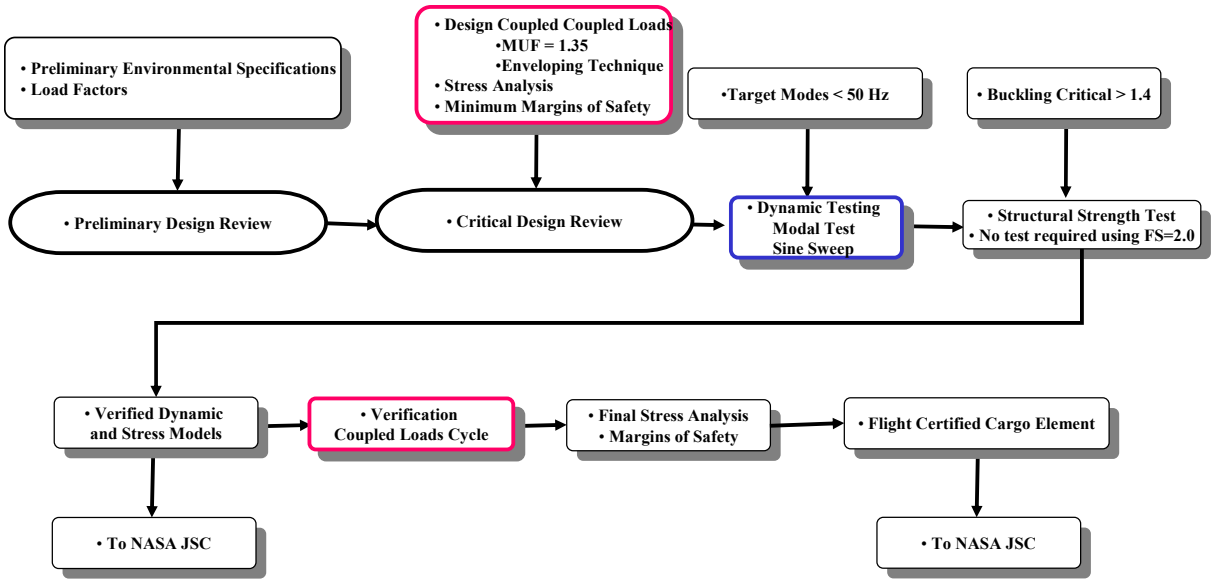

FIGURE 5 - STRUCTURAL CERTIFICATION PROCESS

1.3 Applicable Documents

1. "Payload Verification Requirements," NSTS 14046, Revision E, May 2000.
2. "Rack to Mini Pressurized Logistics Module Interface Control Document," SSP 41017, Part 1, Revision F, May 18, 2001.
3. "Rack to Mini Pressurized Logistics Module Interface Control Document," SSP 41017, Part 2, Revision H, May 18, 2001.
4. "Payload Flight Equipment Requirements and Guidelines for Safety-Critical Structures," SSP 52005, Revision C, Section 7.1 Verification Requirements for Dynamic Structural Models, December 18, 2002.
5. "International Standard Payload Rack (ISPR) Structural Integrator's Handbook," SSP 57007, Revision A, October 31, 2001.

2. Model Correlation

2.1 Requirements

The math model verification requirements for FCF racks are defined in NSTS 14046 and SSP 52005 (see 1.3 Applicable Documents). SSP 52005, Section 7.1 defines that evidence for model correlation is provided through test based frequency and mode shape characterization. The correlation goal for each fundamental frequency is a frequency difference of less than +/- 5%. For higher order frequencies, the correlation goal is a frequency difference of less than +/- 10%.

Cross-orthogonality between the analytical and test mode shapes is evaluated based on the following calculation:

$$[\varnothing]_A^T [M]_A [\varnothing]_T = [C_{ij}]$$

Where:

$[\varnothing]_A^T$ is the transpose of the analytical mode shape matrix

$[M]_A$ is the analytical consistent mass matrix (as defined in NASTRAN manuals)

$[\varnothing]_T$ is the test mode shape matrix

$[C_{ij}]$ is the correlation matrix.

The correlation goal for the diagonal values of the correlation matrix, $[C_{ij}]$, is a value greater than 0.9 for significant modes. For the off-diagonal terms, the correlation goal is a value of less than 0.1.

2.2 Model Correlation Methodology

The CIR model correlation methodology was based on modal testing and correlating each major structural assembly individually (Reference 1). This building block approach facilitates the model correlation process for the CIR. Previous testing by Boeing correlated the rack model in a configuration with various mass weighted horizontal shelves in the rack (Reference 2). The FCF rack structural configuration was different than the Boeing correlated rack configurations as the FCF racks have a vertical plate (optics bench) instead of horizontal shelves, creating a different load path in the rack. The final step in the correlation process was to modal test and model correlate the CIR.

Model correlation for the major structural assemblies is summarized in the following appendices:

Appendix A – CIR Experiment Assembly
Appendix B – CIR ATCU
Appendix C – Rack Door
Appendix D – Lower Structure Assembly

The Lower Structure Assembly model was not correlated as the test measured fundamental frequencies were greater than 100 Hz, outside the model correlation frequency range of interest (0-50 Hz).

3. Test Hardware Configuration

CIR Ground Integration Unit (GIU) hardware was used for the CIR test configuration (Figure 6). The overall dimensions of the rack are given in Figure 7. The test rack was a modified 6-post International Standard Payload Rack (ISPR) made of carbon fiber composite material similar to the flight rack. The rack was supplied by Boeing. The CIR GIU hardware is a structural flight duplicate which will be used as an astronaut trainer and for troubleshooting on-orbit facility problems. The CIR test configuration did not include any wiring or harnessing, however, it did include the environmental control system plumbing. The Passive Rack Isolation System (PaRIS) was not installed (35 lbs distributed mass) in the test configuration.

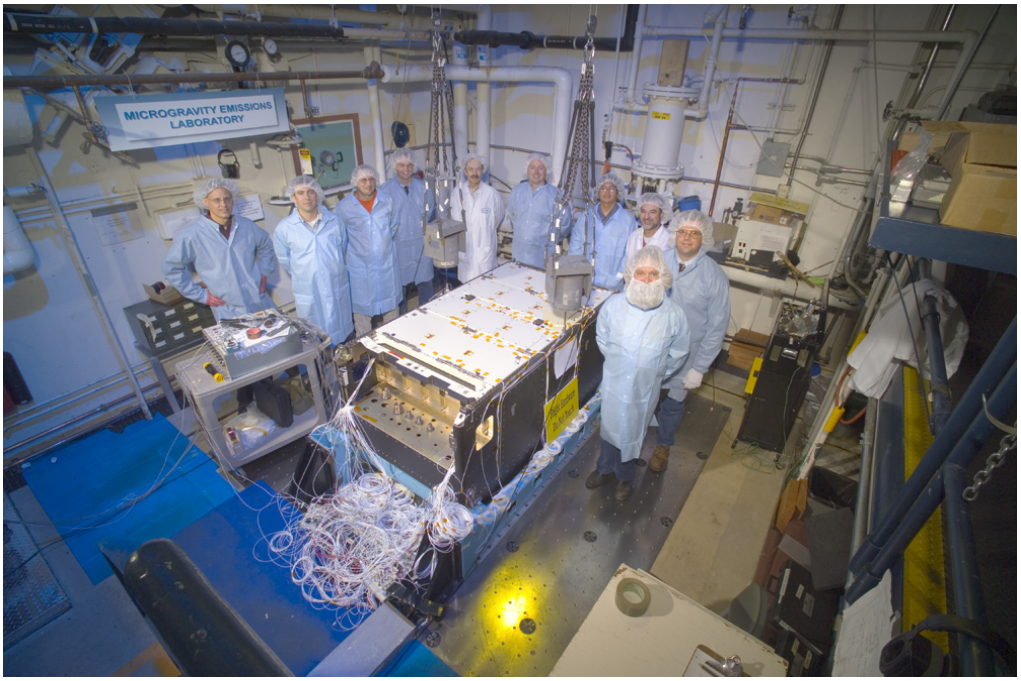

FIGURE 6 - COMBUSTION INTEGRATED RACK TEST CONFIGURATION

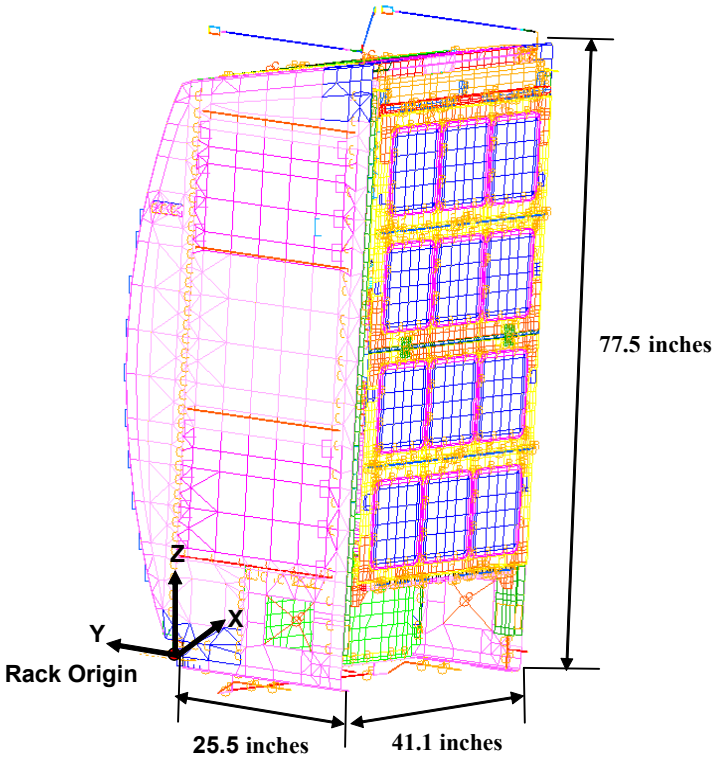

FIGURE 7 - RACK COORDINATE SYSTEM AND OVERALL DIMENSIONS

3.1 Hardware Mass and CG Summary

The CIR test hardware weighs 1516.95 lbs and the CIR flight hardware configuration weighs 1684.00 lbs (Reference 3). The mass difference is 167.05 lbs, representing a difference of 9.9%. A mass and CG summary of the test and flight rack hardware configurations are given in Table 1. The main difference between the test and flight hardware configurations is the test rack does not have wiring or harnessing and PaRIS. The CG properties between the CIR test and flight hardware are very comparable, as seen in Table 1.

Table 1 – CIR Hardware Mass and CG Summary

Subsystems	Weight (lbf)	CG_x (in)	CG_y (in)	CG_z (in)
ATCU	155.47	20.0	-13.2	63.5
Experiment Assembly	785.17	18.9	-13.5	45.0
Door	92.22	19.8	-27.9	43.7
Rack	219.82	19.0	-11.6	33.2
Lower Structure Assembly (Mass Simulator)	206.49	17.5	-12.6	15.1
Tested CIR GIU	1516.95	18.8	-13.6	40.7
CIR Flight	1684.00	18.8	-13.9	40.4

3.2 Rack Hardware Modifications

Test rack hardware modifications were made to reflect the flight rack structural changes. The modifications include removal of the rack center posts, replacement of pressure relief valve assemblies with closeout panels, installation of hardback simulator at bottom of the rack, and removal of a blank Rack Utility Panel (RUP) and installation of a flight-like RUP and RUP extension. The rack modifications are shown in Figure 8.

Structural attachment modifications were made to incorporate FCF hardware in the rack. The Lower Structure Assembly is attached to the rack using modified center-post attachment hardware at the bottom of the rack (Figure 9).

A launch strut (Figure 10) was added between the CIR chamber, upper intercostal, and upper torque tube to increase the rack frequency 1-2 Hz. This CIR rack configuration was used for the Design Coupled Loads Analysis.

A Remove front and rear center posts

B Replace Pressure Relief Assemblies with closeout panels

C Remove blank rack utility panel and install RUP and RUP extension

D Install Hardback simulator at bottom of rack

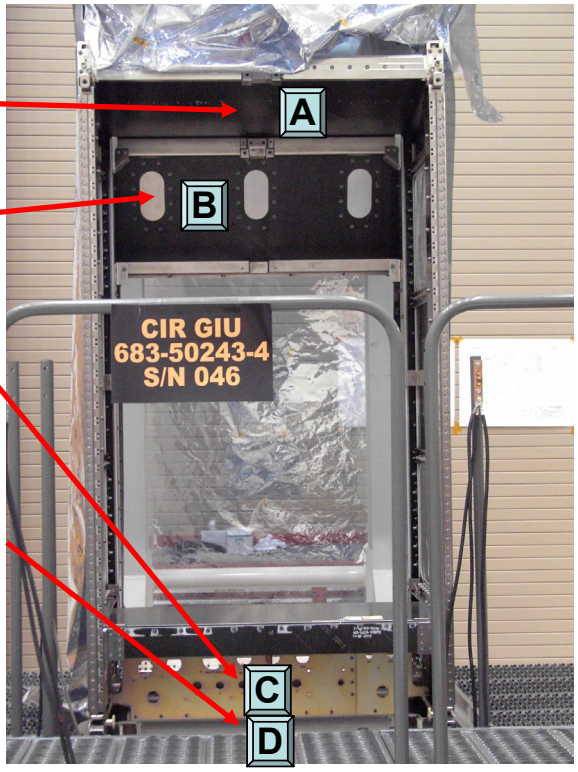

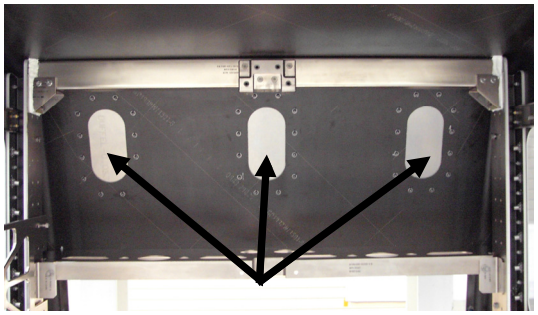

B Pressure Relief closeout panels

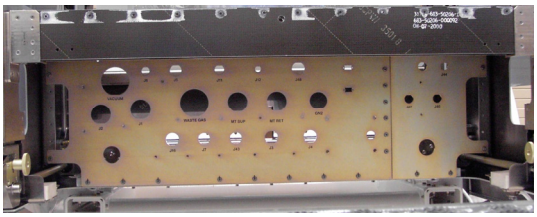

C RUP and RUP extension

D Hardback mass simulator
(looking down at bottom of rack)

FIGURE 8- RACK HARDWARE MODIFICATIONS

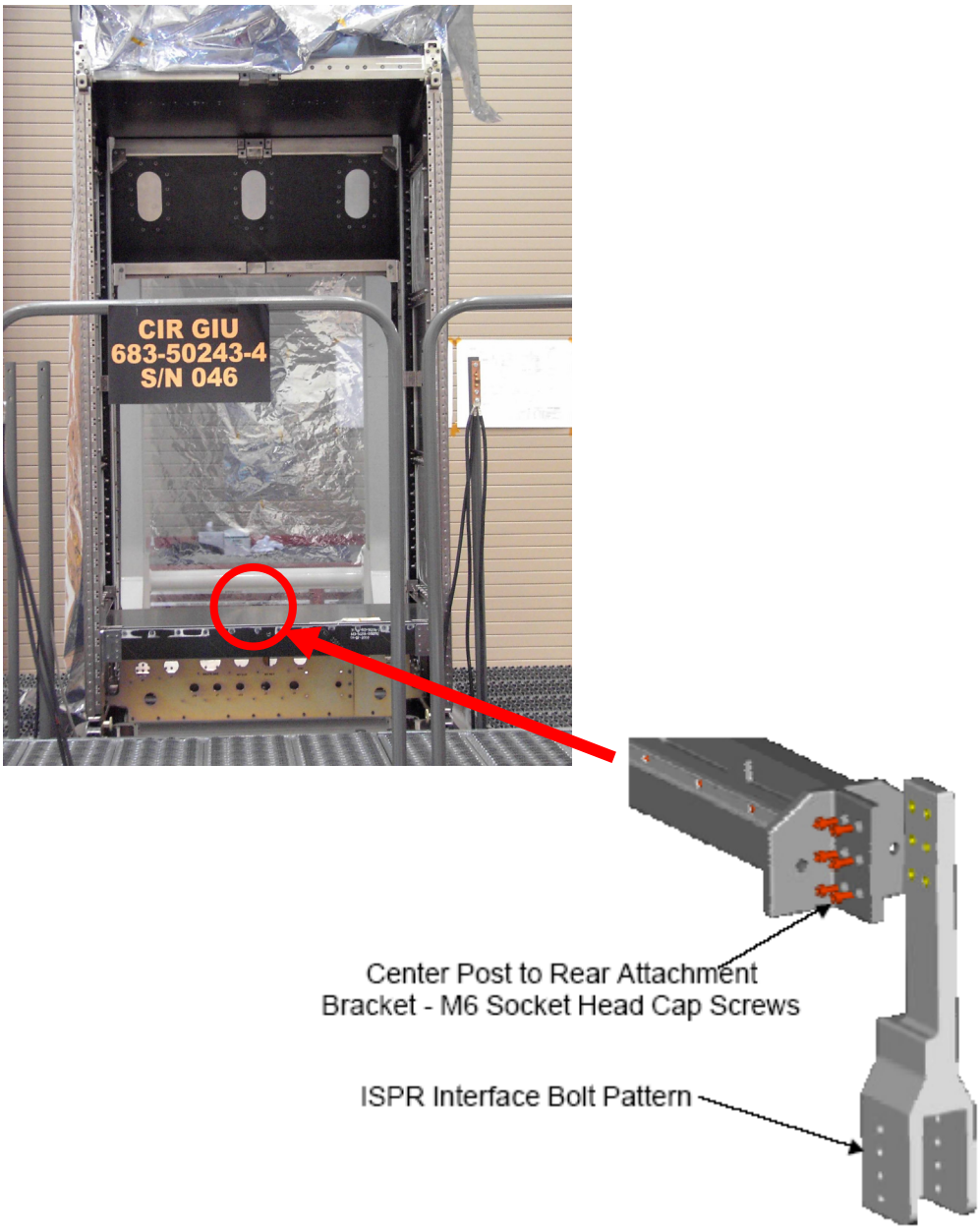

FIGURE 9 - RACK CENTER-POST STRUCTURAL ATTACHMENT MODIFICATION

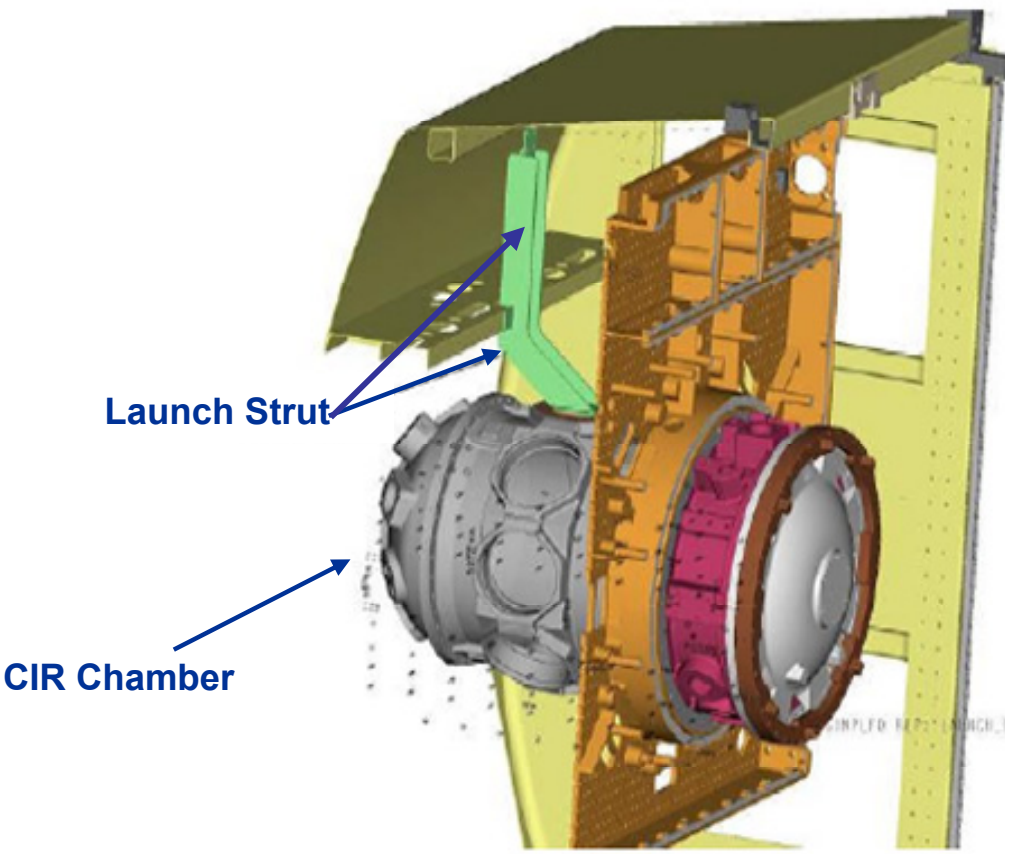

FIGURE 10 - LAUNCH STRUT

3.3 Mass Simulators

The general criteria for using mass simulators in the CIR test configuration is based on providing mass representation for any components weighing greater than 5 lbs. Due to the uncertainty of some component weights at the time of fabrication, a 10% uncertainty factor was added to the mass simulators. The mass simulators incorporated for the CIR modal test are components mounted to the Experiment Assembly including:

Diluent Manifold	16.0 lbs
O2 Manifold	24.0 lbs
N2 Manifold	22.4 lbs
Fuel Manifold	15.8 lbs
Static Mixer	5.8 lbs
Exhaust Manifold	27.0 lbs
Manual Vent Valve	7.8 lbs
Helium GC Manifold	3.7 lbs
GC Argon Manifold	5.2 lbs
GC Check Gas Manifold	2.6 lbs
Vent Manifold	25.6 lbs
Recirculation Pumps (2)	7.1 lbs (each)

4. FEM Model Description

The CIR modal test configuration finite element model (FEM) is shown in Figure 11. The finite element model was created using MSC/NASTRAN and has the following properties:

M O D E L S U M M A R Y

NUMBER OF GRID	POINTS =	103101
NUMBER OF CBAR	ELEMENTS =	4513
NUMBER OF CBUSH	ELEMENTS =	628
NUMBER OF CELAS1	ELEMENTS =	528
NUMBER OF CHEXA	ELEMENTS =	14965
NUMBER OF CONM2	ELEMENTS =	150
NUMBER OF CPENTA	ELEMENTS =	2630
NUMBER OF CQUAD4	ELEMENTS =	59903
NUMBER OF CTETRA	ELEMENTS =	2932
NUMBER OF CTRIA3	ELEMENTS =	9017
NUMBER OF RBAR	ELEMENTS =	239
NUMBER OF RBE2	ELEMENTS =	2205
NUMBER OF RBE3	ELEMENTS =	68

4.1 Rack Coordinate System

The rack coordinate system for the finite element model and modal test is defined in Figure 7. The rack coordinate system is a local coordinate system invariant to the integration position of the rack into the MPLM.

4.2 Rack Modal Test Fixture

The rack modal test fixture is the structural hardware between the rack and the modal floor. The design intent for the rack fixture is to have the fundamental frequency ten times higher than the CIR fundamental frequency to prevent dynamic coupling between the CIR modes and the fixture. The fixture is a frame construction using welded tubular steel with 3/8" wall thickness.

A modal test was conducted on the rack fixture to characterize the fundamental frequencies (Figure 12). The rack fixture finite element model was not correlated. Based on the fixture test results, the fixture stiffness was increased using bookend stiffeners to prevent deflection of the ends of the fixture. Figure 11 illustrates the FEM with rack attachment to the fixture including bookend stiffeners.

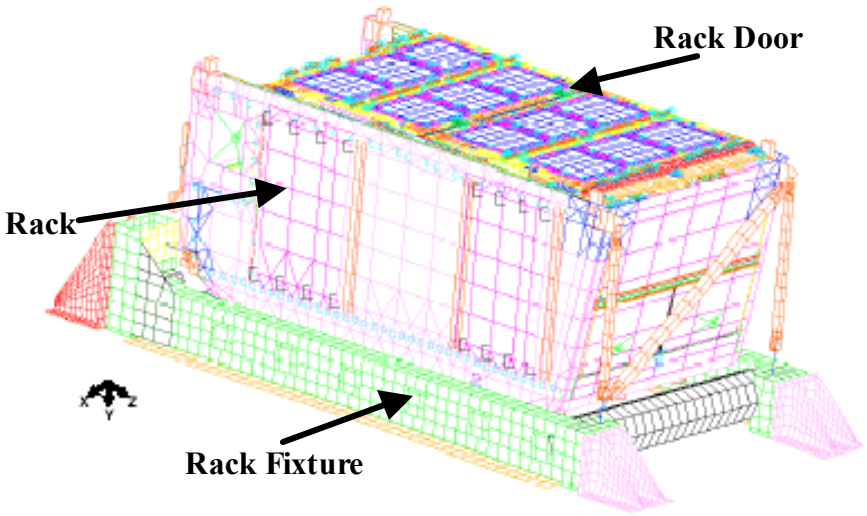

FIGURE 11 – TEST CONFIGURATION FINITE ELEMENT MODEL (FEM)

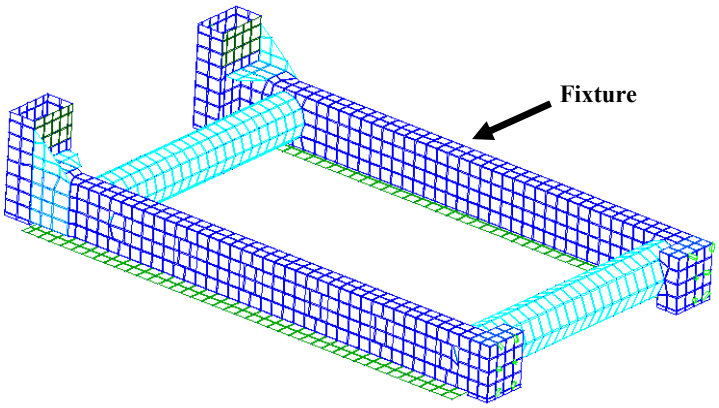

Fixture Modal Test Results without Bookends		
Mode	Axis	Freq (Hz)
1	X	196.6
2	X	201.1
3	Y	243.3
4	X	289.2
5	X	292.4

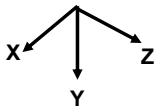

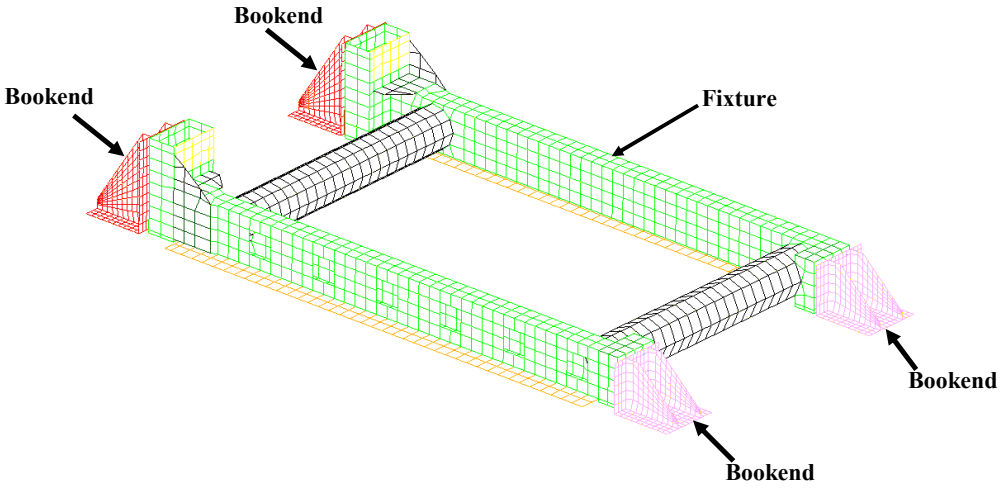

FIGURE 12 – RACK MODAL TEST FIXTURE

4.3 FEM Mass and CG Properties

A mass and CG summary is provided for the CIR test and flight finite element models (FEM) in Tables 2 and 3. The CIR test FEM weighs 1574.87 lbs and the CIR flight FEM weighs 1663.70 lbs. The mass difference between the two finite element models is 88.83 lbs, representing a difference of 5.3%. The CG properties between the test and flight rack are very comparable.

Table 2 – CIR Test Finite Element Model Mass and CG Summary

Subsystems	Weight (lbf)	CG_x (in)	CG_y (in)	CG_z (in)	I_{xx} (lbm-in^2)	I_{yy} (lbm-in^2)	I_{zz} (lbm-in^2)
ATCU	112.91	19.9	-13.2	71.2	17.7	45.7	60.8
Experiment Assembly	833.08	18.2	-13.0	43.9	504.9	691.4	466.5
Door	84.70	19.7	-27.2	41.5	87.0	117.8	30.9
Rack	203.56	19.3	-10.0	33.6	440.7	521.7	255.5
Lower Structure Assembly (Mass Simulator)	139.68	20.2	-10.7	15.8	18.8	43.3	58.0
CIR Test FEM	1574.87	18.5	-12.8	40.1	2053.0	2385.1	1066.6

Table 3 – CIR Flight Finite Element Model Mass and CG Summary

Subsystems	Weight (lbf)	CG_x (in)	CG_y (in)	CG_z (in)	I_{xx} (lbm-in^2)	I_{yy} (lbm-in^2)	I_{zz} (lbm-in^2)
ATCU	112.91	19.9	-13.2	71.2	17.7	45.7	60.8
Experiment Assembly	886.79	18.7	-13.2	44.6	529.9	727.1	479.4
Door	84.70	19.7	-27.2	41.5	87.0	117.8	30.9
Rack	228.21	19.3	-9.9	29.8	514.0	608.3	272.1
Lower Structure Assembly (Mass Simulator)	139.68	20.2	-10.7	15.8	18.8	43.3	58.0
CIR Flight FEM	1663.70	18.7	-12.8	40.0	2221.6	2579.4	1105.7

The mass difference between the CIR test hardware and the test FEM is 57.92 lbs, representing a 3.8% mass difference. The CG properties between the measured CIR test hardware and FEM are very comparable.

The mass difference between the CIR flight hardware and the flight FEM is 20.03 lbs, representing a 1.2% mass difference. The CG properties between the measured CIR flight hardware and FEM are very comparable.

5. Pre-Test Analysis

Pre-test modal analysis was performed to identify target modes between 0-50 Hz and determine the accelerometer instrumentation layout. The methodology used to verify the finite element model is outlined in Figure 13. The criterion used to define the primary target modes are modes with greater than 10% effective mass. Secondary target modes are defined based on modes with less than 10% effective mass. Engineering judgment was also used to select target modes by visualizing animated mode shapes.

Four modes were defined as target modes for the Combustion Integrated Rack (CIR) modal test. Three rack translational modes in the X, Y, and Z-axis were identified as primary target modes. A secondary target mode was identified as the CIR door mode.

The predicted X-axis CIR translational mode was 22.4 Hz, with an effective weight of 1464.5 lbs. The predicted Y-axis CIR translational mode was 36.6 Hz, with an effective weight of 1358.0 lbs. The predicted Z-axis CIR translational mode was 46.2 Hz, with an effective mass of 1444.4 lbs. The predicted CIR door mode was 45.8 Hz, with effective mass of 32.6 lbs. Figures 14–17 illustrate the primary and secondary target modes for the CIR modal test.

The target modes were compared between the CIR test FEM and flight FEM configurations to assure that the test configuration was representative of flight. These comparisons are summarized in Tables 4 and 5, and Figures 14–17 indicating that the test configuration modes are comparable to the flight modes with less than a 3 Hz frequency shift (8% change). There is a 12 Hz frequency shift (21% change) for the Z-axis track translational mode between the flight and test configuration due to the relative flexibility of the fixture.

Selection of the accelerometer locations (NASTRAN A-SET) for the CIR modal test was based on a two-tiered approach using kinetic energy (choosing grid points from the finite element mode with high kinetic energy) and engineering judgment (visualizing the mode shape and placing instrumentation at high deformation locations).

The criterion for selecting the final instrumentation was based on computing the cross-orthogonality between the test finite element model (FEM) and the Test Analysis Model (TAM - test finite element model including only the instrumentation locations). The cross-orthogonality between the test configuration FEM and the TAM are summarized in Table 6 and Figures 18-21. One hundred twenty nine (129) degrees of freedom were used in the TAM. Cross-orthogonality was greater than 90% for the primary target modes satisfying the criteria for instrumentation selection. The secondary target mode for the CIR door had 79% cross-orthogonality. The final instrumentation plan is documented in Appendix E.

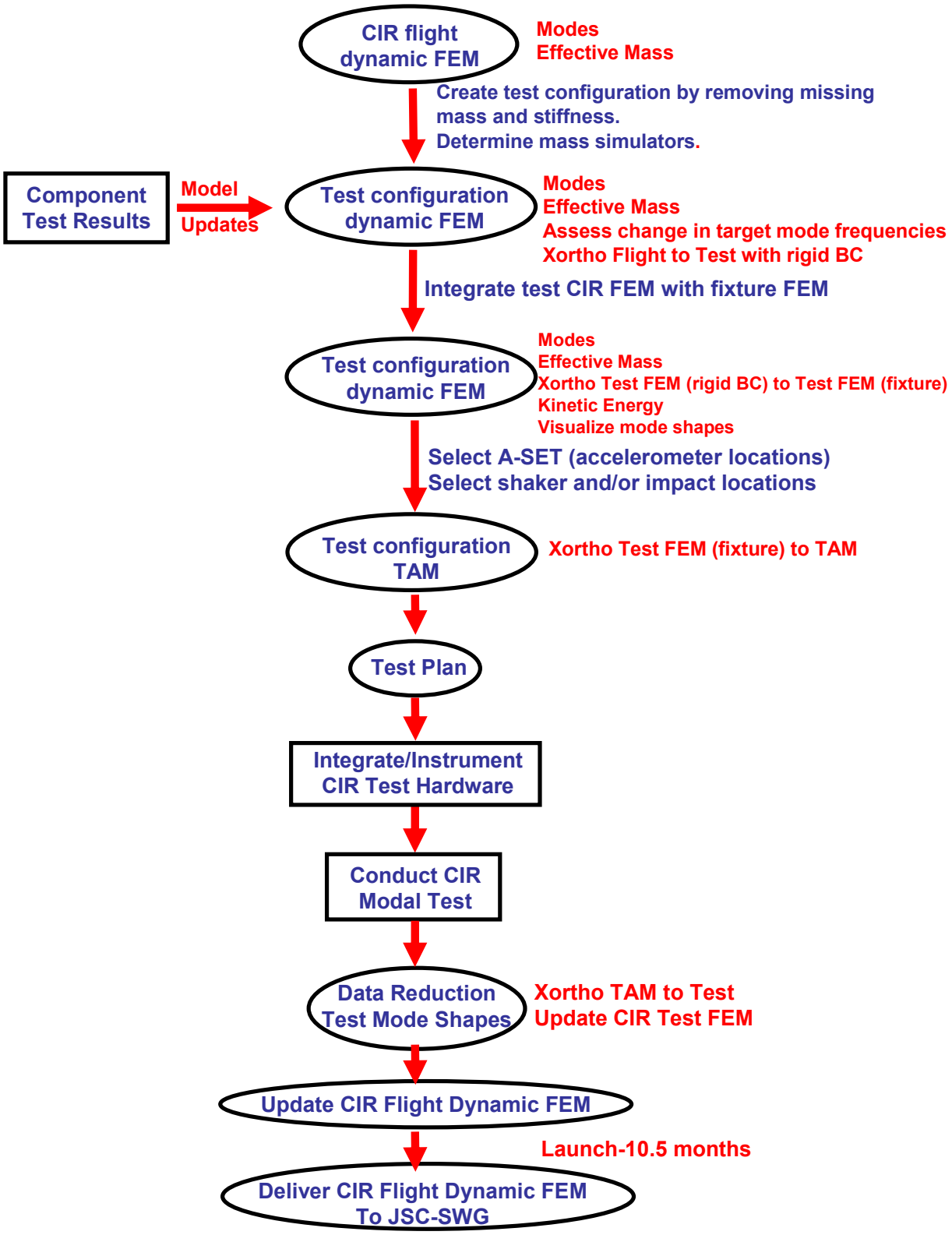

FIGURE 13 - CIR MODEL VERIFICATION METHODOLOGY

TABLE 4 – COMPARISON OF FLIGHT FEM (IN RIGID BOUNDARY CONDITIONS) AND TEST FEM (IN RIGID BOUNDARY CONDITIONS) TARGET MODE FREQUENCY DIFFERENCE AND CROSS-ORTHOGONALITY

			FLIGHT FEM Rigid BC					Delta	Mode Shape
	Mode		1	3	7	13	15	Freq	Description
		Freq (Hz)	23.9	39.7	48.9	57.2	58.5		
Test FEM	1	24.4	-0.971	0	0	0	0	2.2%	Rack X-axis Translation
Rigid BC	3	40.8	0	-0.968	0	0	0	2.9%	Rack Y-axis Translation
	7	48.9	0	0	-0.994	0	0	0.0%	Door Y-axis Bending
	13	58.3	0	0	0	-0.783	-0.480	1.9%	Rack Z-axis Translation
	14	58.7	0	0	0	0.443	-0.866	0.3%	Rack Z-axis Translation

TABLE 5 – COMPARISON OF TEST FEM (IN RIGID BOUNDARY CONDITIONS) AND TEST FEM (IN FIXTURE) TARGET MODE FREQUENCY DIFFERENCE AND CROSS-ORTHOGONALITY

			Test FEM Rigid BC					Delta	Mode Shape
	Mode		1	3	7	13	14	Freq	Description
		Freq (Hz)	24.4	40.8	48.9	58.3	58.7		
	1	22.4	0.996	0	0	0	0	-8.2%	Rack X-axis Translation
Test FEM	2	36.6	0	-0.953	0	0	0	-10.3%	Rack Y-axis Translation
	4	45.8	0	0	-0.954	0	-0.137	-6.3%	Door Y-axis Bending
	5	46.2	0	0.101	0.165	0.660	-0.650	-20.8%	Rack Z-axis Translation

TABLE 6 – COMPARISON OF TEST AND TAM TARGET MODE FREQUENCY DIFFERENCE AND CROSS-ORTHOGONALITY

			TAM				Delta	Mode Shape
	Mode		1	2	4	6	Freq	Description
		Freq (Hz)	22.6	37.1	47.6	49.5		
Test FEM	1	22.4	0.975	0	0	0	-0.9%	Rack X-axis Translation
w/Fixture	2	36.6	0	-0.972	0	0	-1.4%	Rack Y-axis Translation
	5	46.2	0	0	0.926	0	-3.0%	Rack Z-axis Translation
	8	45.8	0	0	0	-0.790	-8.1%	Door Y-axis Bending

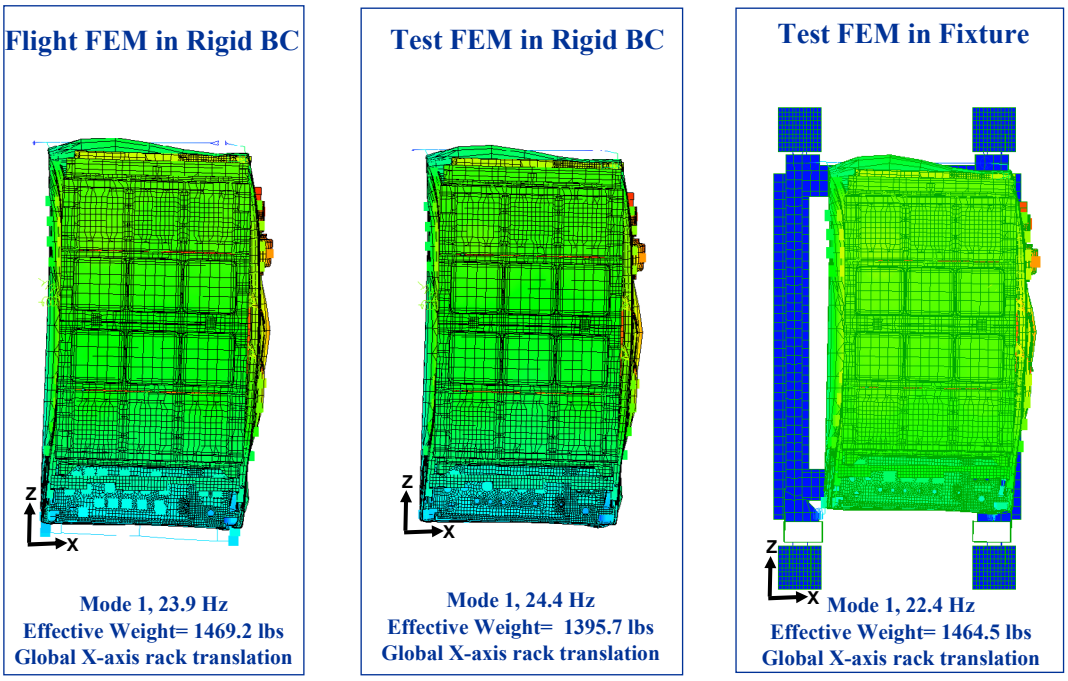

FIGURE 14 – X-AXIS PRIMARY TARGET MODE

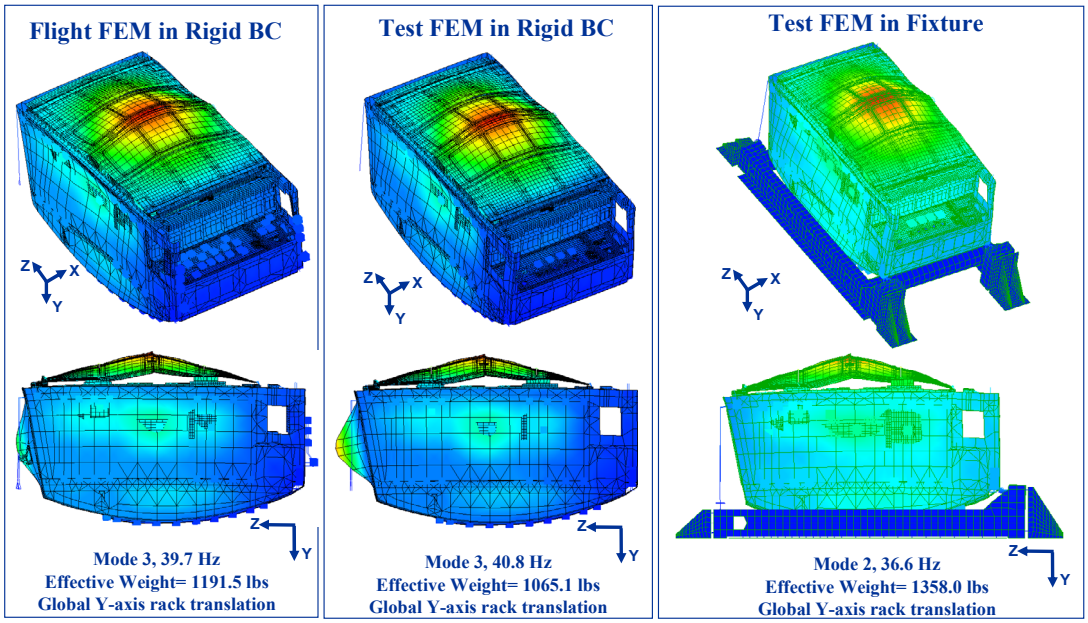

FIGURE 15 – Y-AXIS PRIMARY TARGET MODE

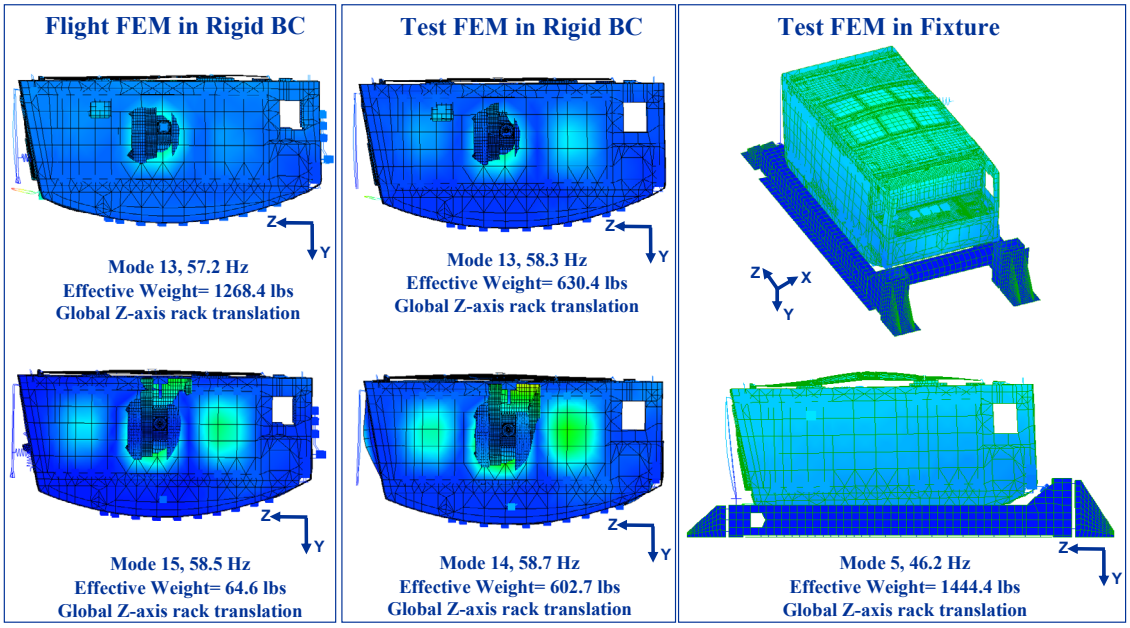

FIGURE 16 – Z-AXIS PRIMARY TARGET MODE

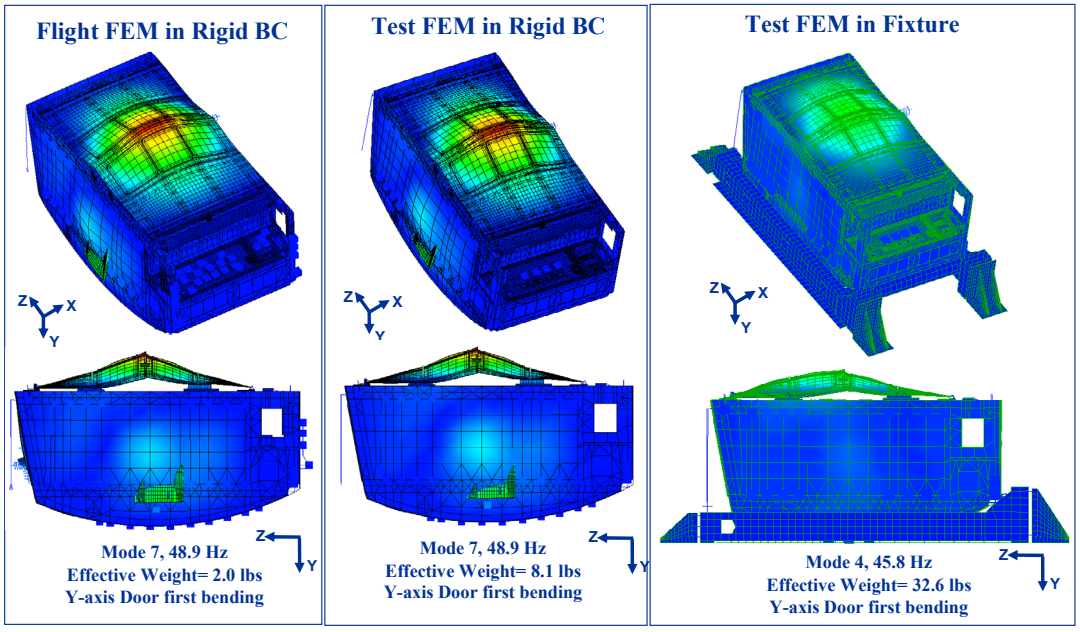

FIGURE 17 – DOOR SECONDARY TARGET MODE

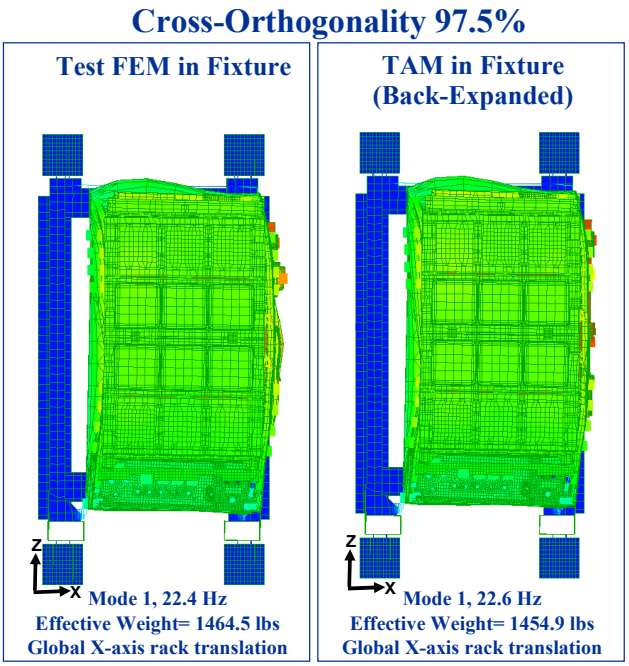

FIGURE 18 – COMPARISON OF TEST FEM TO TAM FOR THE X-AXIS TARGET MODE

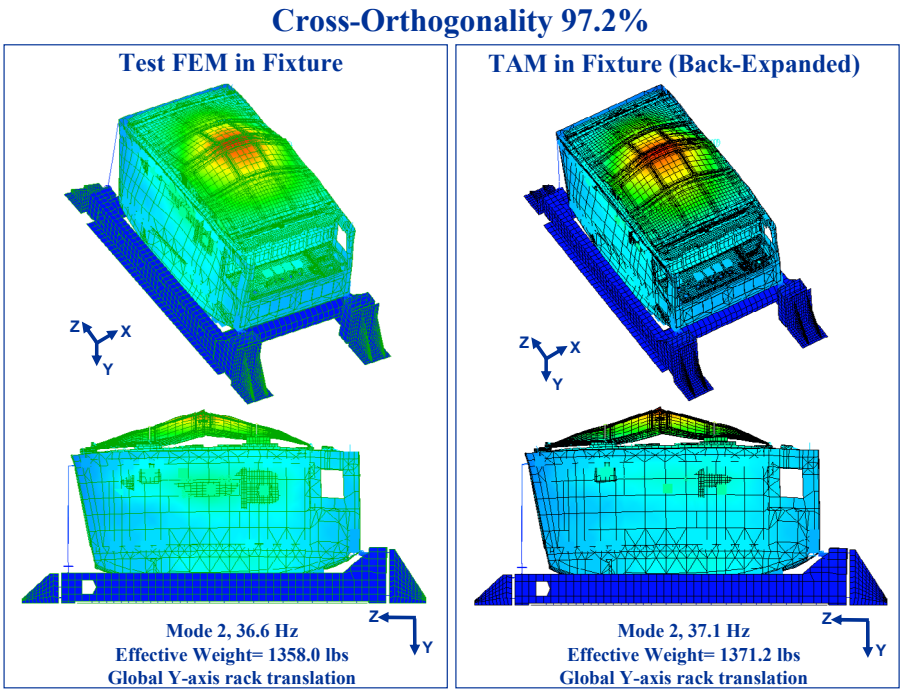

FIGURE 19 – COMPARISON OF TEST FEM TO TAM FOR THE Y-AXIS TARGET MODE

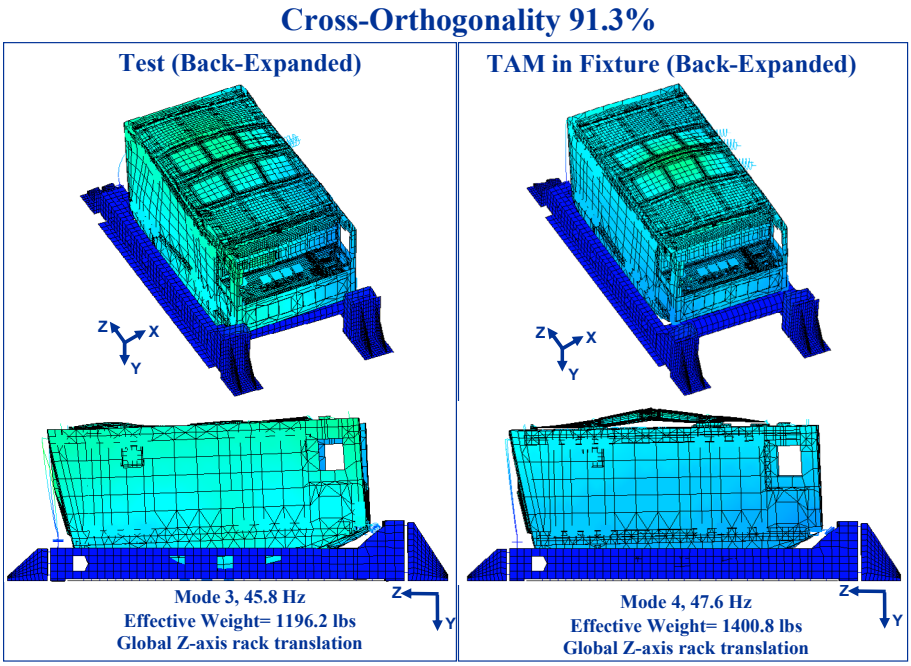

FIGURE 20 – COMPARISON OF TEST FEM TO TAM FOR THE Z-AXIS TARGET MODE

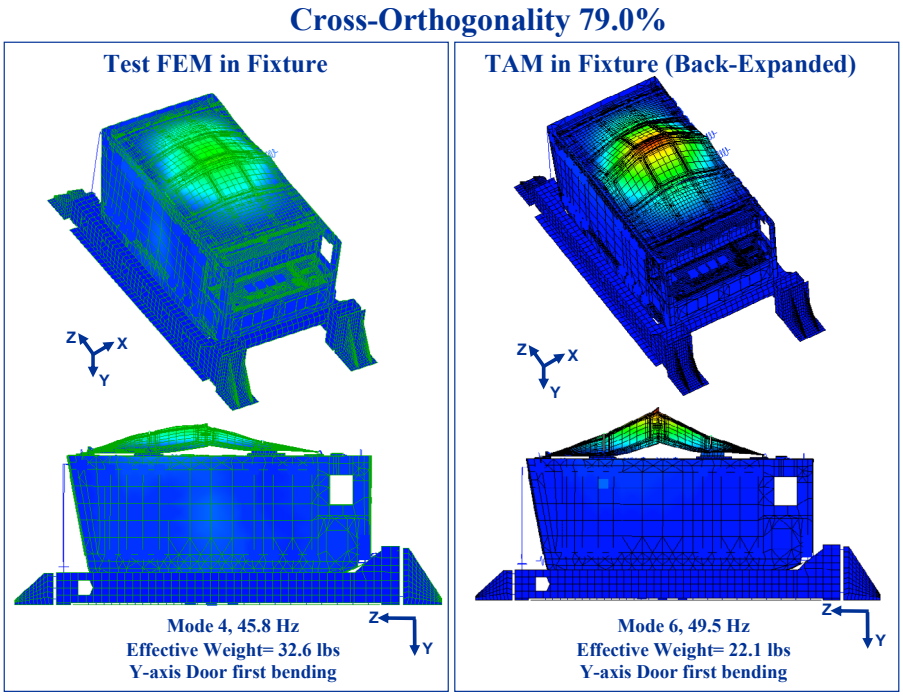

FIGURE 21 – COMPARISON OF TEST FEM TO TAM FOR THE DOOR TARGET MODE

6. Test Results

The Combustion Integrated Rack (CIR) modal test was conducted at the NASA Glenn Research Center Structural Dynamics Laboratory from November 22 – December 3, 2004. The test was performed using a fixed base interface between the test article and the modal floor. One-hundred twenty nine (129) response accelerometers were used during the test. Four (4) load cells were mounted between the rack and fixture attachment locations to measure interface forces (Figure 22). Interface accelerometers were also used to monitor any relative motion between the fixture and rack. Minimal relative interface motion was observed, indicating that the fixture was not participating in the CIR target modes response.

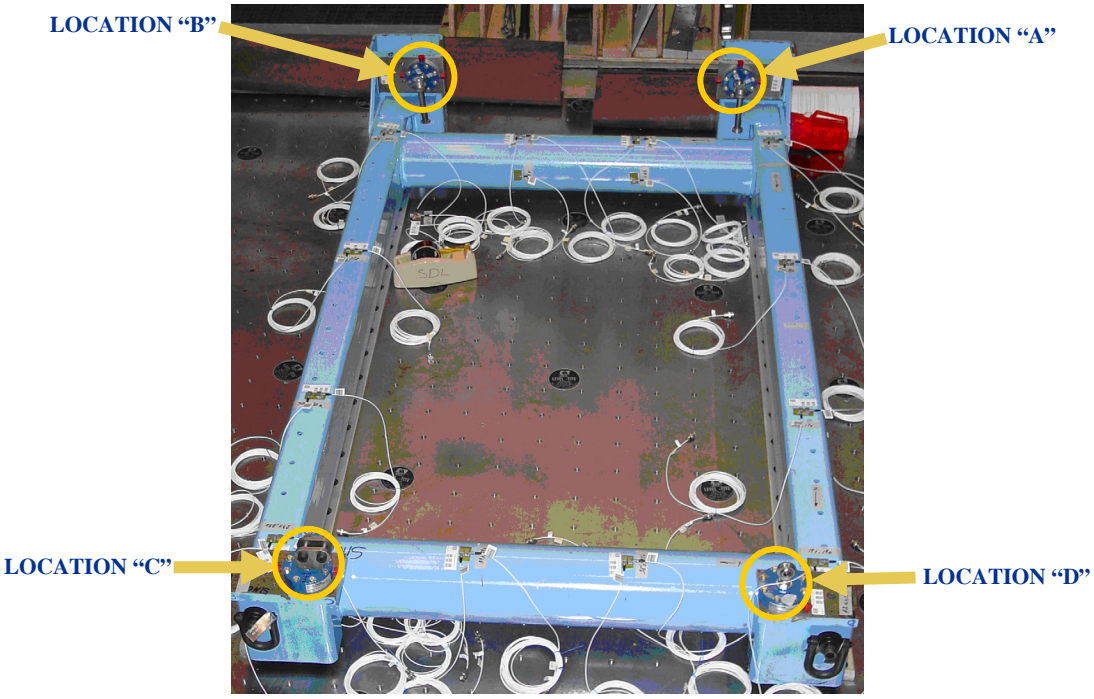

FIGURE 22 – LOAD CELLS

MB Dynamics (Modal 50) 50 lb_{rms} shakers were used to excite the CIR. One shaker was used for X and Z-axis excitation. Two shakers were used in the Y-axis to excite symmetric and anti-symmetric modes. Initially, impact tests were conducted to evaluate data quality, identify potential shaker locations, and to obtain preliminary modal data. Shaker locations were selected at hard points on the rack to optimally excite the target modes (Figures 23– 26). Multiple shaker excitation levels were used to address linearity of the CIR test configuration. Burst random excitation levels included ½, 1, 2, 5, and 10 lb_{rms}. Sine excitation levels included 5, 10, 15, and 20 lb_{peak} from 10-80 Hz. For the X-axis target mode a slight nonlinearity was observed, otherwise linearity was excellent for the target modes (Figures 27– 30). The frequency shift observed was less than 1 Hertz (less than 5%).

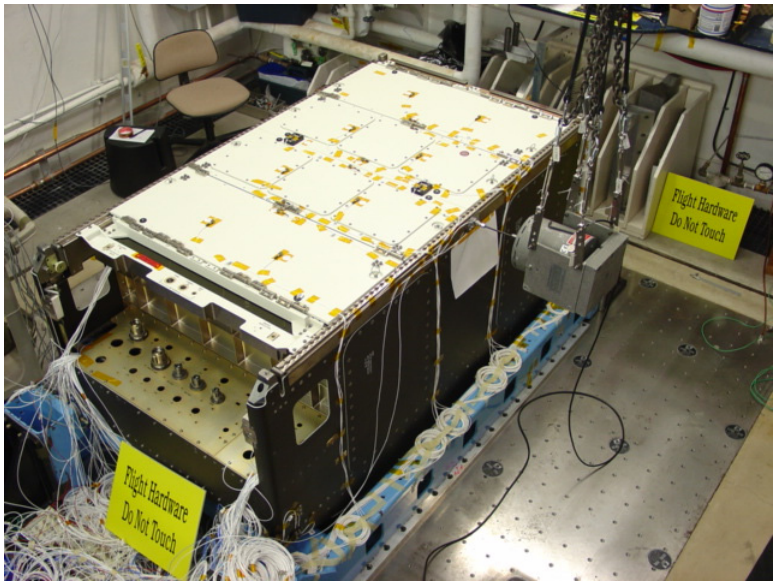

FIGURE 23 – X-AXIS SHAKER EXCITATION

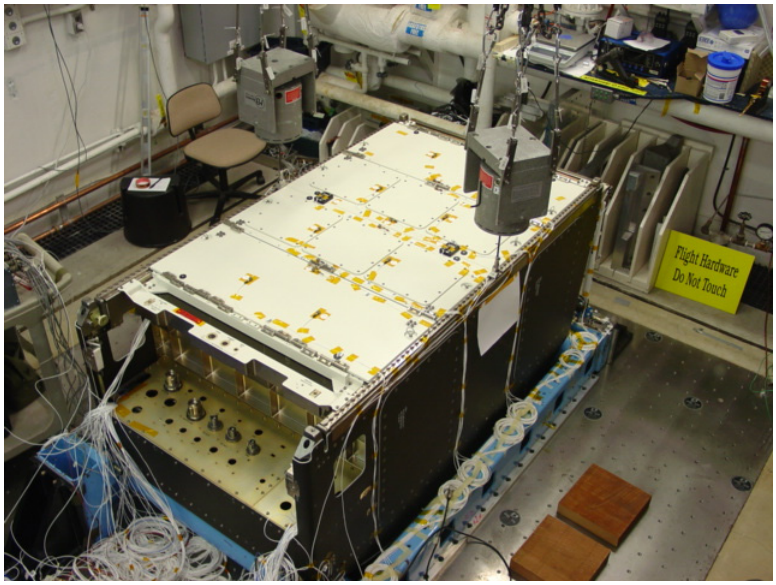

FIGURE 24 – Y-AXIS SHAKER EXCITATION

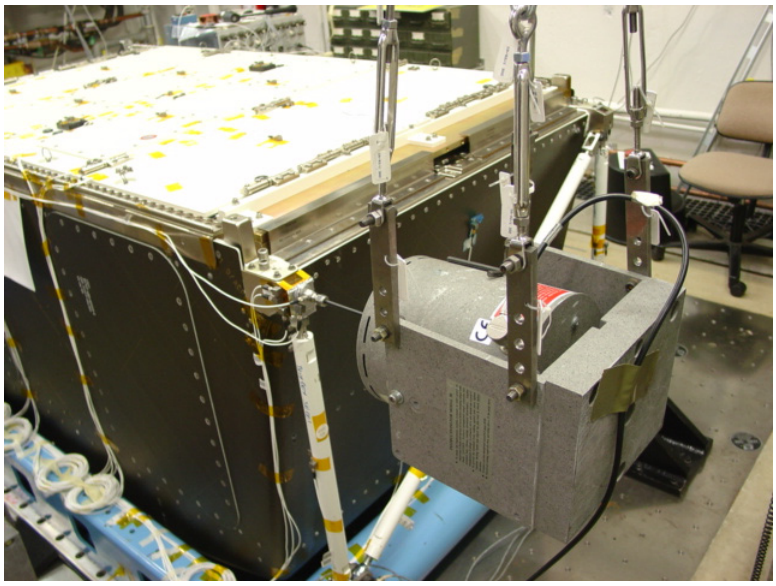

FIGURE 25 – Z-AXIS SHAKER EXCITATION

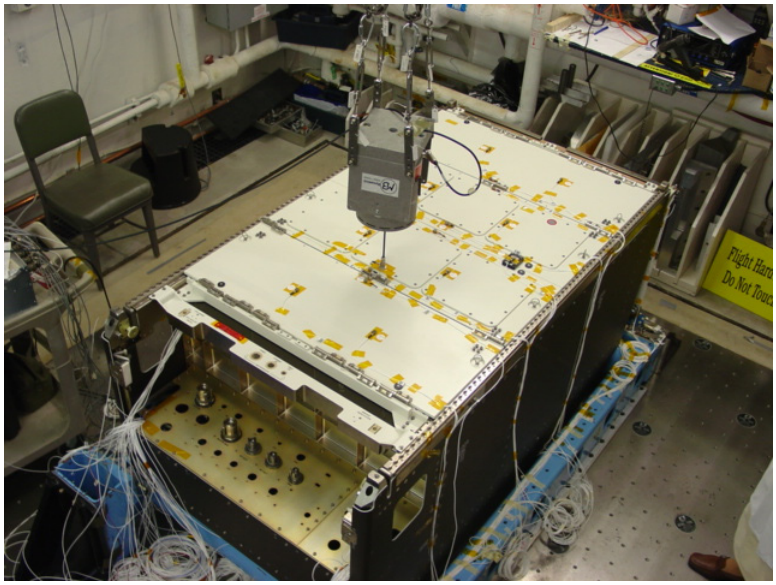

FIGURE 26 – DOOR SHAKER EXCITATION

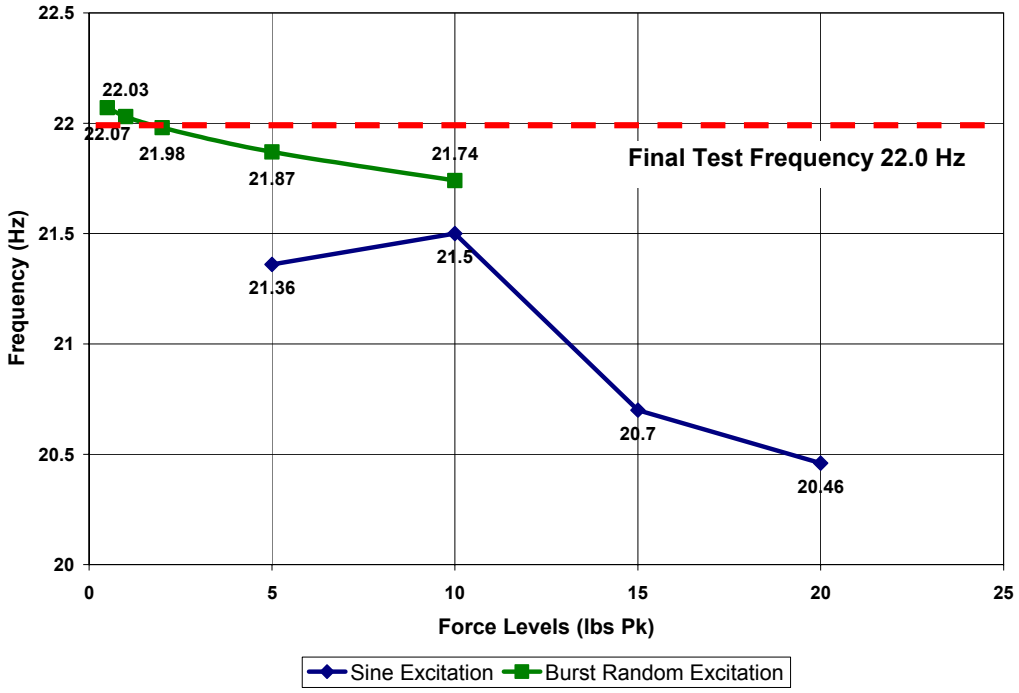

FIGURE 27 – LINEARITY OF X-AXIS RACK TRANSLATION MODE USING SINE SWEEP AND BURST RANDOM EXCITATION

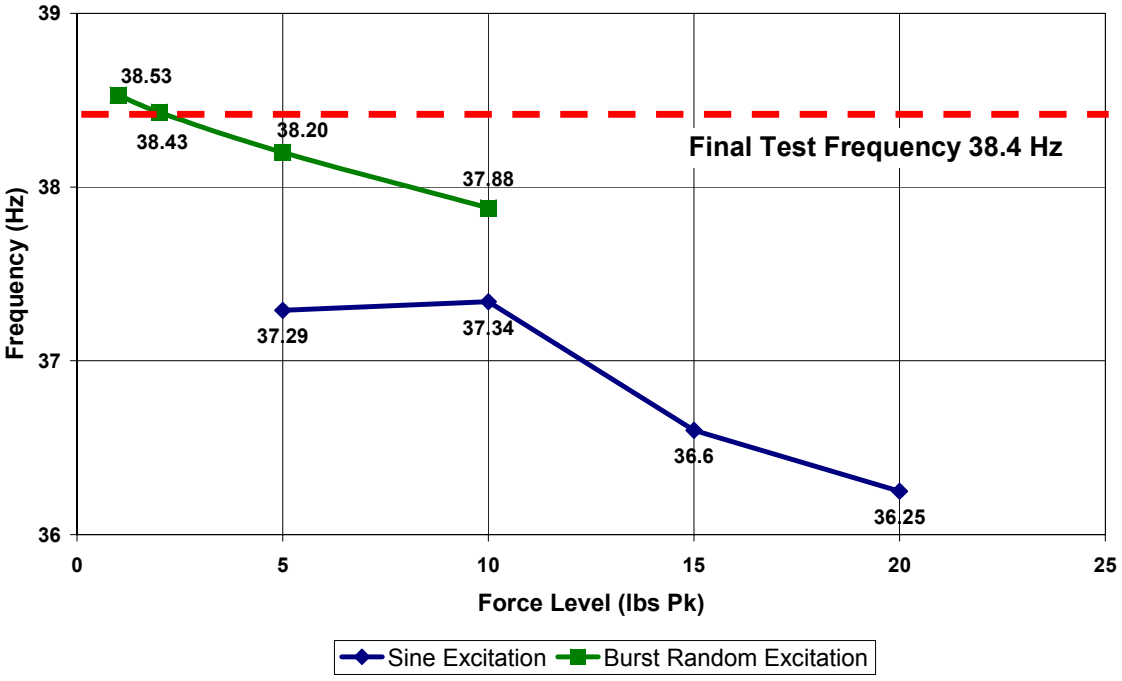

FIGURE 28 – LINEARITY OF Y-AXIS RACK TRANSLATION MODE USING SINE SWEEP AND BURST RANDOM EXCITATION

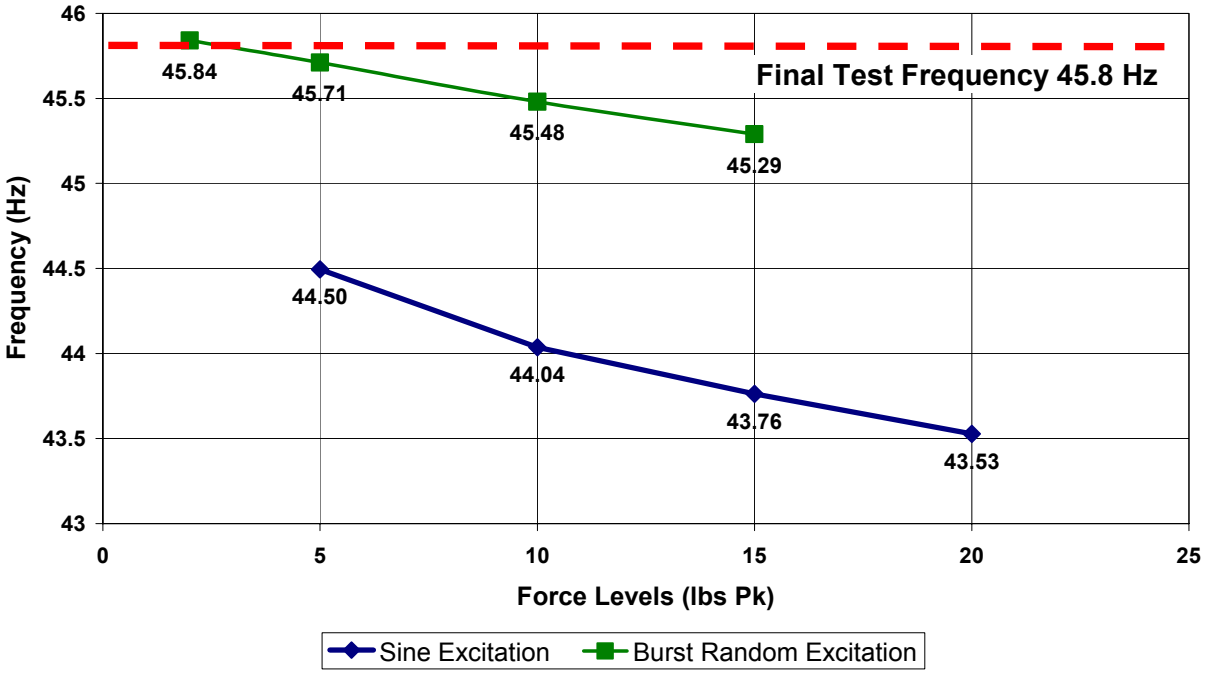

FIGURE 29 – LINEARITY OF Z-AXIS RACK TRANSLATION MODE USING SINE SWEEP AND BURST RANDOM EXCITATION

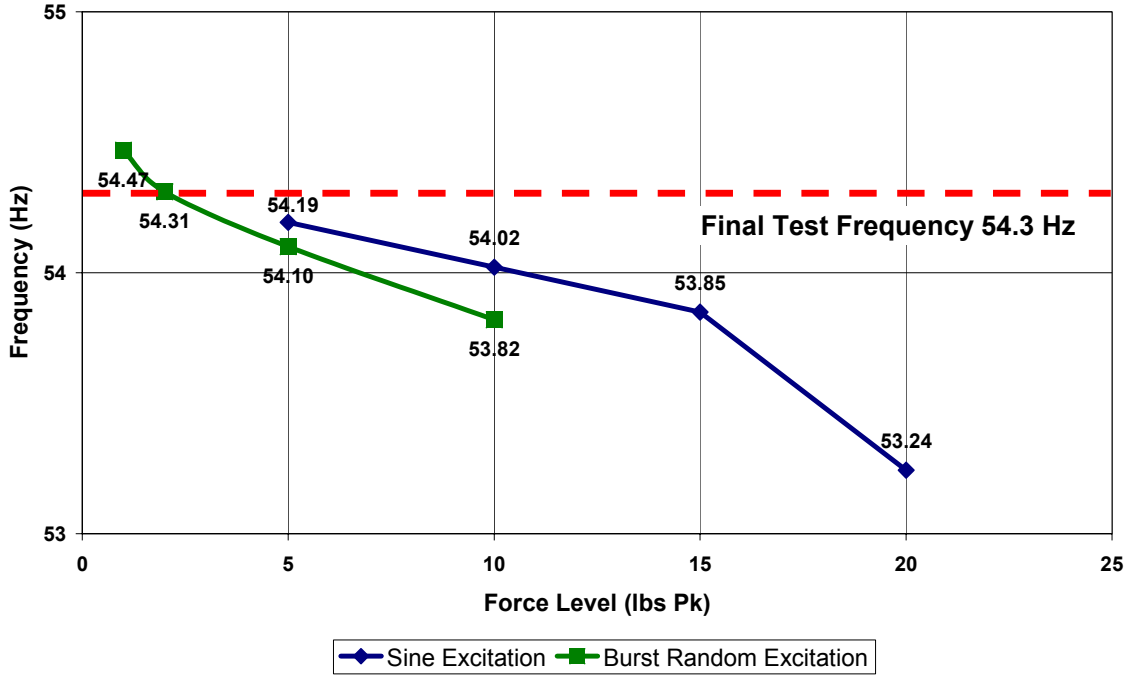

FIGURE 30 – LINEARITY OF Y-AXIS DOOR MODE USING SINE SWEEP AND BURST RANDOM EXCITATION

The CIR modal test had high data quality and low extraneous noise. Typical sine sweep excitation Frequency Response Functions (FRFs) and coherence graphs from the test are shown in Figures 31 – 34. Typical burst random excitation Frequency Response Functions (FRFs) and coherence graphs from the test are shown in Figures 35 – 38. Test data results can be found in the Structural Dynamics Laboratory test report number SDL-TR-04-55 (Reference 4).

Three global rack translational modes were identified during CIR modal testing using burst random excitation. The X-axis mode occurred at 22.0 Hz, the Y-axis mode occurred at 38.4 Hz, and the Z-axis mode occurred at 45.8 Hz. A door mode was also identified at 54.3 Hz.

Two new Z-axis rack rotation modes were identified during testing, occurring at 48.6 Hz and 49.5 Hz. The rotational modes were only predicted with the CIR test FEM using the rack fixture. With CIR test and flight FEMs in rigid boundary conditions, the rotational modes do not exist. The rotational modes are considered to be an artifact of the fixture attachment to the CIR. The rack rotational modes were not correlated as there existence only occurs in the presence of the rack fixture.

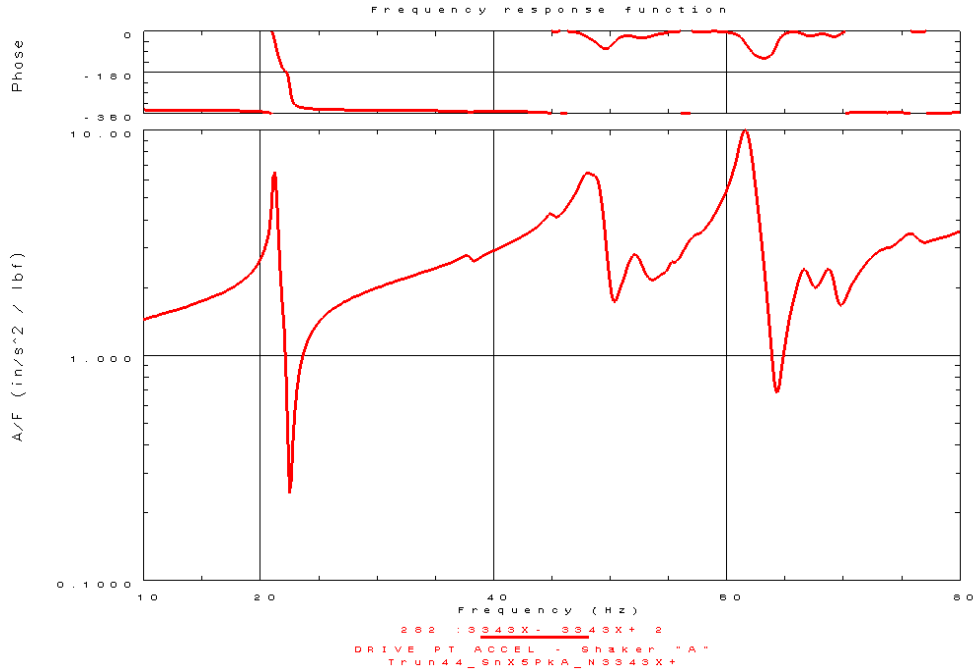

FIGURE 31 – TYPICAL DRIVE POINT FRF FROM X-AXIS SINE SWEEP EXCITATION

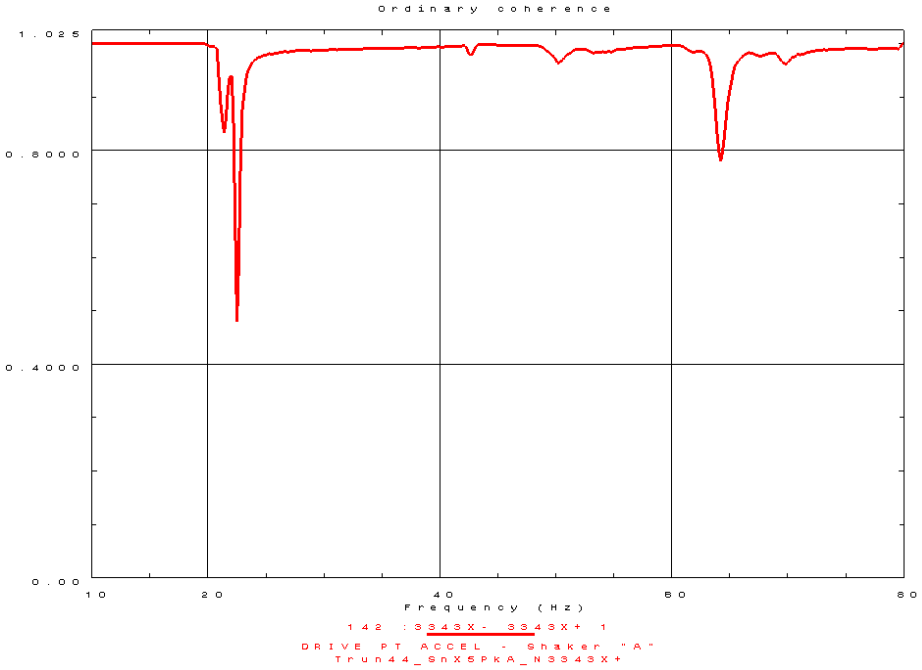

FIGURE 32 – TYPICAL DRIVE POINT COHERENCE FROM X-AXIS SINE SWEEP EXCITATION

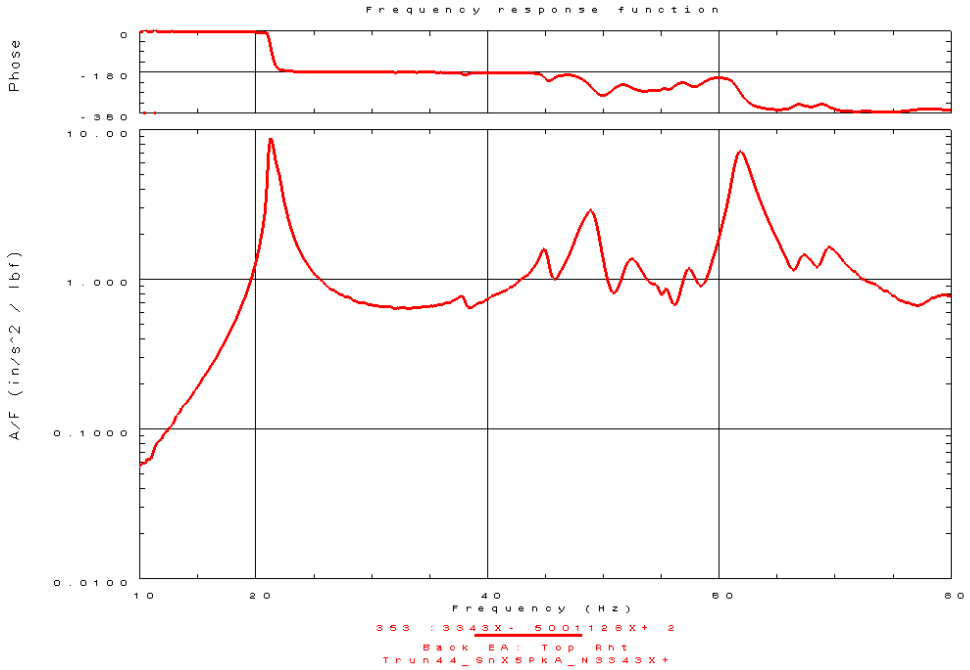

FIGURE 33 – TYPICAL FRF FROM X-AXIS SINE SWEEP EXCITATION

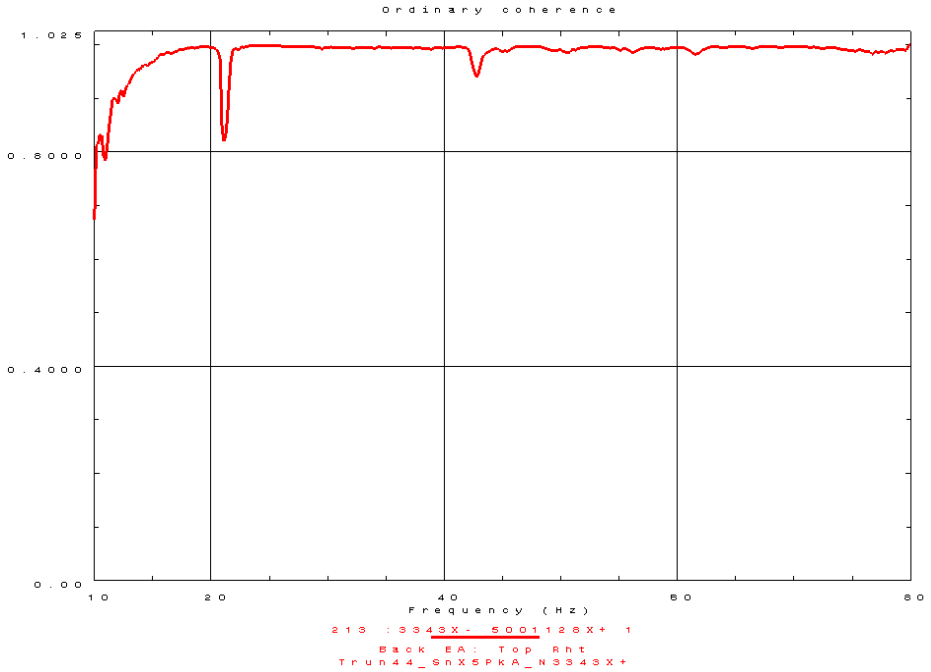

FIGURE 34 – TYPICAL COHERENCE FROM X-AXIS SINE SWEEP EXCITATION

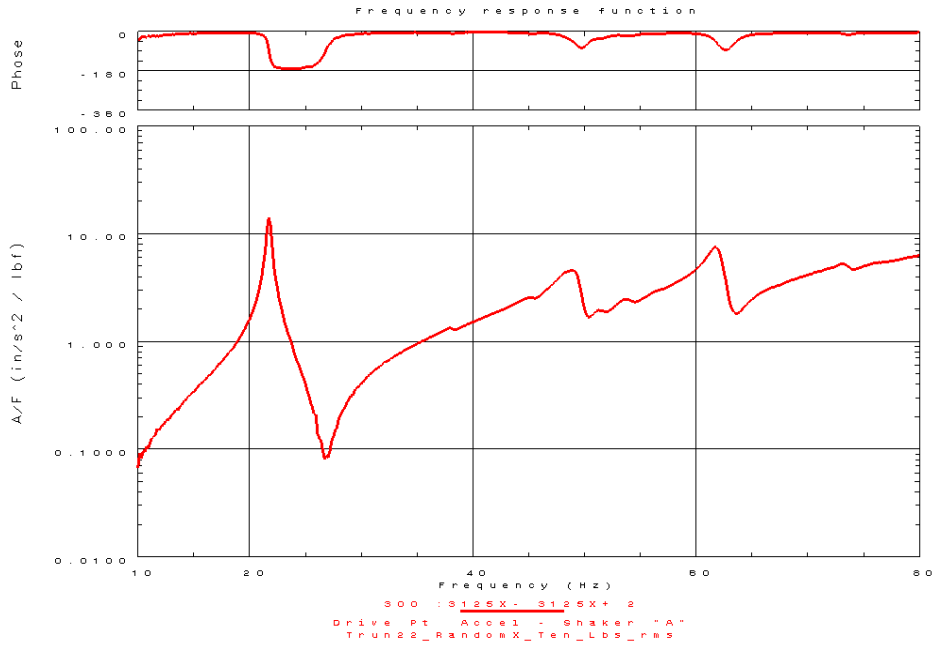

FIGURE 35 – TYPICAL DRIVE POINT FRF FROM X-AXIS BURST RANDOM EXCITATION

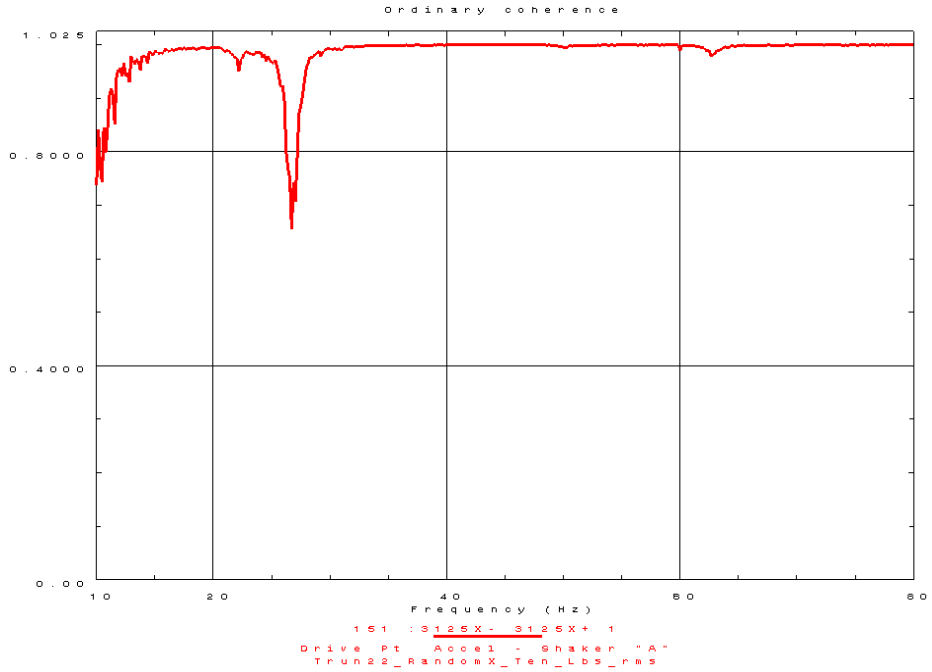

FIGURE 36 – TYPICAL DRIVE POINT COHERENCE FROM X-AXIS BURST RANDOM EXCITATION

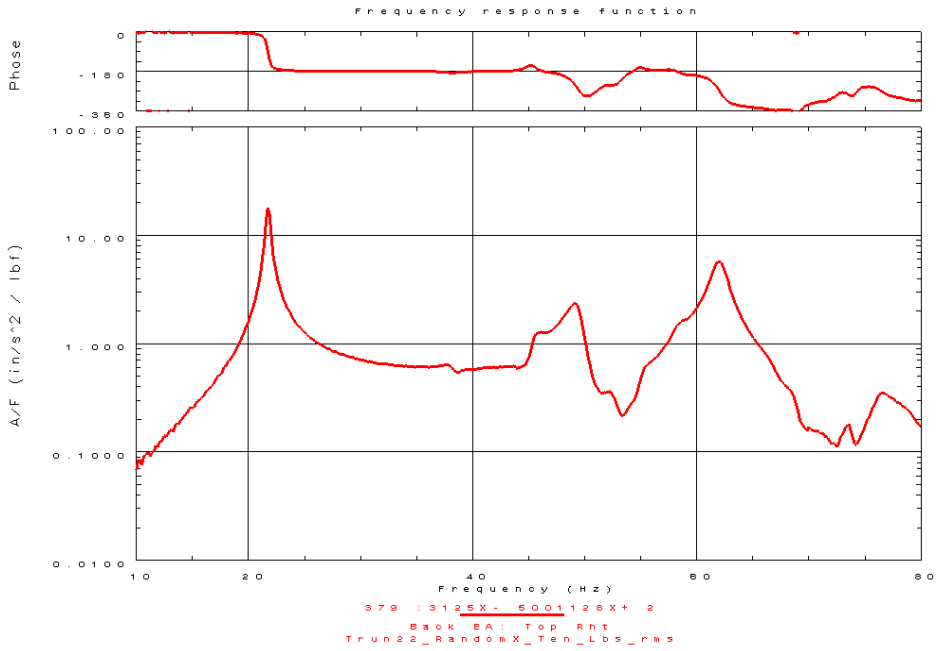

FIGURE 37 – TYPICAL FRF FROM X-AXIS BURST RANDOM EXCITATION

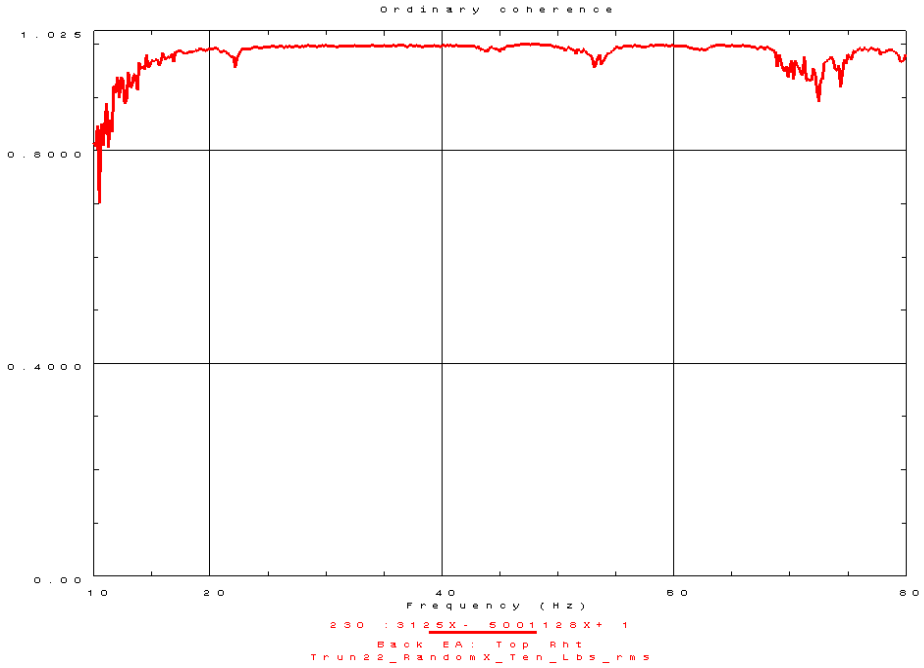

FIGURE 38 – TYPICAL COHERENCE FROM X-AXIS BURST RANDOM EXCITATION

7. Model Correlation

The CIR finite element model was updated based on initial low cross-orthogonality of the primary target modes (rack translation) and the secondary mode (door).

CIR model correlation was accomplished using Attune (Reference 5) test/analysis correlation and model updating software. Attune uses design sensitivity and optimization methods to identify FEM model changes that minimize the difference between test and analysis results (objective function). Design sensitivity coefficients are used that identify important properties in the finite element model (FEM) for optimization. Upper and lower bounds are assigned to the design variables to account for parameter uncertainty. Weights can be assigned to the design variables to emphasize their importance on the objective function. State variables (design constraints) used in the optimization include frequency and cross-orthogonality. The Attune optimization flowchart is shown in Figure 39. After each iteration, the eigensolution is recalculated in Nastran using the updated design variables.

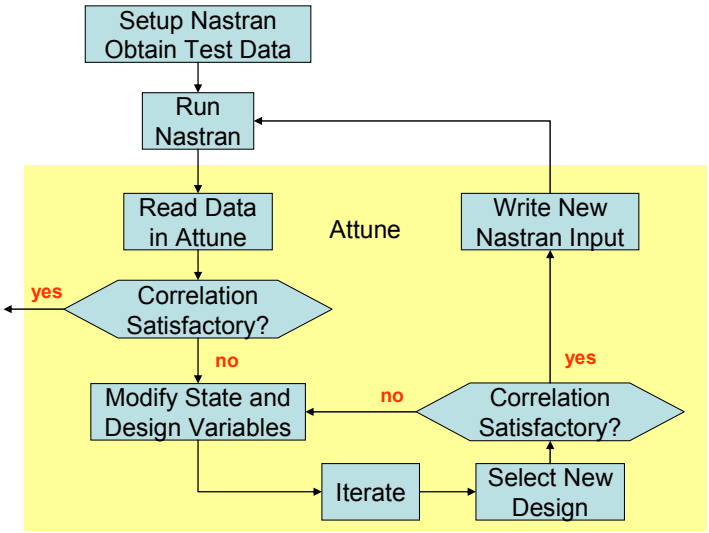

FIGURE 39 – ATTUNE OPTIMIZATION FLOWCHART

The CIR FEM was correlated using three different optimization algorithms: Genetic, Monte Carlo, and Gradient methods.

The Genetic and Monte Carlo algorithms both utilize randomly generated candidate designs, and update the stiffness matrix based on modal matrix sensitivities. The Genetic algorithm evaluates a set of randomly chosen designs against the objective function, and then tries to systematically improve the designs through iteration. The advantage of the Genetic and Monte Carlo methods is that these methods are not trapped by local minima. The Genetic and

Monte Carlo algorithms are generally used to tune the FEM when the design properties are not well known, and there is a large design space.

The Gradient method is best used when the design variables are well known, and only small changes are required to correlate the model. Problems associated with the Gradient method are encountered when the algorithm is trapped in local minima, causing inaccuracies in the linear approximation of the derivatives.

The CIR model correlation methodology was based on modal testing and correlating each major structural assembly FEM individually (CIR Experiment Assembly, CIR Air Thermal Control Unit, Rack Door, and Lower Structure Assembly). This developed confidence that the major assemblies were correlated before the start of the CIR modal test. The final step in the correlation process was to modal test and model correlate the CIR. This building block approach facilitated the model correlation process. Once the major structure assemblies FEMs were individually correlated, the only areas of uncertainty in the fully populated CIR model were the structural connections between the assemblies, the rack, and the fixture.

The CIR FEM was updated using the following design variables:

- Load cell and attachment clevis X, Y, Z-axes translational spring stiffness (PBUSH)
- Door window perimeter stiffness (PBAR)
- Door Young's Modulus (E)
- Door angle bracket thickness (PSHELL)

In order to correlate the CIR FEM, twelve iterations were performed in Attune to update the design parameters. Table 7 summarizes the design parameter changes made between the pre-test and correlated CIR models.

Of primary concern was the spring stiffness representation of the interface load cells that controlled the X, Y, and Z-axes displacement for the rack translational target modes (Figure 40).

Correlation of the door mode was accomplished by updating the stiffness representation of the overlap between the window panels and the door frame. CBARS were added around the perimeter of each window panel to increase the local stiffness around the door frame without adding mass. The door Young's Modulus was increased by 11.4% in order to account for underestimation of the door stiffness and to correlate the door mode shape. In addition, the door mounting bracket thickness was also increased to reflect the as-built configuration (increased the FEM bracket section thickness from 0.25" to 1" on the web and from 0.50" to 1" on the flange). Figure 41 shows the door window panel region where stiffness (CBARs) was added to the model. Figure 42 shows the door mounting bracket locations.

Table 7 – Comparison of CIR FEM Design Variable Sensitivities Between the Pre-Test and Correlated Models

Description	Type	PID	Property	Design Variable	Design Sensitivity	Pre-Test Model	Correlated Model	Percent Change
Load Cell Translational Spring Stiffness at "C" fixture location	**PBUSH**	14000010	**Stiffness (lb/in)**					
			Kx	KCTX	1.095E-03	1.000E+08	8.529E+07	-17.2%
			Ky	KCTY	9.033E-09	1.000E+06	1.084E+06	7.7%
			Kz	KCTZ	1.351E-09	1.000E+08	8.529E+07	-17.2%
Load Cell Translational Spring Stiffness at "D" fixture location	**PBUSH**	14000011	**Stiffness (lb/in)**					
			Kx	KDTX	-7.377E-03	1.000E+08	1.05E+08	4.8%
			Ky	KDTY	-2.484E-03	1.000E+06	1.23E+06	18.7%
			Kz	KDTZ	-5.870E-02	1.000E+08	8.53E+07	-17.2%
Load Cell Translational Spring Stiffness at "A and B" fixture locations	**PBUSH**	14000012	**Stiffness (lb/in)**					
			Kx	KABTX	4.360E-02	5.500E+04	6.438E+04	14.6%
			Ky	KABTY	6.871E-02	3.000E+05	1.500E+05	-100.0%
			Kz	KABTZ	-1.377E-02	5.000E+05	5.850E+05	14.5%
Window Perimeter Stiffness	**PBAR**	1001	**Inertia (in^4)**					
			I1	PBI1	8.337E-04	0.0400	0.05388	25.8%
Door Young's Modulus	**MAT1**	7231184	**Modulus (lb/in^2)**					
			E	DOORE	8.676E-10	1.010E+07	1.140E+07	11.4%
Door Bracket Web Thickness	**PSHELL**	4981589	**Thickness (in)**					
			T	WEBT	2.117E-05	0.25	0.99	74.7%
Door Bracket Flange Thickness	**PSHELL**	4981588	**Thickness (in)**					
			T	FLANGET	1.784E-03	0.50	0.998	49.9%

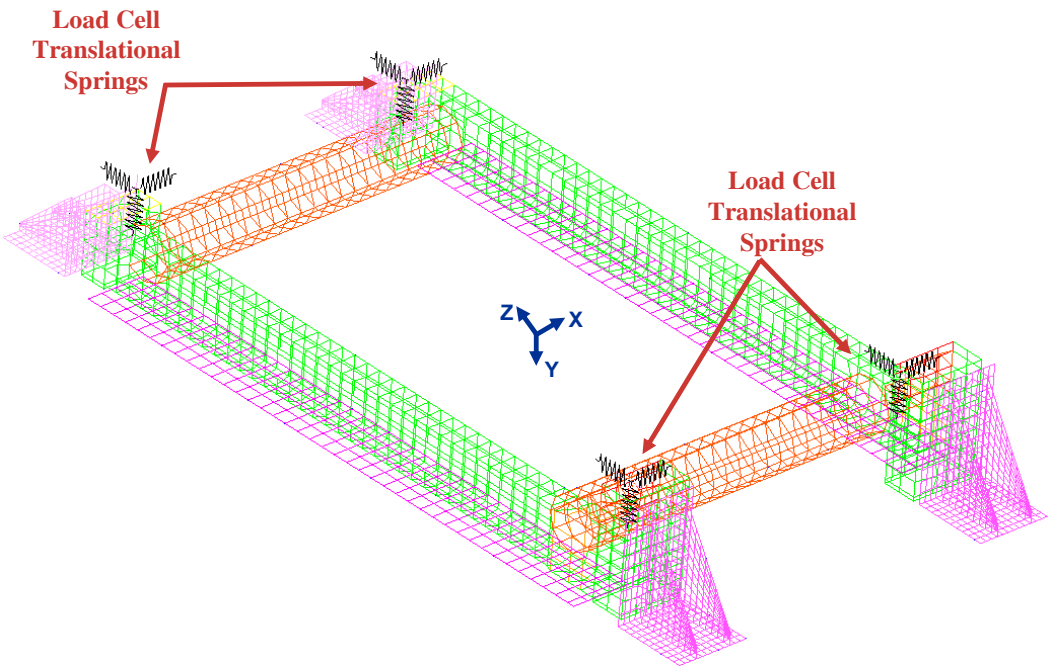

FIGURE 40– LOAD CELL TRANSLATIONAL SPRINGS

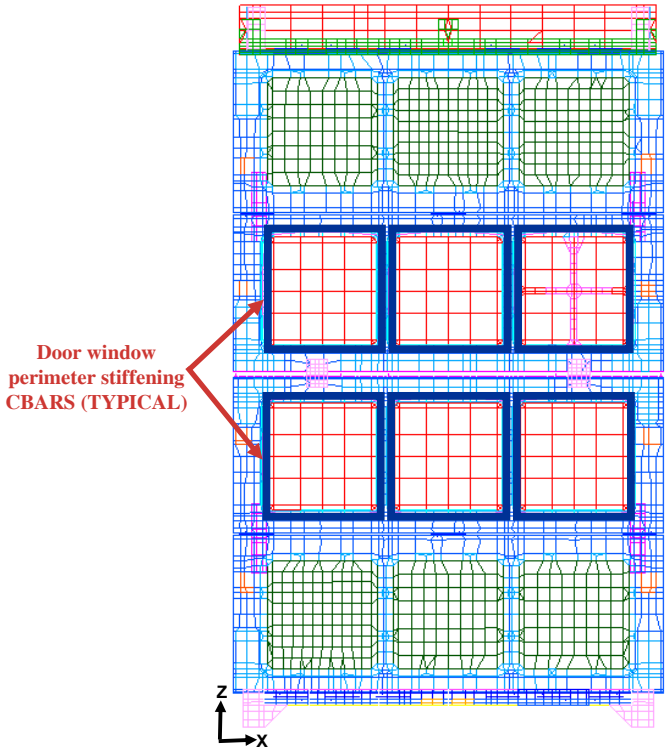

FIGURE 41– DOOR WINDOW PERIMETER STIFFENING

Design variables having the greatest change from the pre-test model to the correlated model were the Load Cell “A and B” location Y-axis translational stiffness (-100% change), door mounting bracket web thickness (+74.7% change), door mounting bracket flange thickness (+49.9% change), and the door window perimeter stiffness (+25.8% change). The FEM did not reflect the as-built door bracket design.

The Genetic algorithm was primarily used to correlate the model, with an overall RMS state variable error of 6.28% for the objective function (comparing the test and TAM target mode frequencies and cross-orthogonalities). The X-axis target mode frequency difference was -2.7%, the Y-axis target mode frequency difference was 3.4%, the Z-axis target mode frequency difference was -3.9%, and the door target mode frequency difference was 8.8%. All target mode cross-orthogonality values were greater than 90% (Figure 43). These results are summarized in Table 8.

Figures 44 – 47 illustrate a comparison between the test and TAM modes, effective weight, and cross-orthogonality. The test and TAM modes shapes are dynamically back-expanded to improve visualization. The correlated model has high cross-orthogonality (>90%), satisfying the ISS model correlation criteria.

The correlated models are enclosed on Compact Disk and have the following MSC/NASTRAN run deck and bulk data file names:

Folder: Correlated CIR Test FEM
Run Deck
cir_tam_12_02_04_full_model.dat

Bulk Data
CIR_TAM_11_04_04_REV15_test_fm_Ypin_ModCS_EAMassSimBC.bdf
Load_Cell_springs.bdf
Window_Reinforcement.bdf

Folder: Correlated CIR Flight FEM
Run Deck
CIR_DYNAMIC_LAUNCH_12-17-04.dat

Bulk Data
CIR_DYNAMIC_LAUNCH_10-5-04_REV2.bdf
Window_Reinforcement.bdf

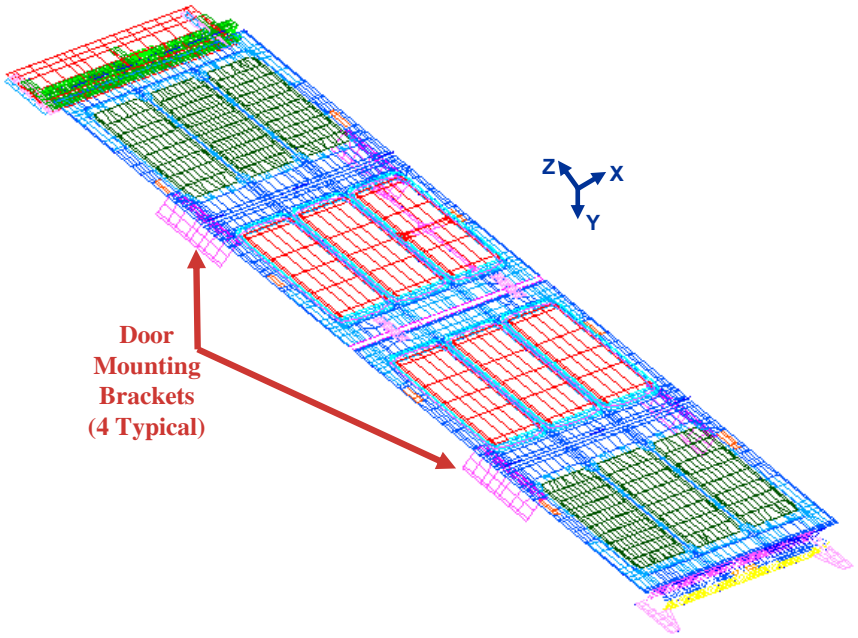

FIGURE 42– DOOR MOUNTING BRACKETS

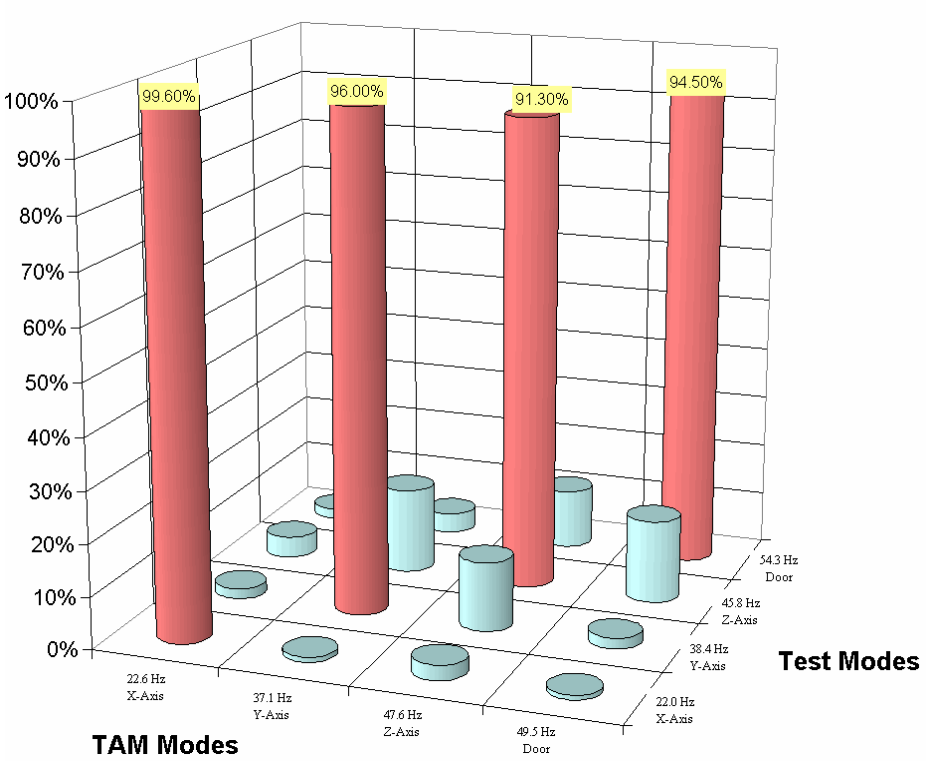

FIGURE 43 – FINAL CROSS-ORTHOGONALITY FOR TARGET MODES

Table 8 – Comparison of Test and TAM Target Mode Frequency Difference and Cross-Orthogonality

	Mode		TAM 1	TAM 2	TAM 4	TAM 6	Delta Freq	Mode Shape Description
		Freq (Hz)	22.6	37.1	47.6	49.5		
	1	22.0	0.996	-0.010	-0.029	-0.008	-2.7%	Rack X-axis Translation
	2	38.4	0.020	-0.960	0.133	-0.020	3.4%	Rack Y-axis Translation
Test	3	45.8	-0.040	0.166	0.913	-0.160	-3.9%	Rack Z-axis Translation
	6	54.3	-0.020	-0.039	-0.114	-0.945	8.8%	Door Y-axis Bending

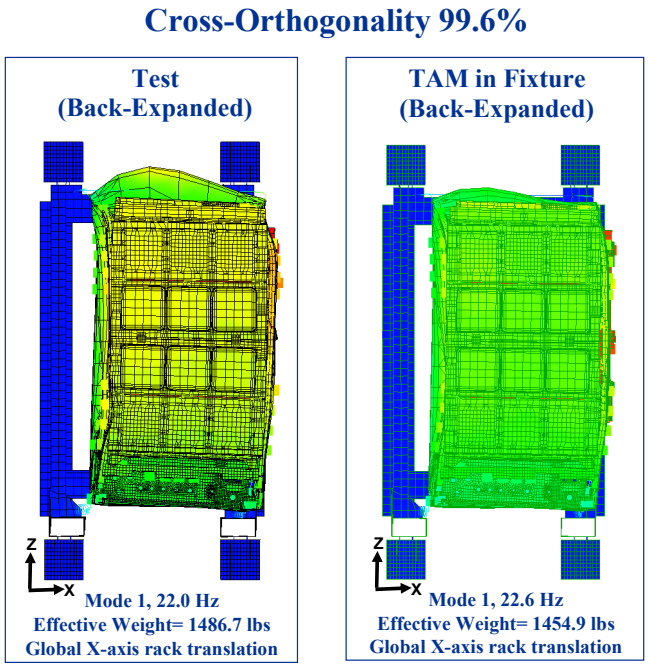

FIGURE 44 – X-AXIS TARGET MODE SHAPES, EFFECTIVE WEIGHT, AND CROSS-ORTHOGONALITY

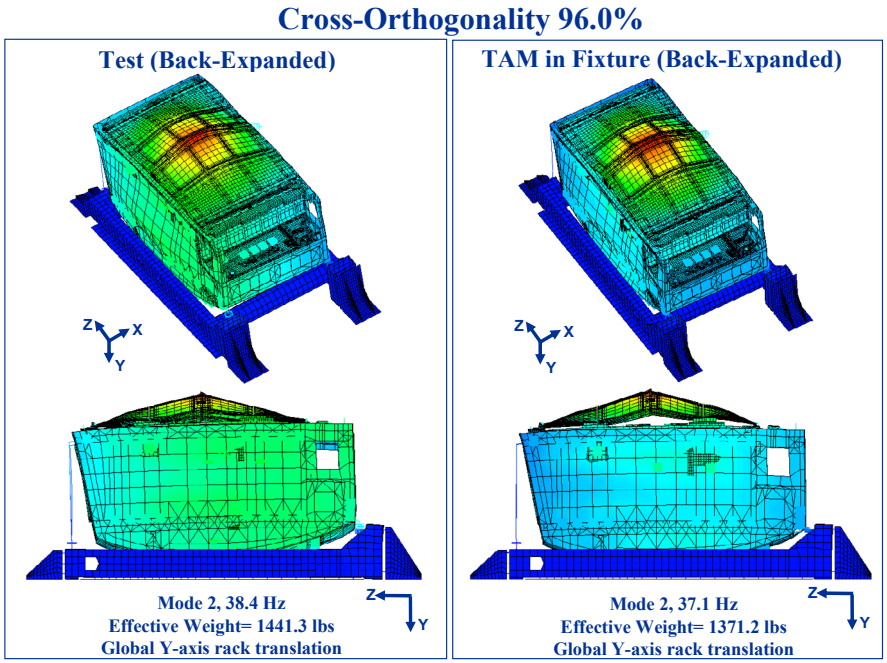

FIGURE 45 – Y-AXIS TARGET MODE SHAPES, EFFECTIVE WEIGHT, AND CROSS-ORTHOGONALITY

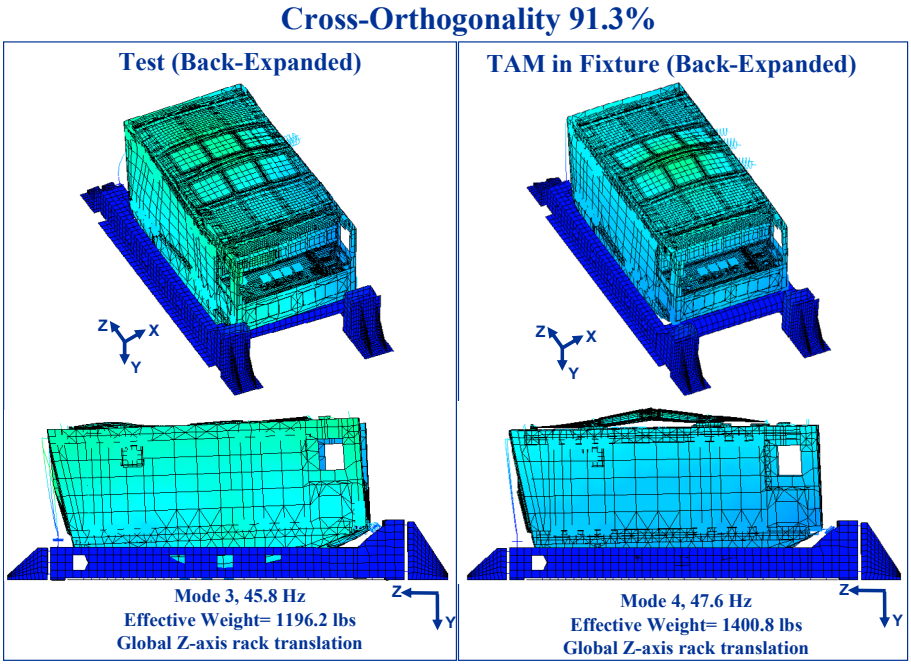

FIGURE 46 – Z-AXIS TARGET MODE SHAPES, EFFECTIVE WEIGHT, AND CROSS-ORTHOGONALITY

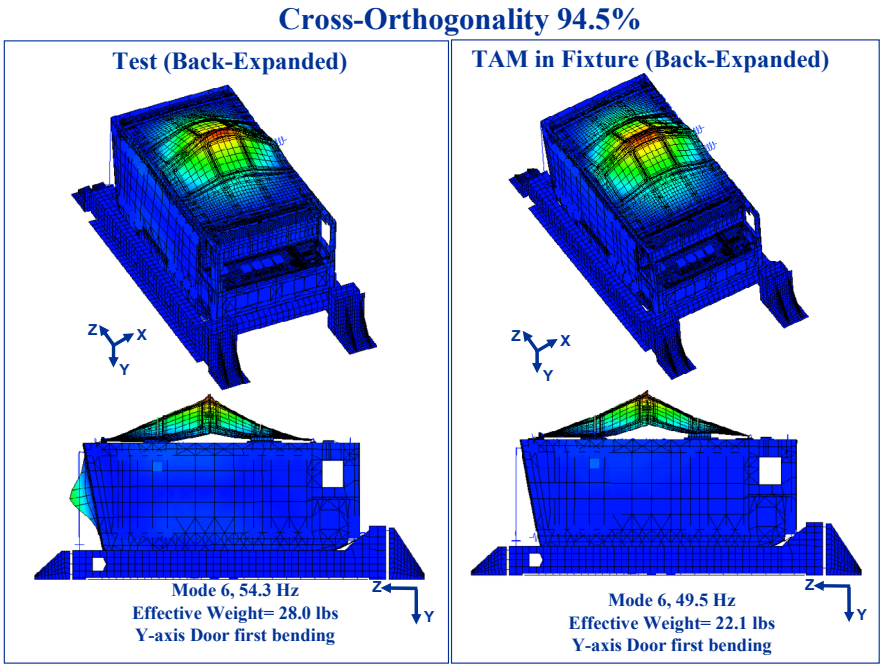

FIGURE 47 – DOOR MODE SHAPES, EFFECTIVE WEIGHT, AND CROSS-ORTHOGONALITY

8. Conclusions

The CIR rack finite element model was successfully correlated based on the International Space Station model correlation criteria.

Four target modes were identified in test including three primary rack translation modes (X, Y, and Z-axes) and a secondary door mode. All model primary target modes had frequency differences less than 5% compared to test. The model secondary target mode has a frequency difference less than 9% compared to test (Table 8). The final cross-orthogonality between the correlated TAM and test mode shapes (Figure 43) was greater than 90% for all target modes.

9. References

1. "ISS Fluids and Combustion Facility Loads Model Verification Plan," NASA GRC presentation to the NASA JSC Structures Working Group, September 24, 2003.
2. "ISPR Qualification Modal Test Correlation," prepared by J. A. Knoll and H. A. Britt, Boeing rack model correlation report, 2-8F1A-HAB-049/95, Revision A, January 12, 1996.
3. "CIR Mass Properties Report," CIR-RPT-3855, Final, March 11, 2005.
4. "FCF CIR GIU Rack Modal Test Report," SDL TR-04-55.
5. "Attune User's Guide," test/analysis correlation and modal updating software, Version 1.1, ATA Engineering, January 2005.

10. Acronym List

ARIS	Active Rack Isolation Subsystem
ATCS	Air Thermal Control System
ATCU	Air Thermal Control Unit
CDR	Critical Design Review
CIR	Combustion Integrated Rack
CSCI	Computer Software Configuration Item
DCM	Diagnostics Control Module
ECS	Environmental Control Subsystem
EDA	Engineering Development Article
EDU	Experiment Development Unit
EM	Engineering Model
EMI	Electro- Magnetic Interference
EA	Experiment Assembly
EPCU	Electrical Power Control Unit
EVP	Exhaust Vent Package
Fab	Fabrication
FCF	Fluids and Combustion Facility
FCU	FOMA Control Unit
FDSS	Fire Detection and Suppression System
FEA	Fluids Experiment Assembly
FHA	Flight Hardware Availability
FIR	Fluids Integrated Rack
FMEA	Failure Modes and Effects Analysis
FOMA	Fuel/Oxidizer Management Assembly
FSAP	Fluids Science Avionics Package
FSR	Flight Safety Review
GCIP	Gas Chromatograph Instrumentation Package
GN2	Gaseous Nitrogen
GIS	Gas Interface System
GIU	Ground Integration Unit
GSE	Ground Support Equipment
HFR	High Frame Rate
HiBMs	High Bit depth Multi Spectral Camera Package
HR	High Resolution
H/W	Hardware
I&T	Integration and Test
IAM	Image Acquisition Module
ICD	Interface Control Document
I/F	Interface
IOP	Input/ Output Processor
IPP	Image Processing Package
IPSU	Image Processing and Storage Unit
IPSU-A	Image Processing and Storage Unit, Version A
IR	Infrared
ISPR	International Standard Payload Rack
ISS	International Space Station
LED	Light Emitting Diode
LLL	Low Light Level
LMM	Light Microscopy Module
MDCA	Multi-user Droplet Combustion Assembly
MEL	Microgravity Emissions Laboratory
MFC	Mass Flow Controller
MRDOC	Microgravity Research, Development and Ops Contract
NGIT	Northrop Grumman Information Technology
OB	Optics Bench
OM	Optics Module
OPI	Optics Plate Interface
PaRIS	Passive Rack Isolation System
PCS	Portable Computer System
PFE	Portable Fire Extinguisher
PI	Principal Investigator
PIA	Payload Integration Agreement
PPH	Program-Provided Hardware
PSH	Payload Support Hardware
PSR	Pre-Ship Review
PTCU	Payload Training Center Unit
Qual	Qualification
REU	Remote Electronic Unit
RFCA	Rack Flow Control Assembly
RHA	Rack Handling Adapter
RMSA	Rack Maintenance Switch Assembly
RPC	Remote Power Controller
RPCM	Remote Power Controller Module
RUP	Rack Utility Panel
SAMS	Space Acceleration Measurement System
SDL	Serial Data Link
SEI	Software Engineering Institute
SMD	Silicon Mountain
SPEL	Station Power Electronics Laboratory
SSC	Station Support Computer
Temp	Temporary
TSC	Telescience Support Center
TSH	Tri-axial Sensor Head
T/O	Turnover
UIP	Utility Interface Panel
UF	Utilization Flight
ULF	Utilization and Logistics Flight
UV	Ultraviolet
VES	Vacuum Exhaust System
VP	Verification Plan
VRS	Vacuum Resource System
VTR	Verification and Test Readiness
VVS	Vacuum Vent System
WFCA	Water Flow Control Assembly
WTCS	Water Thermal Control System

11. Appendices

Appendix A CIR Experiment Assembly Model Correlation

Appendix B Air Thermal Control Unit (ATCU) Model Correlation

Appendix C Rack Door Model Correlation

Appendix D Lower Package Structure Model Correlation

Appendix E CIR Rack Modal Instrumentation Plan

Appendix A

CIR Experiment Assembly Model Correlation

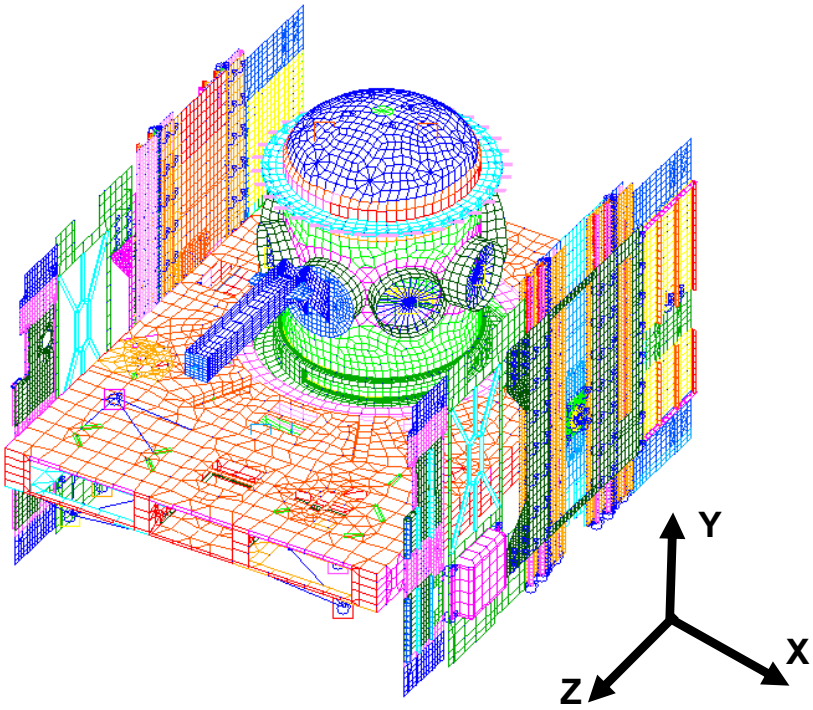

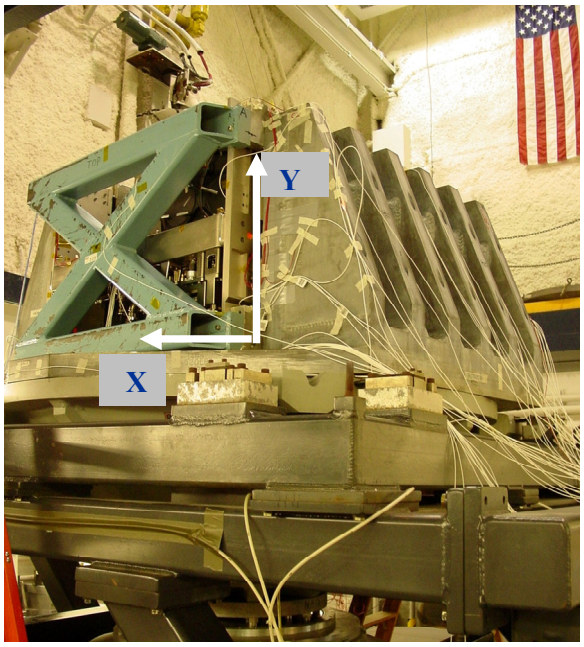

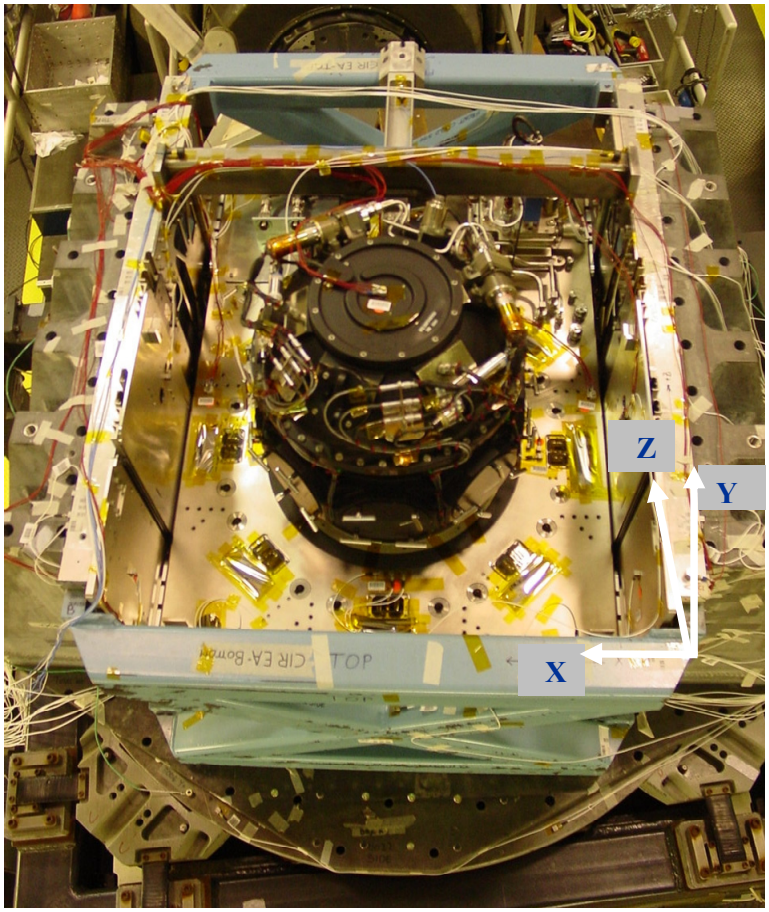

CIR Experiment Assembly Test Configuration

CIR Experiment Assembly
Comparison of FEM to TAM

FEM (178,884 DoF)			TAM (78 DoF)		
Mode	**Frequency (Hz)**	**Effect Mass (%)**	**Mode**	**Frequency (Hz)**	**Effect Mass (%)**
1	**50.6**	**86.3-X**	**1**	**50.9**	**97.5-X**
2	60.0		**2**	**72.4**	**81.5-Y**
3	61.9		3	96.1	RX
4	65.2		4	100.9	
5	67.4		5	113.9	
8	**71.4**	**60.4-Y**	6	159.8	42.6-Z
26	151.0	53.6-Z	7	170.7	40.5-Z
27	158.6	12.8-Z	8	175.8	

BOLD INDICATES TARGET MODES

Comparison of CIR Experiment Assembly
FEM with TAM

MODE SHAPE DESCRIPTION	FEM FREQ (Hz)	TAM FREQ (Hz)	XORTHO %	% FREQ DIFF
Translation of the Chamber in the X-axis	50.6	50.9	98.5	0.6
Translation of the Chamber in the Y-axis	71.4	72.4	95.8	1.3

CIR Experimental Assembly
Cross Orthogonality
FEM vs TAM

			TAM MODE								
	Mode Number		1	2	3	4	5	6	7	8	9
		Hz	50.9	72.4	96.1	101.0	113.9	159.9	170.7	175.9	191.5
	1	50.6	98.5	0.0	0.0	0.0	0.0	0.0	0.0	0.0	0.0
	2	60.0	0.0	0.0	0.0	0.0	0.0	0.0	0.0	0.0	0.0
	3	61.9	0.0	0.0	0.0	0.0	0.0	0.0	0.0	0.0	0.0
	4	65.2	0.0	0.0	0.0	0.0	0.0	0.0	0.0	0.0	0.0
	5	67.4	0.0	11.9	0.0	0.0	0.0	0.0	0.0	0.0	0.0
	6	69.6	0.0	0.0	0.0	0.0	0.0	0.0	0.0	0.0	0.0
	7	69.7	0.0	0.0	0.0	0.0	0.0	0.0	0.0	0.0	0.0
	8	71.4	0.0	95.8	0.0	0.0	0.0	0.0	0.0	0.0	0.0
	9	71.7	0.0	0.0	0.0	0.0	0.0	0.0	0.0	0.0	0.0
	10	80.8	0.0	0.0	18.5	0.0	0.0	0.0	0.0	0.0	0.0
	11	84.2	0.0	0.0	0.0	0.0	0.0	0.0	0.0	0.0	0.0
	12	85.5	0.0	0.0	0.0	0.0	0.0	0.0	0.0	0.0	0.0
FEM	13	87.3	0.0	0.0	0.0	0.0	0.0	0.0	0.0	0.0	0.0
MODE	14	94.0	0.0	0.0	77.0	29.5	0.0	0.0	0.0	0.0	0.0
	15	94.1	0.0	0.0	17.3	0.0	0.0	0.0	0.0	0.0	0.0
	16	96.3	0.0	0.0	48.7	64.8	0.0	0.0	0.0	0.0	0.0
	17	101.8	0.0	0.0	0.0	0.0	0.0	0.0	0.0	0.0	0.0
	18	105.2	0.0	0.0	12.3	63.7	0.0	0.0	0.0	0.0	0.0
	19	106.4	0.0	0.0	0.0	12.5	0.0	0.0	0.0	0.0	0.0
	20	112.4	0.0	0.0	0.0	0.0	95.9	0.0	0.0	0.0	0.0
	21	126.3	0.0	0.0	0.0	0.0	0.0	0.0	0.0	0.0	0.0
	22	130.4	0.0	0.0	0.0	0.0	0.0	0.0	0.0	0.0	0.0
	23	139.3	0.0	0.0	0.0	0.0	0.0	0.0	0.0	0.0	0.0
	24	141.2	0.0	0.0	0.0	0.0	0.0	0.0	0.0	0.0	0.0
	25	145.1	0.0	0.0	0.0	0.0	0.0	0.0	0.0	0.0	0.0
	26	151.0	0.0	0.0	0.0	0.0	0.0	80.9	22.7	10.9	0.0
	27	158.6	0.0	0.0	0.0	0.0	0.0	33.6	75.3	12.3	0.0

CIR Experimental Assembly
Cross Orthogonality Graph
FEM vs TAM

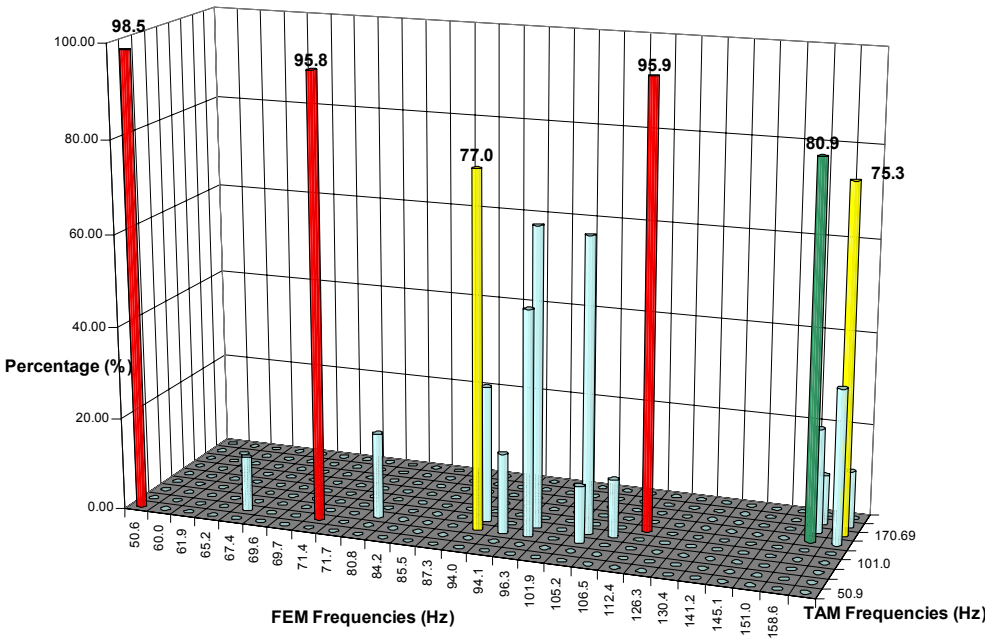

Comparison of CIR Experiment Assembly TAM with Test

MODE SHAPE DESCRIPTION	TAM FREQ (Hz)	Test FREQ (Hz)	XORTHO (%)	FREQ DIFF(%)
Translation of the Chamber in the X-axis	50.9	48.1	99.2	5.5
Translation of the Chamber in the Y-axis	72.4	73.0	89.8	0.9

CIR Experimental Assembly Cross Orthogonality TAM vs TEST

			TEST MODE		
	Mode Number		1	3	4
TAM		Freq (Hz)	**48.1**	**73.0**	**92.4**
MODE	1	**50.9**	99.2	0.1	1.1
	2	**72.4**	0.1	89.8	21.0
	3	**96.1**	0.2	0.3	80.3

CIR Experimental Assembly Cross Orthogonality Graph TAM vs TEST

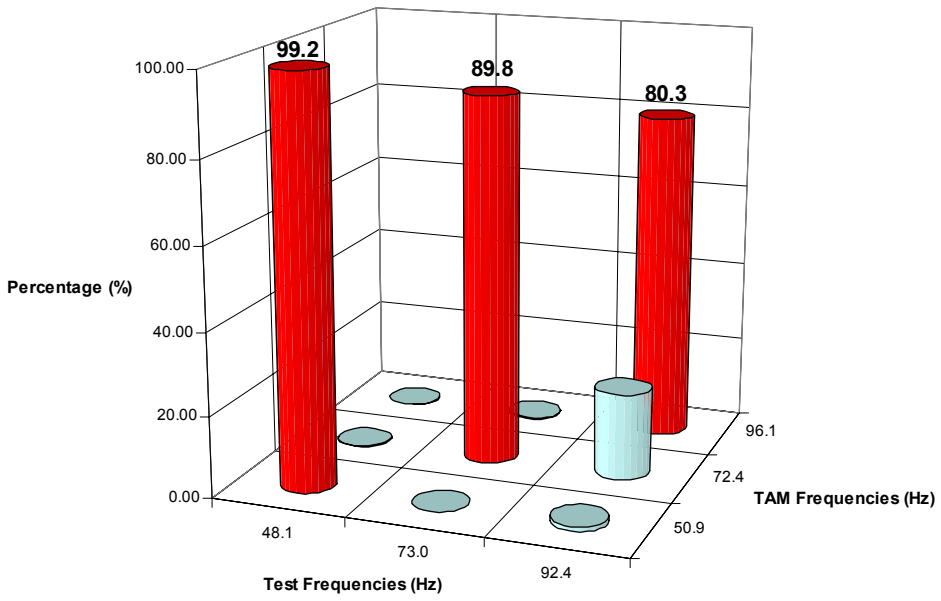

Comparison of CIR Experiment Assembly FEM with Test

MODE SHAPE DESCRIPTION	FEM FREQ (Hz)	TEST FREQ (Hz)	% FREQ DIFF
Translation of the Chamber in the X-axis	50.6	48.1	5.1
Translation of the Chamber in the Y-axis	71.4	73.0	2.2

Comparison of CIR Experiment Assembly FEM with Test

Mode Shapes - X Axis

Cross-Orthogonality 99.2%

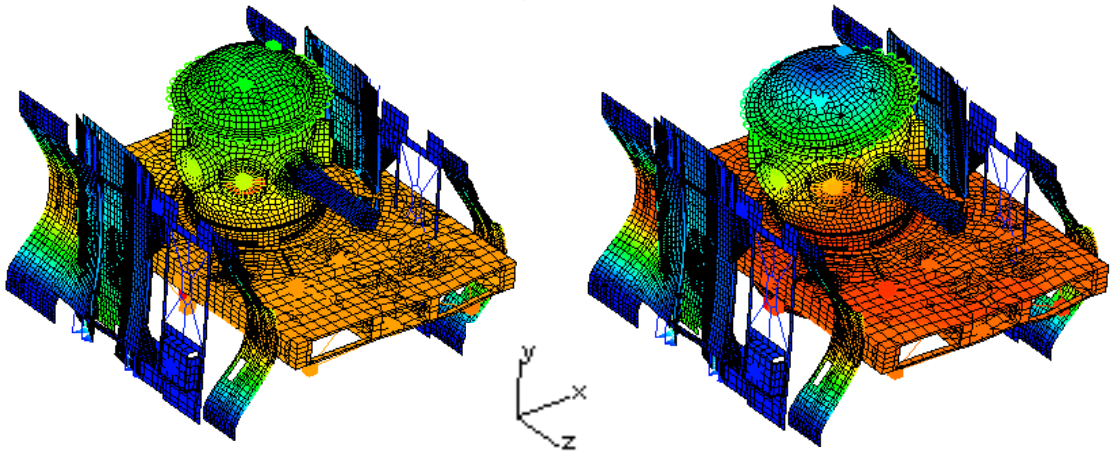

FEM
Mode 1, 50.6 Hz
86.3% Effective Mass

TEST
48.1 Hz
Damping = 3.55, MCF = 0.910

Translation of the Chamber in the X-axis

Comparison of CIR Experiment Assembly FEM with Test

Mode Shapes - Y Axis

Cross-Orthogonality 89.8%

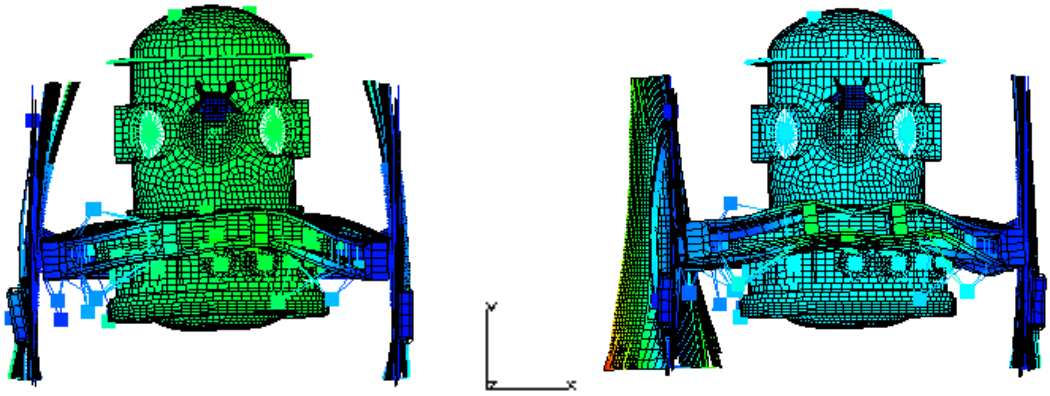

FEM Mode 8, 71.4 Hz 60.4% Effective Mass	TEST 73.0 Hz Damping = 4.0, MCF = 0.903

Translation of the Chamber in the Y-axis

Appendix B

CIR Air Thermal Control Unit (ATCU)
Final Revised Design
Model Correlation

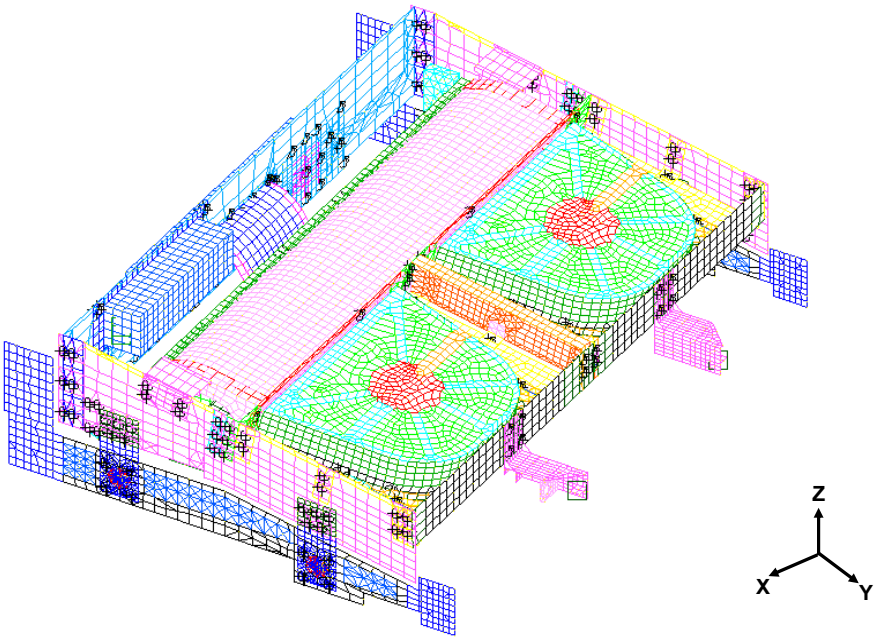

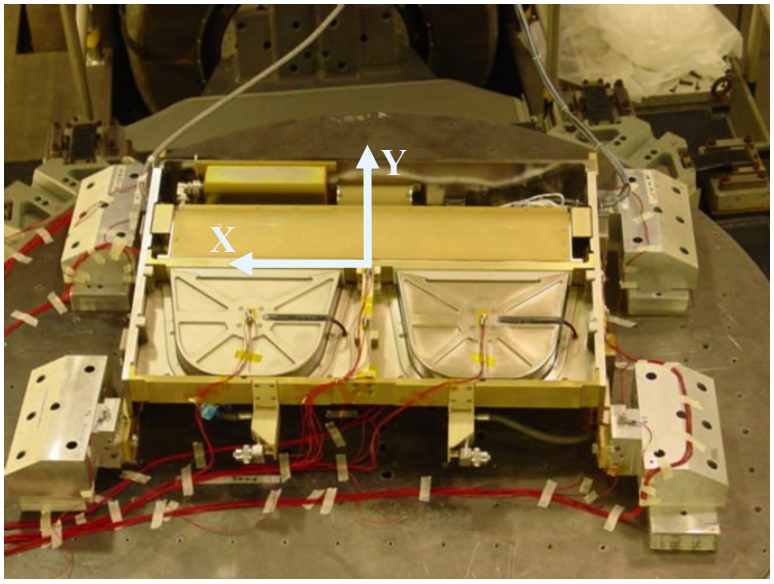

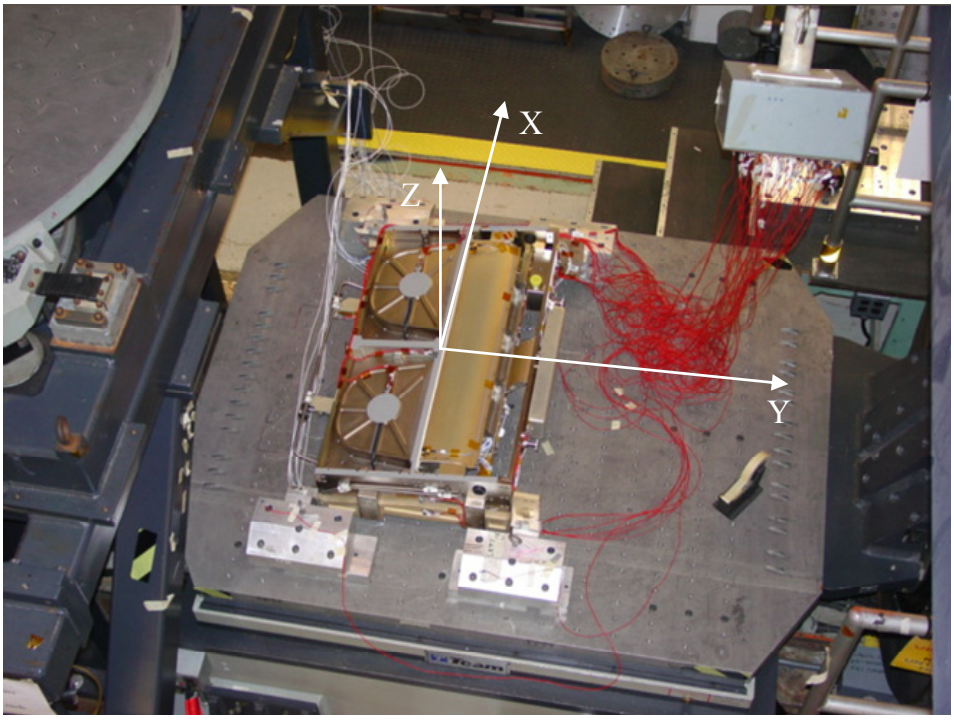

ATCU Test Configuration

CIR ATCU Final Design
Comparison of FEM to TAM

FEM (150,072 DoF)			TAM (52 DoF)		
Mode	Frequency (Hz)	Effective Mass (%)	Mode	Frequency (Hz)	Effective Mass (%)
1	**67.4**	**94.6 - X**	**1**	**67.8**	**96.9 - X**
2	**75.9**	**29.9 - Z**	**2**	**77.3**	**32.1 - Z**
3	88.4		3	88.8	
4	92.6	20.1 - Z	4	95.9	25.0 - Z
5	118.0		**5**	**121.0**	**83.8 - Y**
6	**119.0**	**55.5 - Y**			

BOLD INDICATES TARGET MODES

Comparison of CIR ATCU
FEM with TAM

MODE SHAPE DESCRIPTION	FEM FREQ (Hz)	TAM FREQ (Hz)	XORTHO %	% FREQ DIFF
Translation of the ATCU in the X-axis	67.4	67.8	98.9	0.6
Translation of the ATCU in the Z-axis	75.9	77.3	96.2	1.7
Translation of the ATCU in the Y-axis	119.0	121.0	93.1	1.6

CIR ATCU Final Revised Design
Cross Orthogonality
FEM vs TAM

						TAM MODE					
	Mode Number		1	2	3	4	5	6	7	8	9	10
		Hz	67.8	77.3	88.8	95.9	121.0	133.5	137.3	172.6	176.9	194.8
	1	67.4	98.9	0.0	0.0	0.0	0.0	0.0	0.0	0.0	0.0	0.0
	2	75.9	0.0	96.2	0.0	0.0	0.0	0.0	0.0	0.0	0.0	0.0
	3	88.4	0.0	0.0	99.0	0.0	0.0	0.0	0.0	0.0	0.0	0.0
FEM	4	92.6	0.0	12.8	0.0	92.3	0.0	0.0	0.0	0.0	0.0	0.0
MODE	5	118.0	0.0	0.0	0.0	15.7	25.5	44.6	53.6	0.0	0.0	0.0
	6	119.0	0.0	0.0	0.0	0.0	93.1	12.2	15.5	0.0	0.0	0.0
	7	124.4	0.0	0.0	0.0	0.0	0.0	67.1	48.6	0.0	0.0	0.0
	8	148.8	0.0	0.0	0.0	0.0	0.0	0.0	0.0	0.0	0.0	0.0
	9	148.9	0.0	0.0	0.0	0.0	0.0	0.0	0.0	0.0	0.0	0.0
	10	151.4	0.0	0.0	0.0	0.0	0.0	0.0	0.0	0.0	0.0	0.0
	11	151.5	0.0	0.0	0.0	0.0	0.0	12.7	0.0	0.0	0.0	0.0

CIR ATCU Final Revised Design
Cross Orthogonality Graph
FEM vs TAM

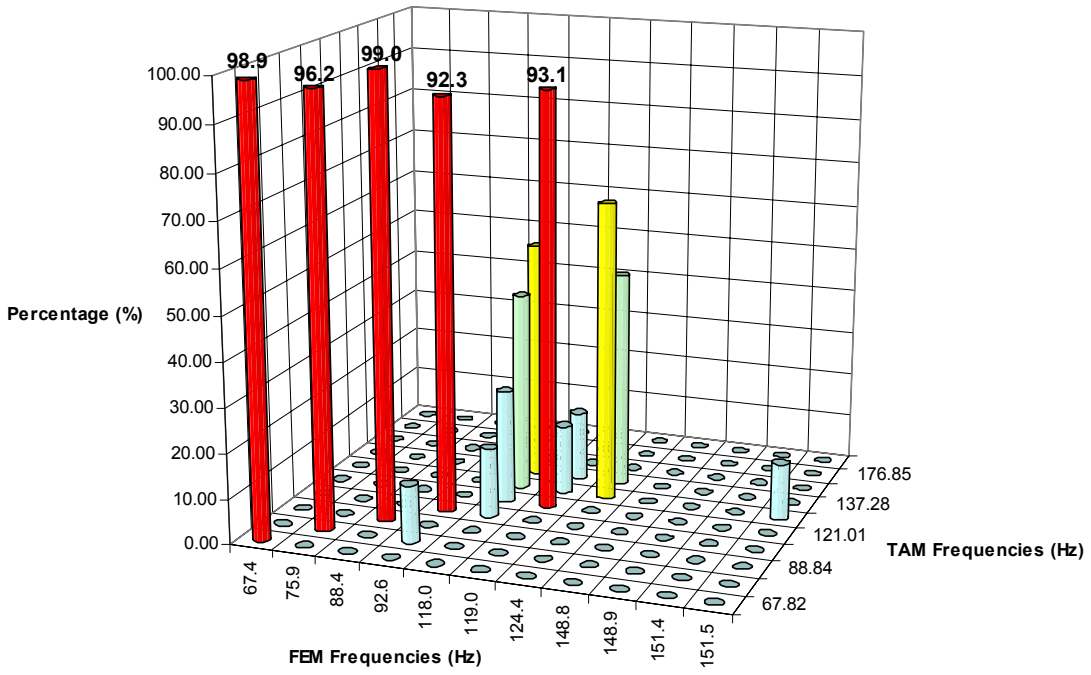

Comparison of CIR ATCU TAM with TEST

MODE SHAPE DESCRIPTION	TAM FREQ (Hz)	TEST FREQ (Hz)	XORTHO %	% FREQ DIFF
Translation of the ATCU in the X-axis	67.8	67.7	99.8	0.1
Translation of the ATCU in the Z-axis	77.3	72.3	96.9	6.4
Translation of the ATCU in the Y-axis	121.0	120.2	97.1	0.6

CIR ATCU Cross Orthogonality TAM vs TEST

			TEST MODE		
	Mode Number		1	2	3
		Freq (Hz)	**67.7**	**72.3**	**120.2**
TAM	1	**67.8**	**99.8**	6.0	1.7
MODE	2	**77.3**	1.3	**96.9**	3.1
	5	**121.0**	1.2	9.0	**97.1**

CIR ATCU Final Revised Design Cross Orthogonality Graph TAM vs TEST

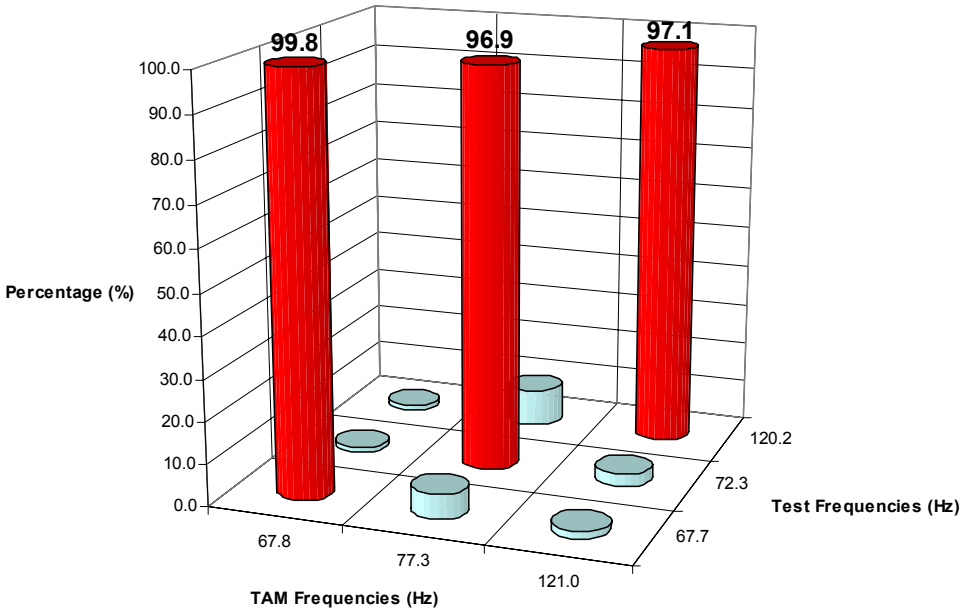

Comparison of CIR ATCU FEM with Test

MODE SHAPE DESCRIPTION	FEM FREQ (Hz)	TEST FREQ (Hz)	% FREQ DIFF
Translation of the ATCU in the X-axis	67.4	67.7	0.4
Translation of the ATCU in the Z-axis	75.9	72.3	4.7
Translation of the ATCU in the Y-axis	119.0	120.2	1.0

Comparison of CIR ATCU FEM with Test
Mode Shapes - X Axis
Cross-Orthogonality 99.8%

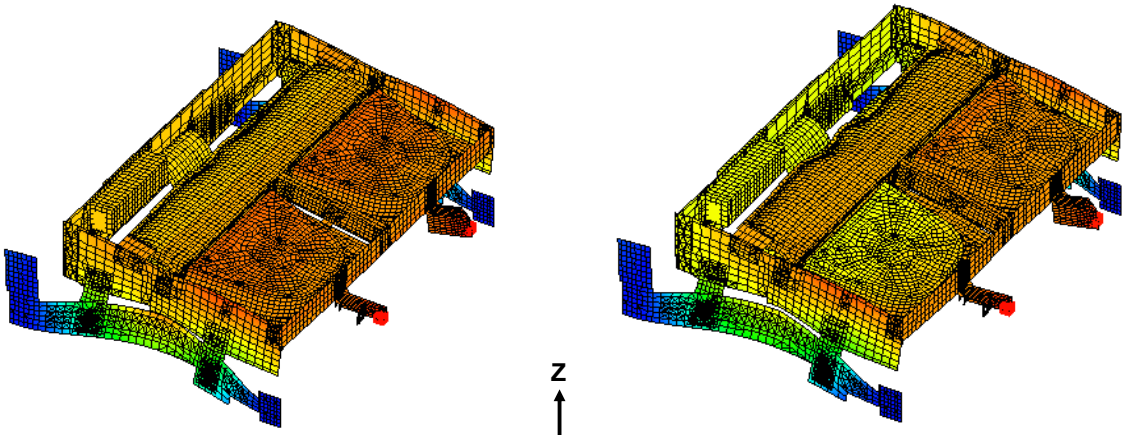

FEM
Mode 1, 67.4 Hz
94.6% Effective Mass

TEST
67.7 Hz
Damping = 0.71, MCF = 1.000

Translation of the ATCU in the X-Axis

Comparison of CIR ATCU FEM with Test

Mode Shapes - Z Axis

Cross-Orthogonality 96.9%

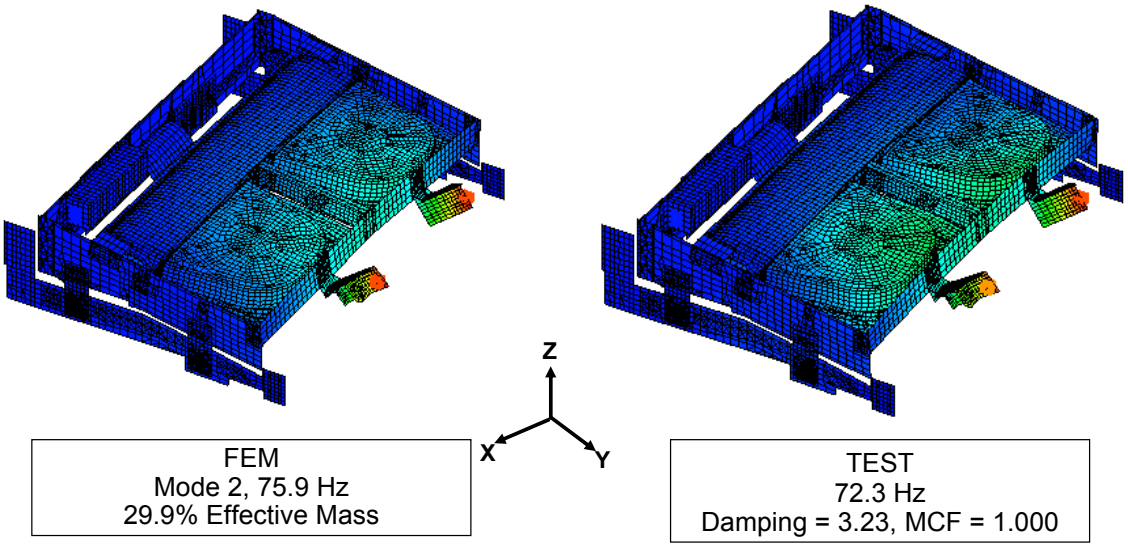

Translation of the ATCU in the Z-Axis

Comparison of CIR ATCU FEM with Test

Mode Shapes - Y Axis

Cross-Orthogonality 97.1%

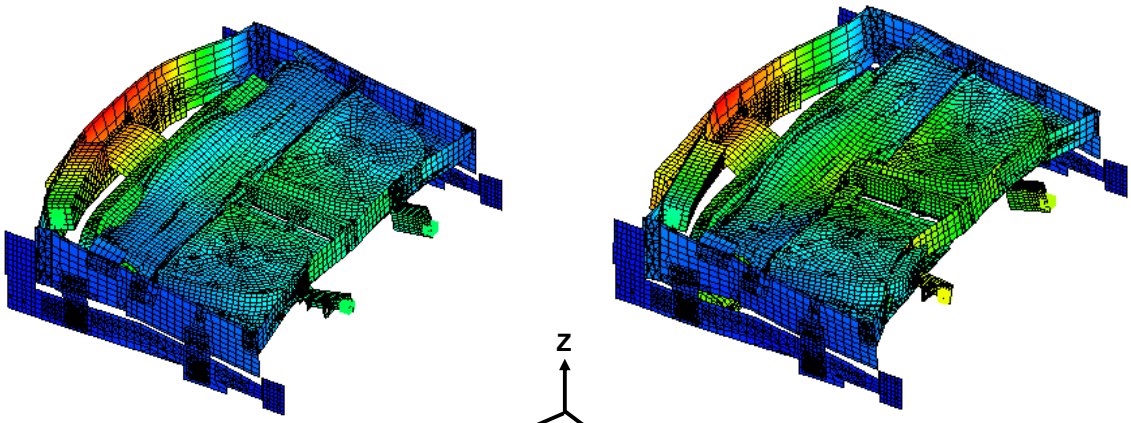

FEM
Mode 6, 119.0 Hz
55.5% Effective Mass

TEST
120.2 Hz
Damping = 1.38, MCF = 1.000

Translation of the ATCU in the Y-Axis

Appendix C

CIR Rack Door
Model Correlation

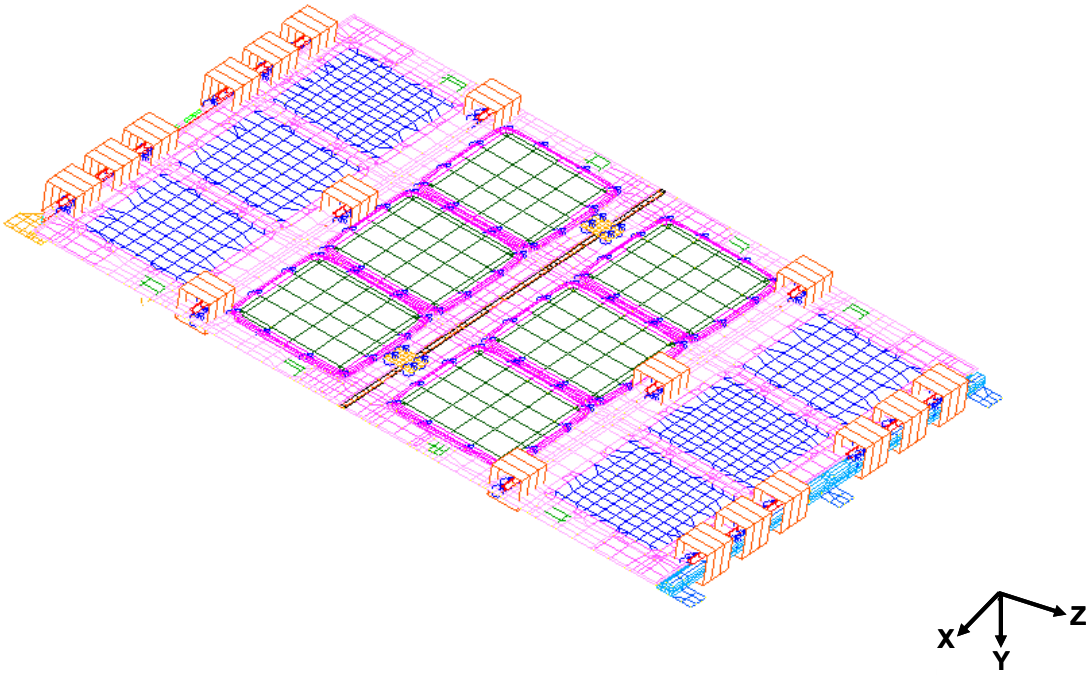

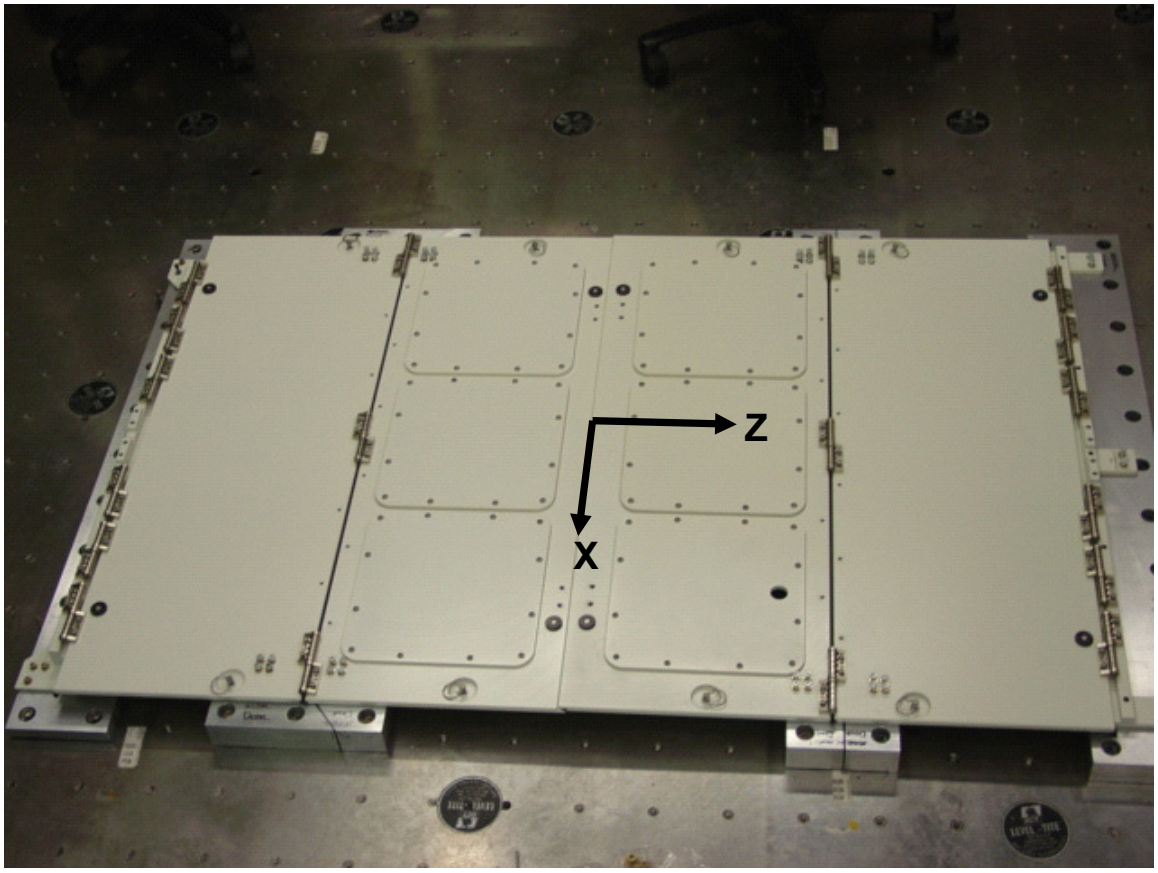

Rack Door Test Configuration

CIR Rack Door
Comparison of FEM to TAM

FEM (33,396 Grid Pts)			TAM (39 DoF)		
Mode	Frequency (Hz)	Effect Mass (%)	Mode	Frequency (Hz)	Effect Mass (%)
1	**57.9**	**33.3-Y**	**1**	**58.2**	**57.3-Y**
2	**90.1**	**1.6-Y**	**2**	**91.5**	
3	**99.7**	**12.3-Y**	**3**	**101.6**	**17.1-Y**
4	112.1		4	113.9	

BOLD INDICATES TARGET MODES

Comparison of CIR Rack Door
FEM with TAM

MODE SHAPE DESCRIPTION	FEM FREQ (Hz)	TAM FREQ (Hz)	XORTHO %	% FREQ DIFF
Y-axis First Bending Mode of the Doors	57.9	58.2	99.0	0.5
Y-axis Second Bending Mode of the Doors	90.1	91.5	96.8	1.6
Y-axis Third Bending Mode of the Doors	99.7	101.6	96.1	1.9

CIR Rack Door
Cross Orthogonality
FEM vs TAM

			TAM MODE									
	Mode Number		1	2	3	4	5	6	7	8	9	10
		Hz	58.2	91.5	101.6	113.9	163.3	176.0	203.3	223.7	230.3	247.3
	1	57.9	99.0	0.0	0.0	0.0	0.0	0.0	0.0	0.0	0.0	0.0
FEM	2	90.1	0.0	96.8	0.0	0.0	0.0	0.0	0.0	0.0	0.0	0.0
MODE	3	99.7	0.0	0.0	96.1	0.0	0.0	0.0	0.0	0.0	0.0	0.0
	4	112.1	0.0	0.0	0.0	96.9	0.0	0.0	0.0	0.0	0.0	0.0

CIR Rack Door
Cross Orthogonality Graph
FEM vs TAM

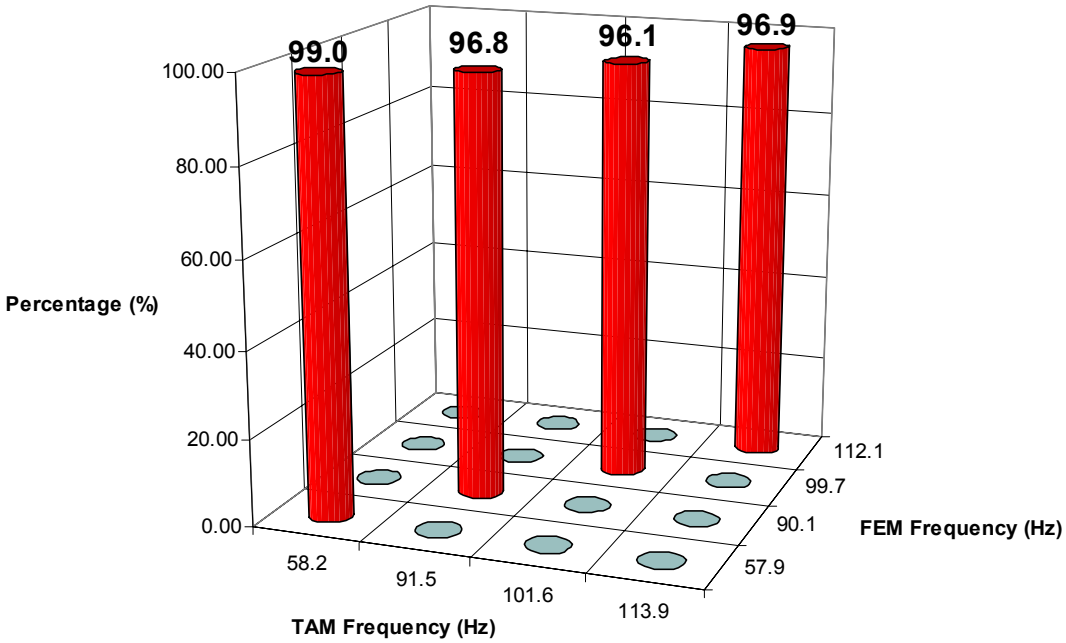

Comparison of CIR Rack Door TAM with Test

MODE SHAPE DESCRIPTION	TAM FREQ (Hz)	TEST FREQ (Hz)	XORTHO %	% FREQ DIFF
Y-axis First Bending Mode of the Doors	58.2	55.2	99.8	5.2
Y-axis Second Bending Mode of the Doors	91.5	81.4	97.0	11.1
Y-axis Third Bending Mode of the Doors	101.6	90.7	96.4	10.8

CIR Rack Door Cross Orthogonality TAM vs TEST

			TEST MODE		
	Mode Number		1	2	3
TAM		Freq (Hz)	55.2	81.4	90.7
MODE	1	58.2	99.8	1.7	17.5
	2	91.5	0.4	97.0	13.7
	3	101.6	4.9	19.7	96.4

CIR Rack Door Cross Orthogonality Graph TAM vs TEST

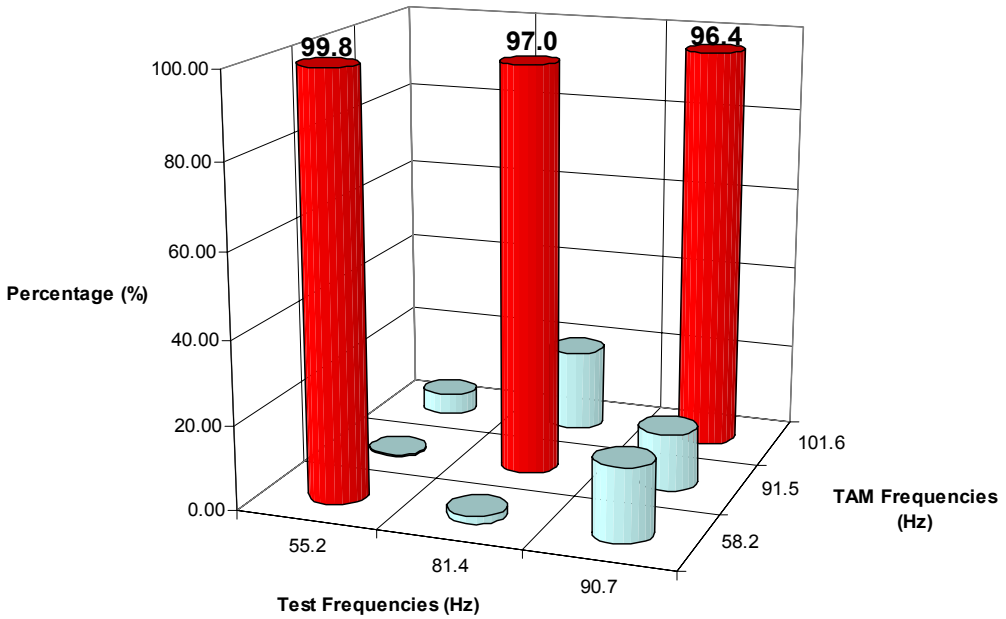

Comparison of CIR Rack Door FEM with Test

MODE SHAPE DESCRIPTION	FEM FREQ (Hz)	TEST FREQ (Hz)	% FREQ DIFF
Y-axis First Bending Mode of the Doors	57.9	55.2	4.9
Y-axis Second Bending Mode of the Doors	90.1	81.4	10.7
Y-axis Third Bending Mode of the Doors	99.7	90.7	9.9

Comparison of CIR Rack Door FEM with Test

Mode Shapes - Y Axis

Cross-Orthogonality 99.8%

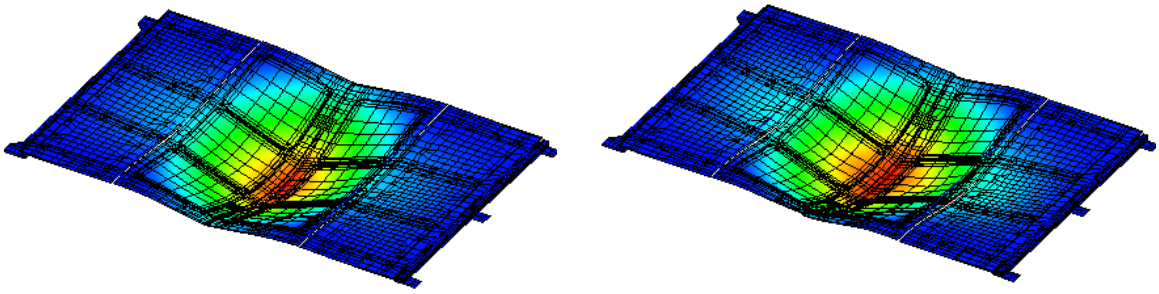

FEM
Mode 1, 57.9 Hz
33.3 % Effective Mass

TEST
55.2 Hz
Damping = 0.636 , MCF = 1.000

Y-axis First Bending Mode of the Doors

Comparison of CIR Rack Door FEM with Test

Mode Shapes - Y Axis

Cross-Orthogonality 97.0%

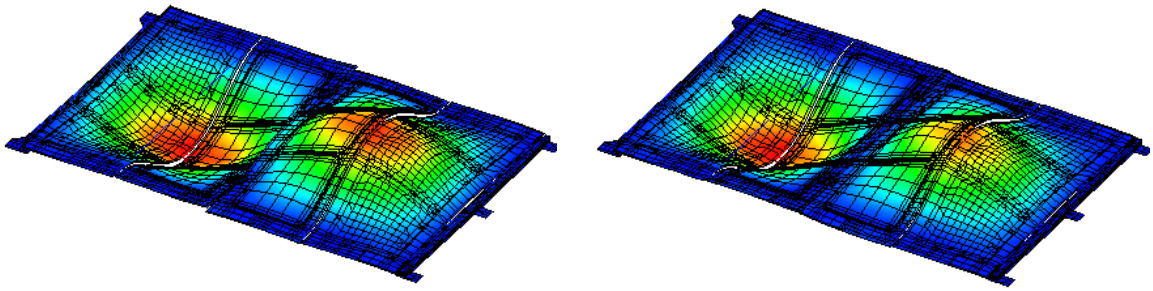

FEM	TEST
Mode 2, 90.1 Hz 1.6 % Effective Mass	81.4 Hz Damping = 1.666 , MCF = 0.997

Y-axis Second Bending Mode of the Doors

Comparison of CIR Rack Door FEM with Test
Mode Shapes - Y Axis
Cross-Orthogonality 96.4%

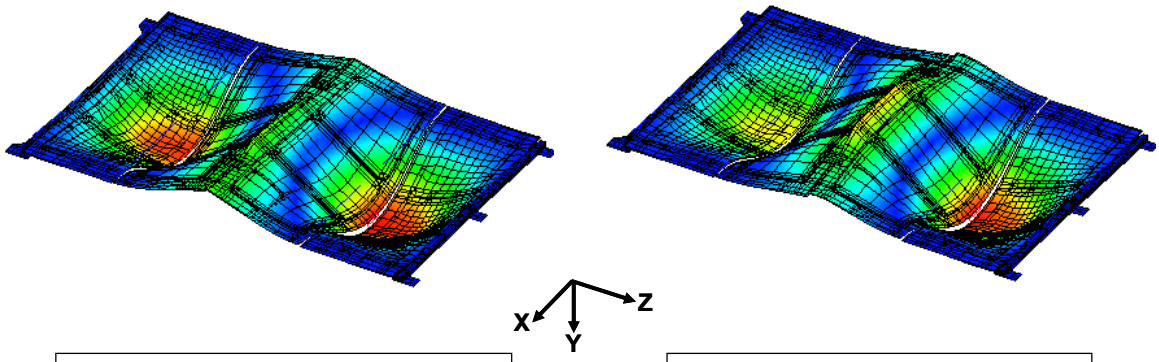

FEM	TEST
Mode 3, 99.7 Hz 12.3 % Effective Mass	90.7 Hz Damping = 1.384, MCF = 0.999

Y-axis Third Bending Mode of the Doors

Appendix D

CIR Lower Structure Assembly Model Correlation

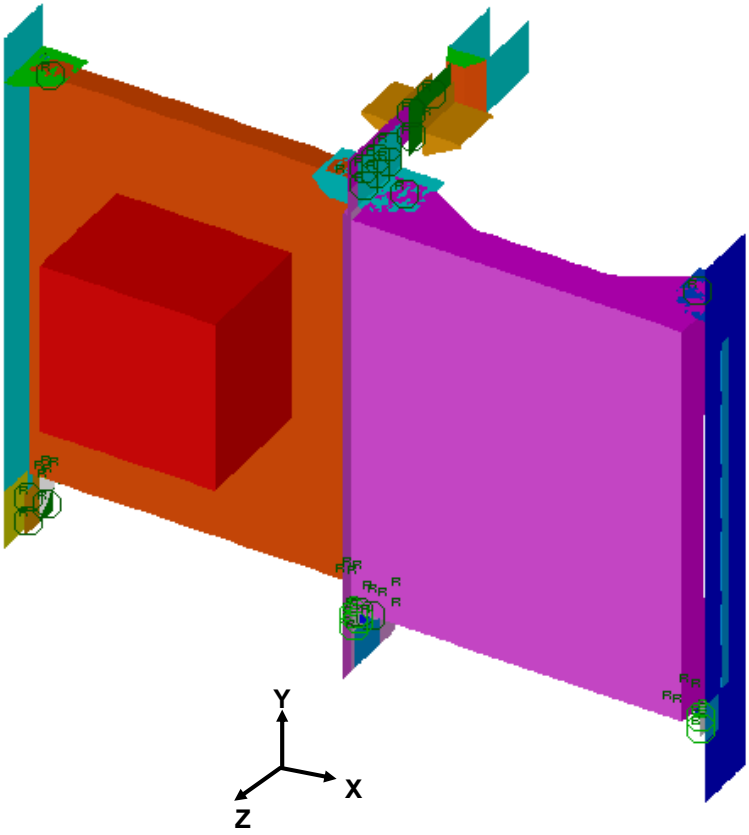

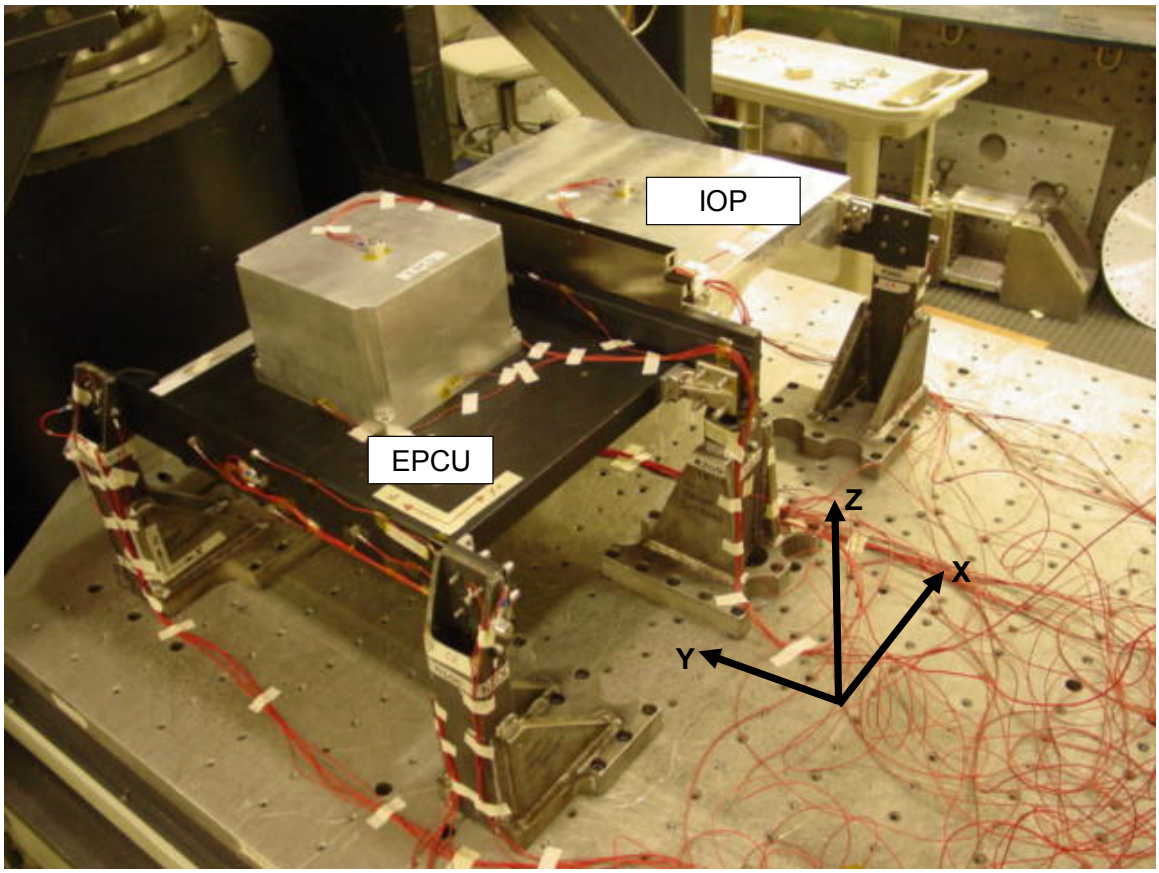

Lower Structure Assembly Test Configuration

CIR Lower Structure Assembly
Comparison of FEM to TAM

FEM (100,944 DoF)			TAM (38 DoF)		
Mode	Frequency (Hz)	Effect Mass (%)	Mode	Frequency (Hz)	Effect Mass (%)
1	**105.7**	**25.8-X**	**1**	**106.4**	**29.5-X**
2	**125.2**	**44.5-Z**	**2**	**127.3**	**55.7-Z**
3	143.9	21.4-X	3	145.7	25.5-X
4	173.8		4	176.7	
5	**175.2**	**60.2-Y**	**5**	**177.9**	**56.3-Y**

BOLD INDICATES TARGET MODES

Comparison of CIR Lower Structure FEM with TAM

MODE SHAPE DESCRIPTION	FEM FREQ (Hz)	TAM FREQ (Hz)	XORTHO %	% FREQ DIFF
Translation of the Lower Structure in the X-Axis	105.7	106.4	98.7	0.6
Translation of the EPCU in the Z-Axis	125.2	127.3	96.7	1.7
Translation of the Lower Structure in the Y-Axis	175.2	177.9	96.1	1.6

CIR Lower Structure Assembly
Cross Orthogonality
FEM vs TAM

			TAM MODE										
	Mode Number		1	2	3	4	5	6	7	8	9	10	11
		Hz	106.4	127.3	145.7	176.5	177.9	192.4	202.4	219.0	229.7	331.5	350.2
	1	105.7	98.7	0.0	0.0	0.0	0.0	0.0	0.0	0.0	0.0	0.0	0.0
	2	125.2	0.0	96.7	0.0	0.0	0.0	0.0	0.0	0.0	0.0	0.0	0.0
	3	143.9	0.0	0.0	97.4	0.0	0.0	0.0	0.0	0.0	0.0	0.0	0.0
FEM	4	173.8	0.0	0.0	0.0	96.1	11.0	0.0	0.0	0.0	0.0	0.0	0.0
MODE	5	175.2	0.0	0.0	0.0	11.3	96.1	0.0	0.0	0.0	0.0	0.0	0.0
	6	189.1	0.0	0.0	0.0	0.0	0.0	96.3	0.0	0.0	0.0	0.0	0.0
	7	198.5	0.0	0.0	0.0	0.0	0.0	0.0	96.0	0.0	0.0	0.0	0.0
	8	212.2	0.0	0.0	0.0	0.0	0.0	0.0	0.0	93.2	0.0	0.0	0.0
	9	224.8	0.0	0.0	0.0	0.0	0.0	0.0	0.0	0.0	95.4	0.0	0.0
	10	290.4	0.0	0.0	0.0	0.0	0.0	0.0	0.0	0.0	0.0	67.7	30.1
	11	311.4	0.0	0.0	0.0	0.0	0.0	0.0	0.0	0.0	0.0	30.4	54.7

CIR Lower Structure Assembly
Cross Orthogonality Graph
FEM vs TAM

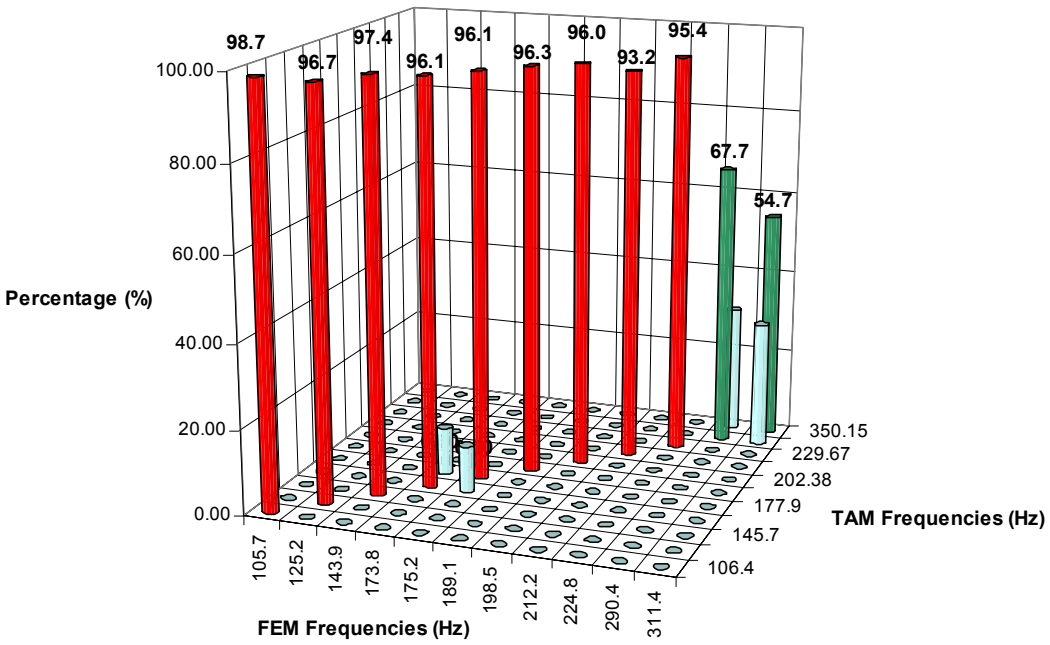

Comparison of CIR Lower Structure TAM with TEST

MODE SHAPE DESCRIPTION	TAM FREQ (Hz)	TEST FREQ (Hz)	XORTHO %	FREQ DIFF (%)
Translation of the Lower Structure in the X-Axis	106.4	112.5	54.9	5.4
Translation of the EPCU in the Z-Axis	127.3	138.5	39.9	8.1
Translation of the Lower Structure in the Y-Axis	177.9	169.5	29.9	5.0

CIR Lower Structure Assembly Cross Orthogonality TAM vs TEST

			TEST MODE		
			1	2	4
		Freq (Hz)	112.5	138.5	169.5
TAM	1	106.4	54.9	44.9	14.9
MODE	2	127.3	0.0	39.9	15.9
	5	177.9	0.3	52.2	25.9

CIR Lower Structure Assembly Cross Orthogonality Graph TAM vs TEST

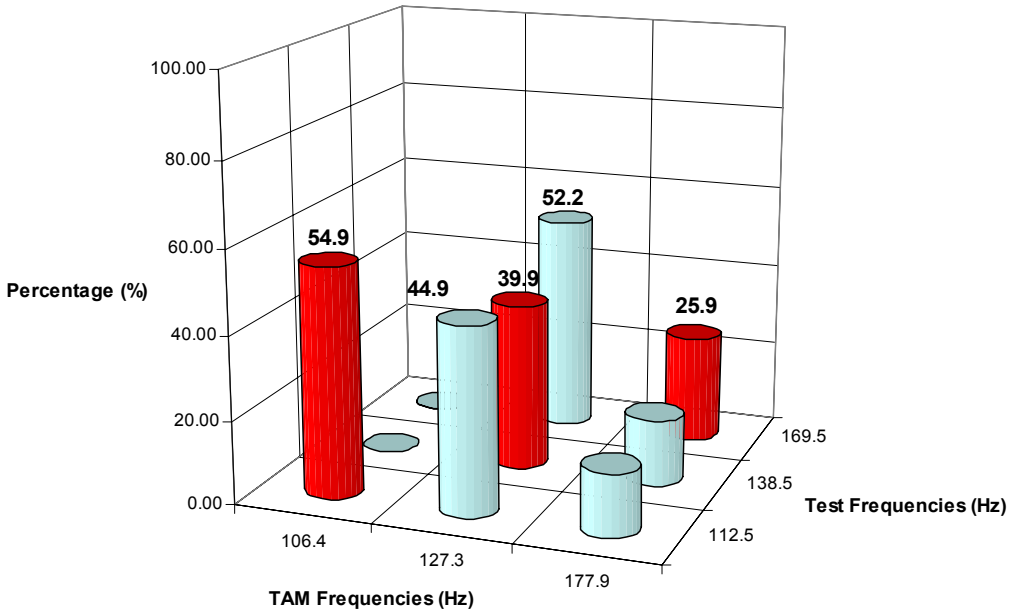

Comparison of CIR Lower Structure FEM with TEST

MODE SHAPE DESCRIPTION	FEM FREQ (Hz)	TEST FREQ (Hz)	FREQ DIFF (%)
Translation of the Lower Structure in the X-Axis	105.7	112.5	6.1
Translation of the EPCU in the Z-Axis	125.2	138.5	9.6
Translation of the Lower Structure in the Y-Axis	175.2	169.5	3.3

Comparison of CIR Lower Structure Assembly FEM with Test

Mode Shapes - X Axis

Cross-Orthogonality 54.9%

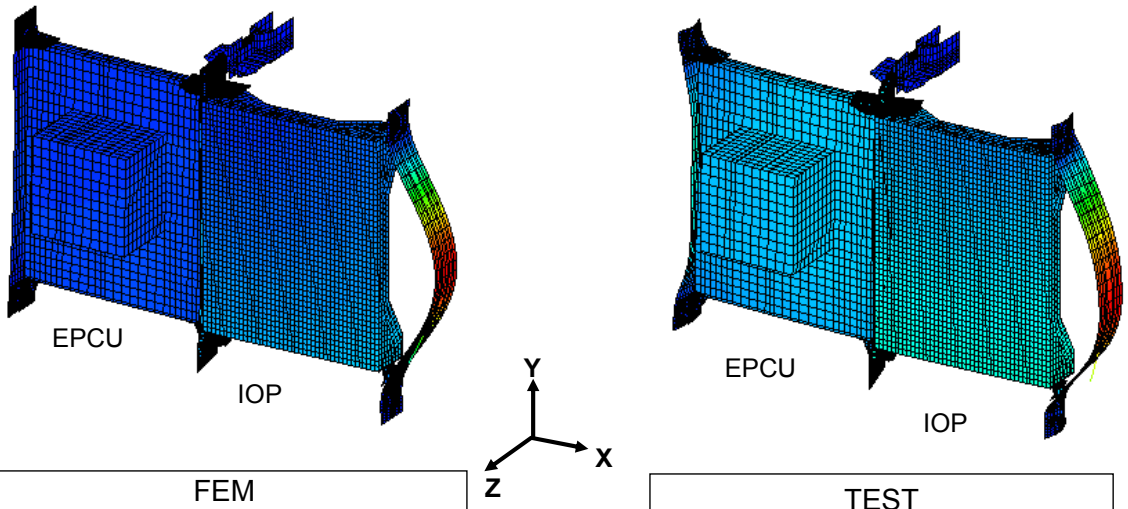

FEM
Mode 1, 105.7 Hz
25.8 % Effective Mass

TEST
112.5 Hz
Damping = 1.46 %, MCF = 1.00

Translation of the Lower Structure in the X-Axis

Comparison of CIR Lower Structure Assembly FEM with Test

Mode Shapes - Z Axis

Cross-Orthogonality 39.9%

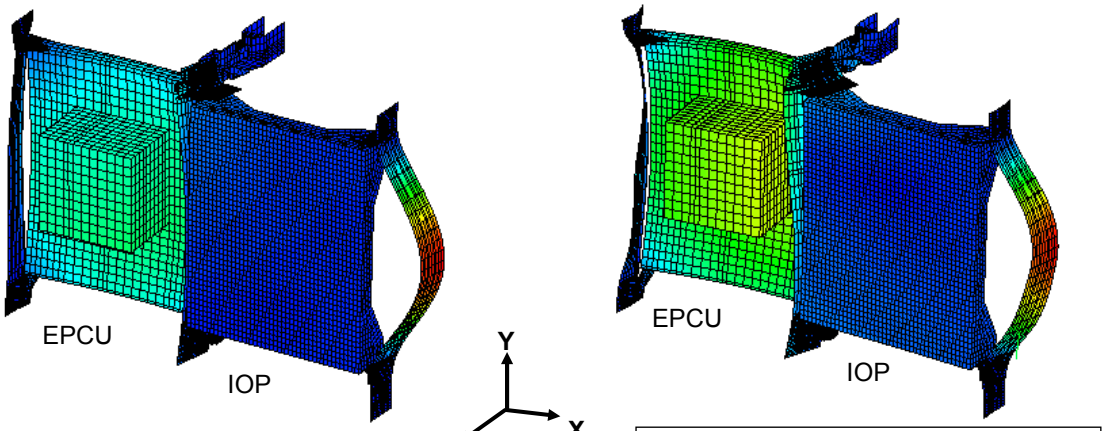

FEM
Mode 2, 125.2 Hz
44.5% Effective Mass

TEST
138.5 Hz
Damping = 0.95 , MCF = 1.00

Translation of the EPCU in the Z-Axis

Comparison of CIR Lower Structure Assembly FEM with Test

Mode Shapes - Y Axis

Cross-Orthogonality 25.9%

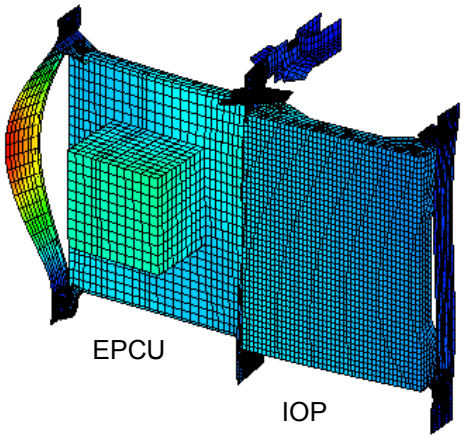

FEM
Mode 5, 175.2 Hz
60.2 % Effective Mass

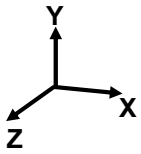

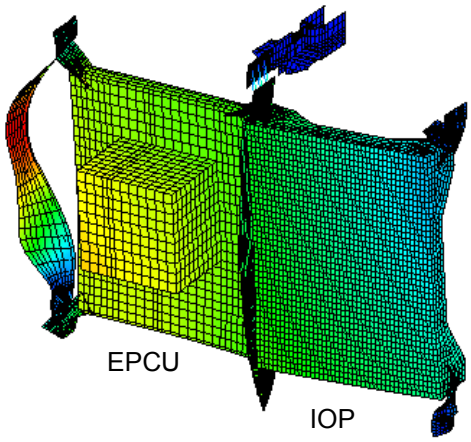

TEST
169.5 Hz
Damping =1.08 , MCF = 1.00

Translation of the Lower Structure in the Y-Axis

Appendix E

CIR Rack
Modal Instrumentation Plan

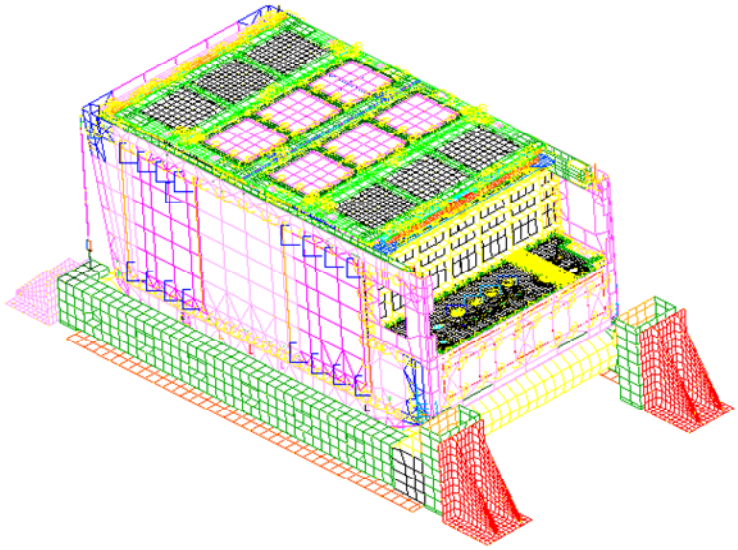

Modal Rack Instrumentation Plan
ISPR (8 locations, 16 accels)

Rack Front View
Rear Right Post Locations

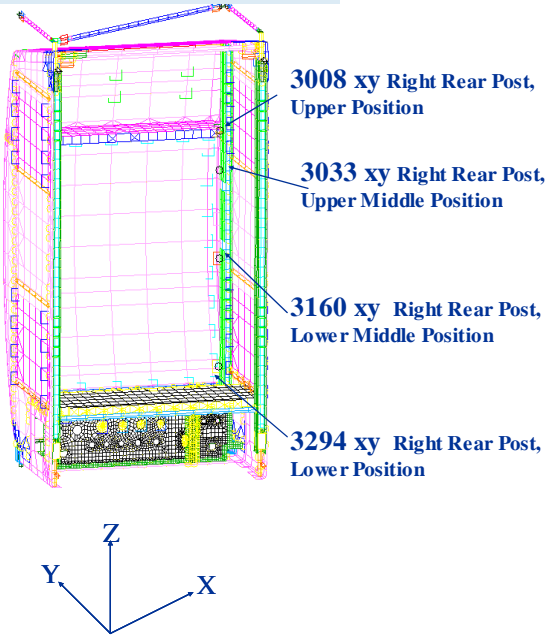

Rack Front View
Rear Left Post Locations

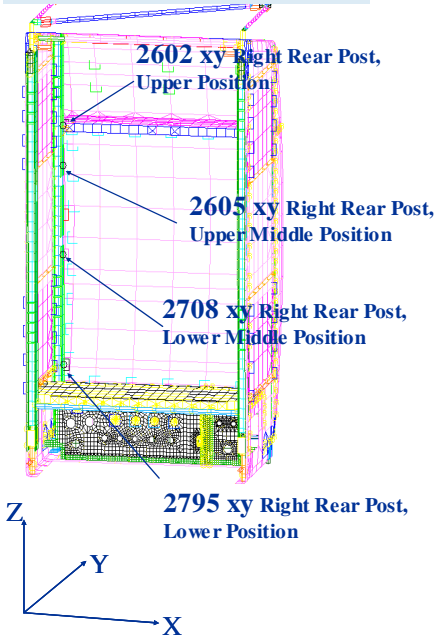

Modal Rack Instrumentation Plan
ISPR (5 locations, 5 accels)

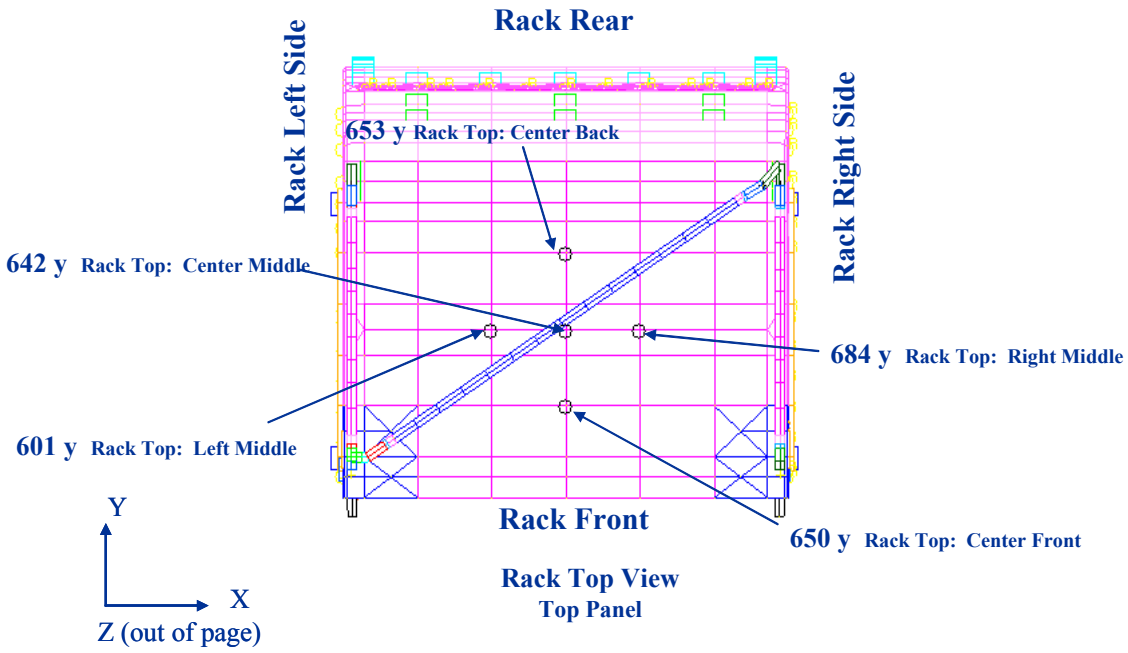

CIR Modal Rack Instrumentation Plan
Strut (5 locations, 12 accels)

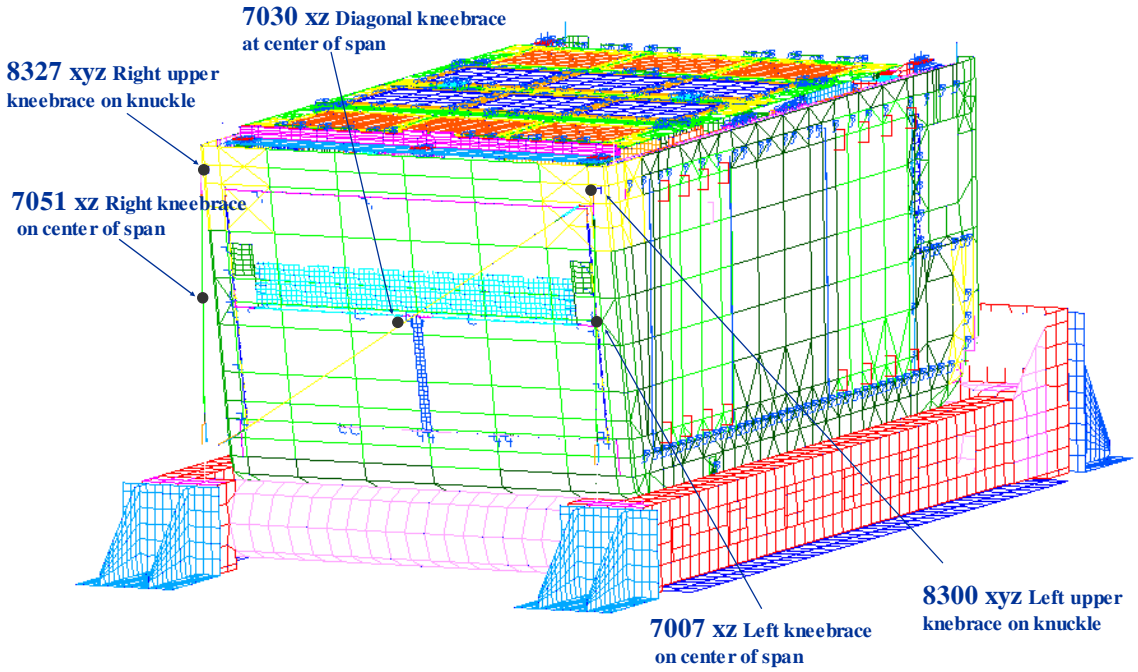

CIR Modal Rack Instrumentation Plan

Blue Boy Control Accelerometers (6 locations, 24 accels)

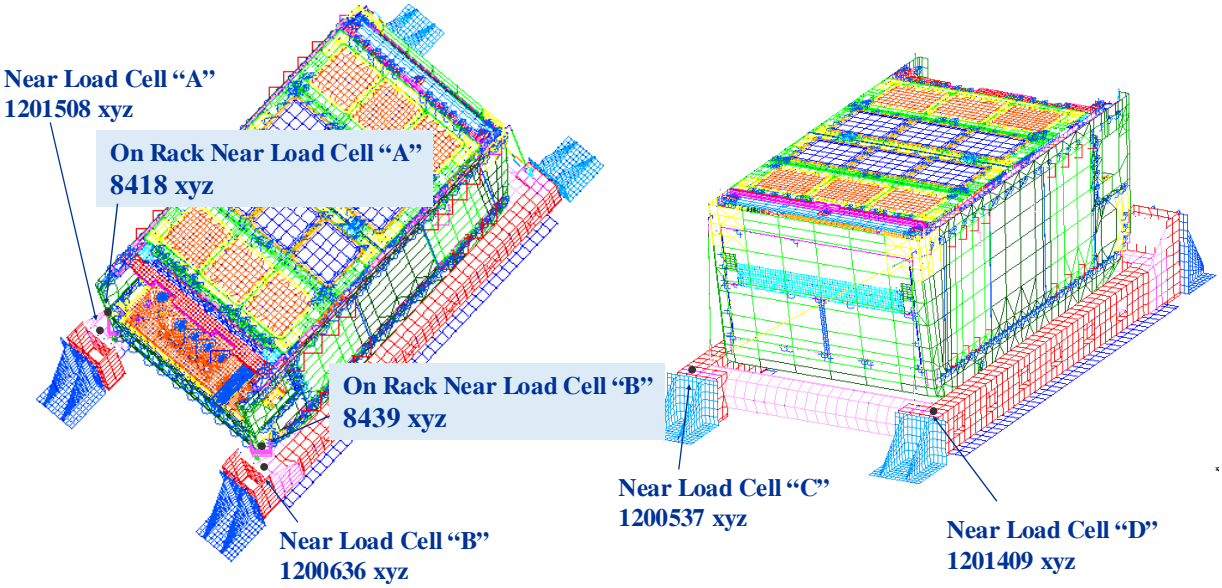

Modal Rack Instrumentation Plan
ATCU (2 locations, 2 accels)

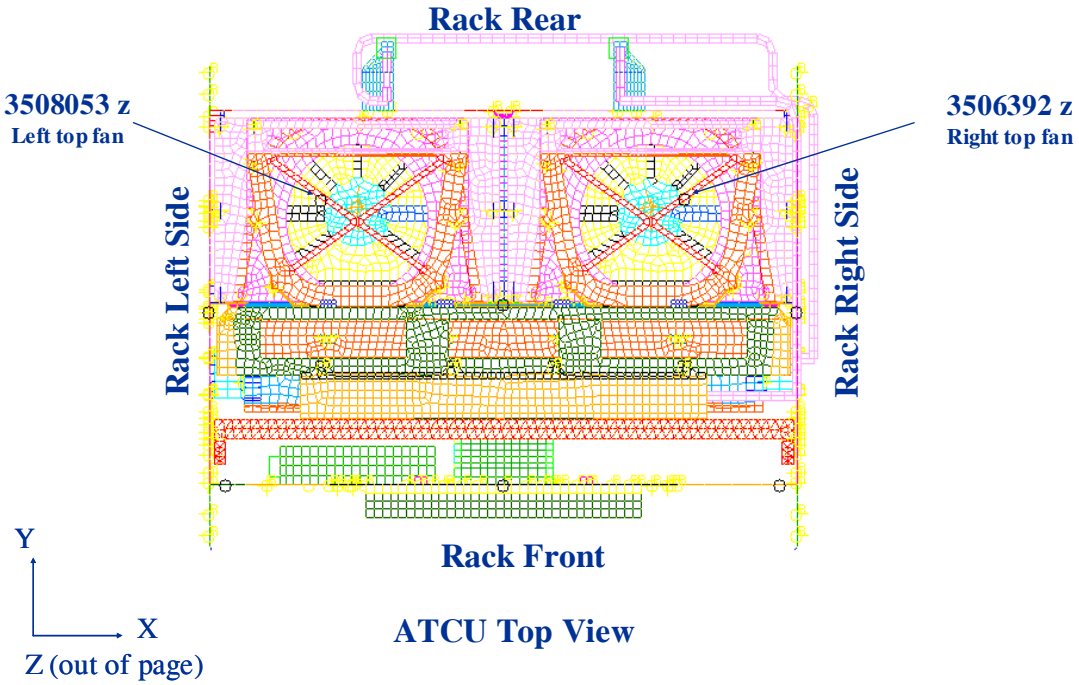

ATCU Top View

Modal Rack Instrumentation Plan
ATCU (4 locations, 4 accels)

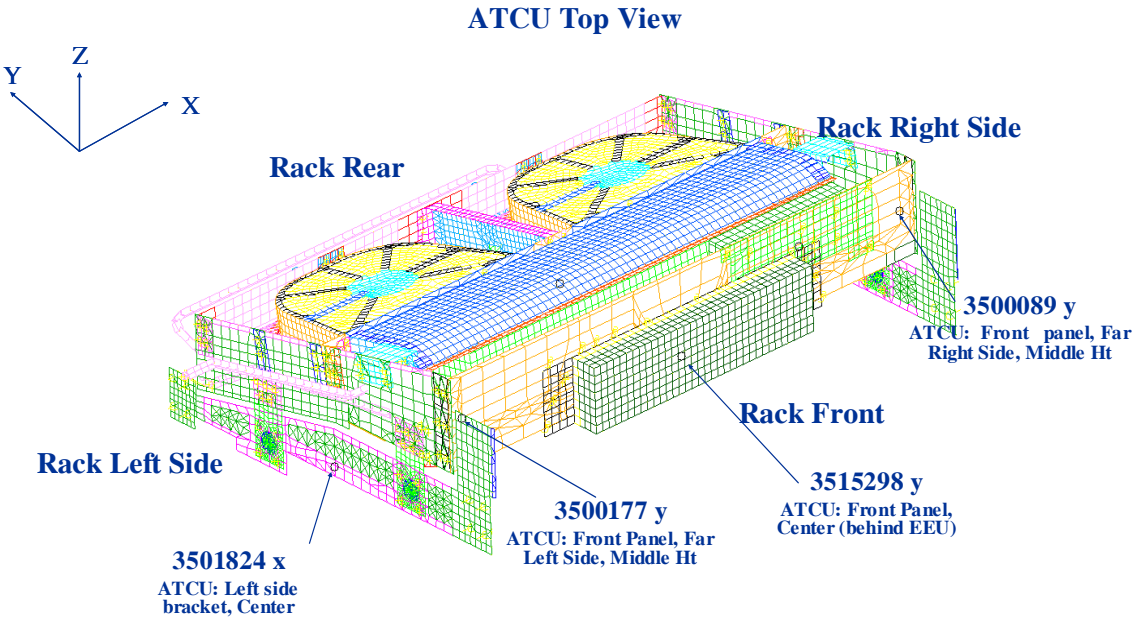

Modal Rack Instrumentation Plan
ATCU (4 locations, 4 accels)

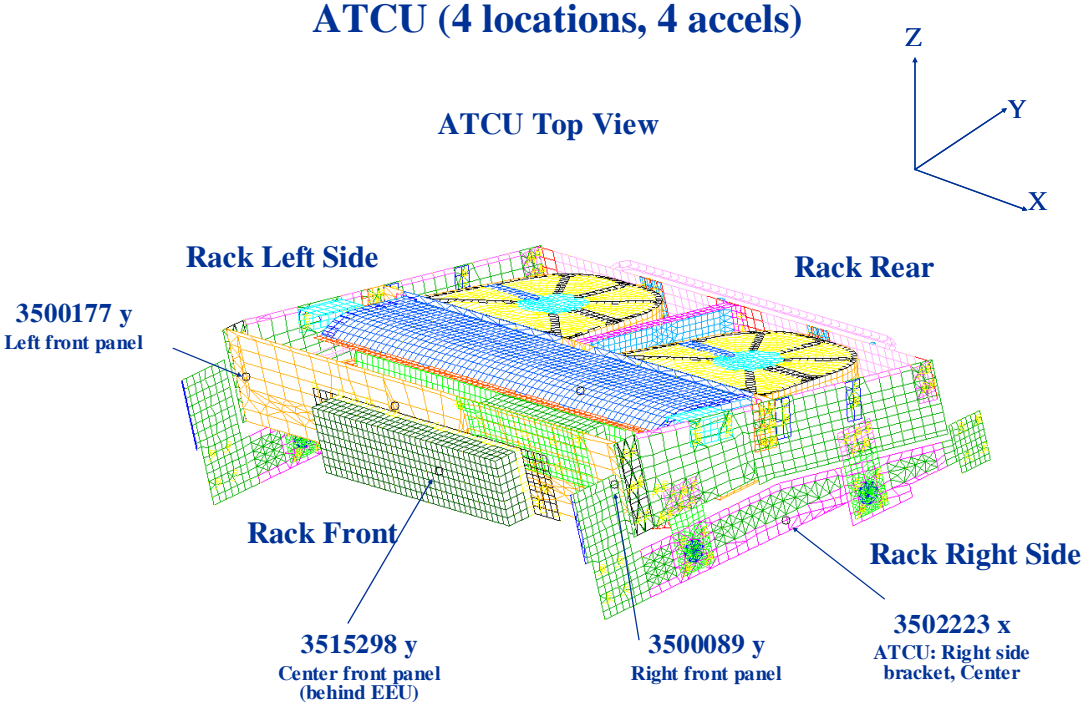

Modal Rack Instrumentation Plan
ATCU (2 locations, 4 accels)

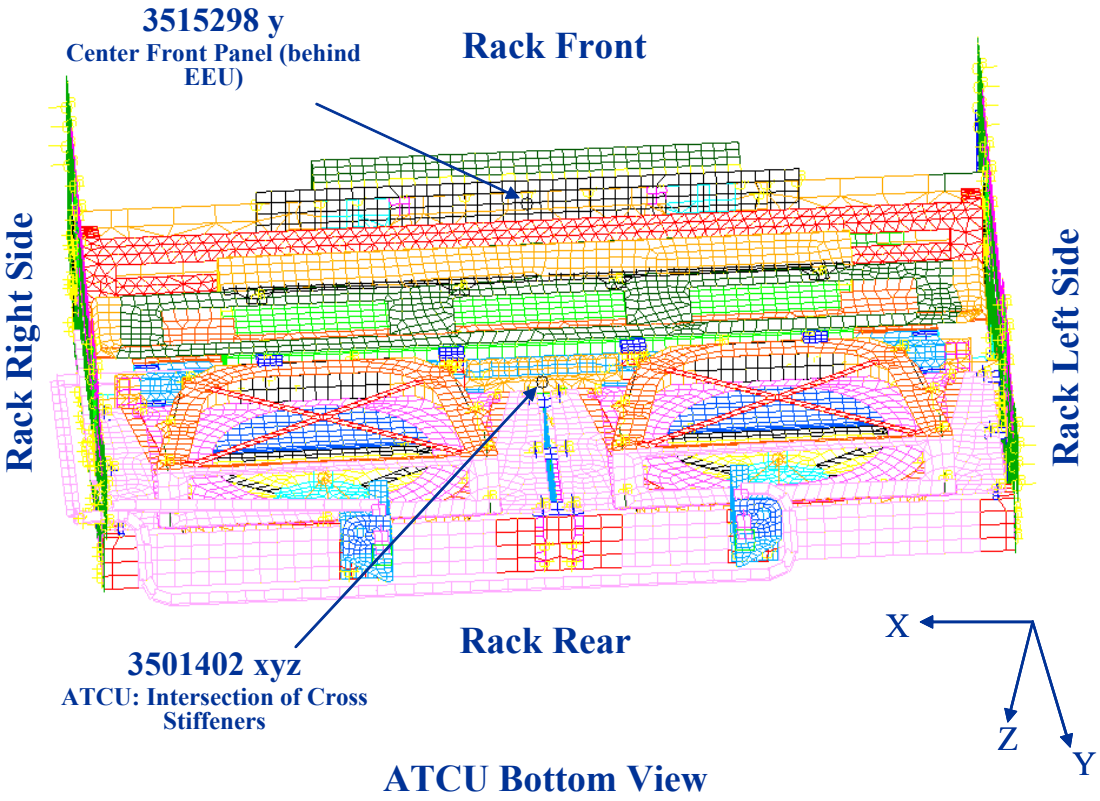

ATCU Bottom View

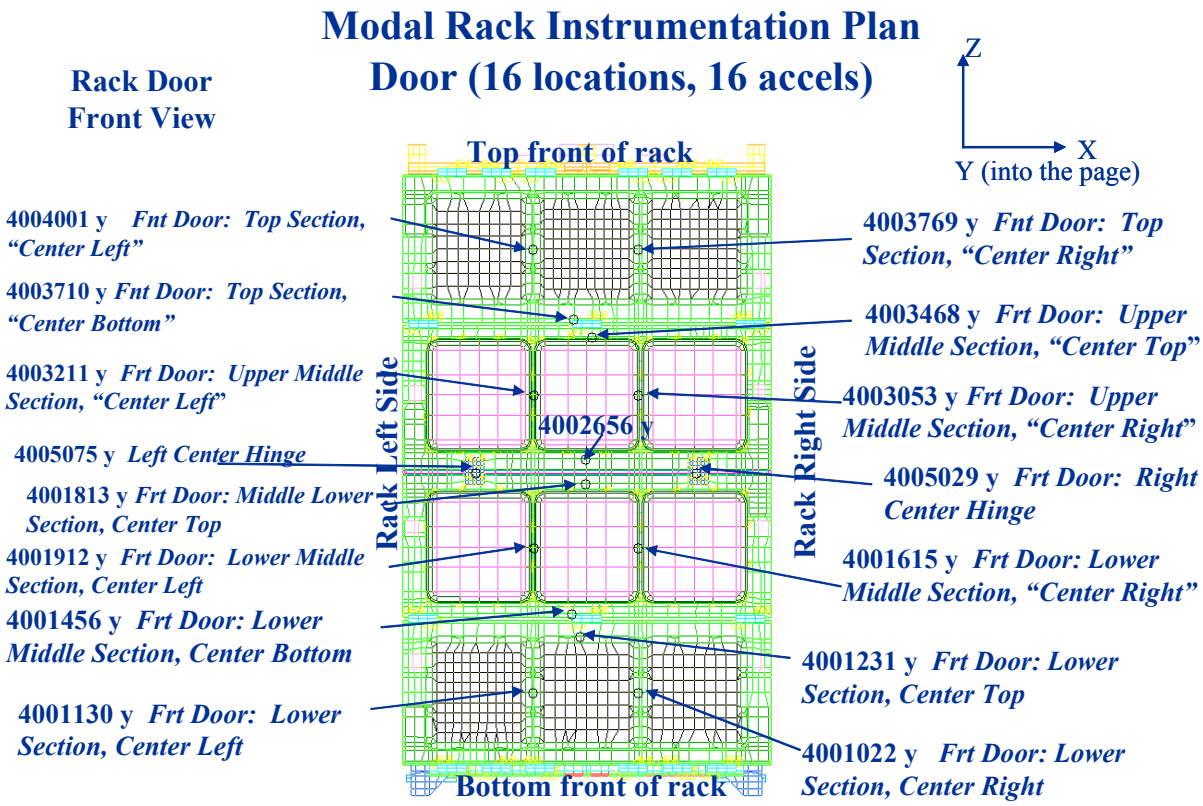
Modal Rack Instrumentation Plan
Door (16 locations, 16 accels)
Rack Door
Front View
Z
X
Y (into the page)
Top front of rack
4004001 y Fnt Door: Top Section, "Center Left"
4003710 y Fnt Door: Top Section, "Center Bottom"
4003211 y Frt Door: Upper Middle Section, "Center Left"
4005075 y Left Center Hinge
4001813 y Frt Door: Middle Lower Section, Center Top
4001912 y Frt Door: Lower Middle Section, Center Left
4001456 y Frt Door: Lower Middle Section, Center Bottom
4001130 y Frt Door: Lower Section, Center Left
Rack Left Side
4002656 y
Rack Right Side
4003769 y Fnt Door: Top Section, "Center Right"
4003468 y Frt Door: Upper Middle Section, "Center Top"
4003053 y Frt Door: Upper Middle Section, "Center Right"
4005029 y Frt Door: Right Center Hinge
4001615 y Frt Door: Lower Middle Section, "Center Right"
4001231 y Frt Door: Lower Section, Center Top
4001022 y Frt Door: Lower Section, Center Right
Bottom front of rack

Modal Rack Instrumentation Plan
Lower Structure Assembly (5 locations, 9 accels)

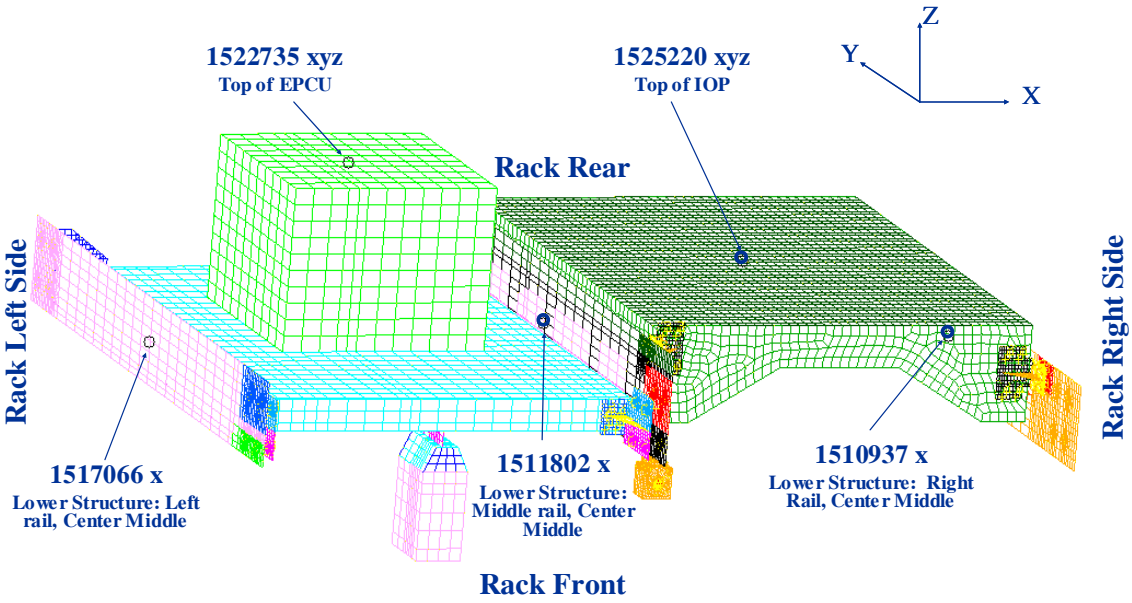

Front Perspective View of Lower Structure Assembly

Modal Rack Instrumentation Plan
Experiment Assembly (9 locations, 18 accels)

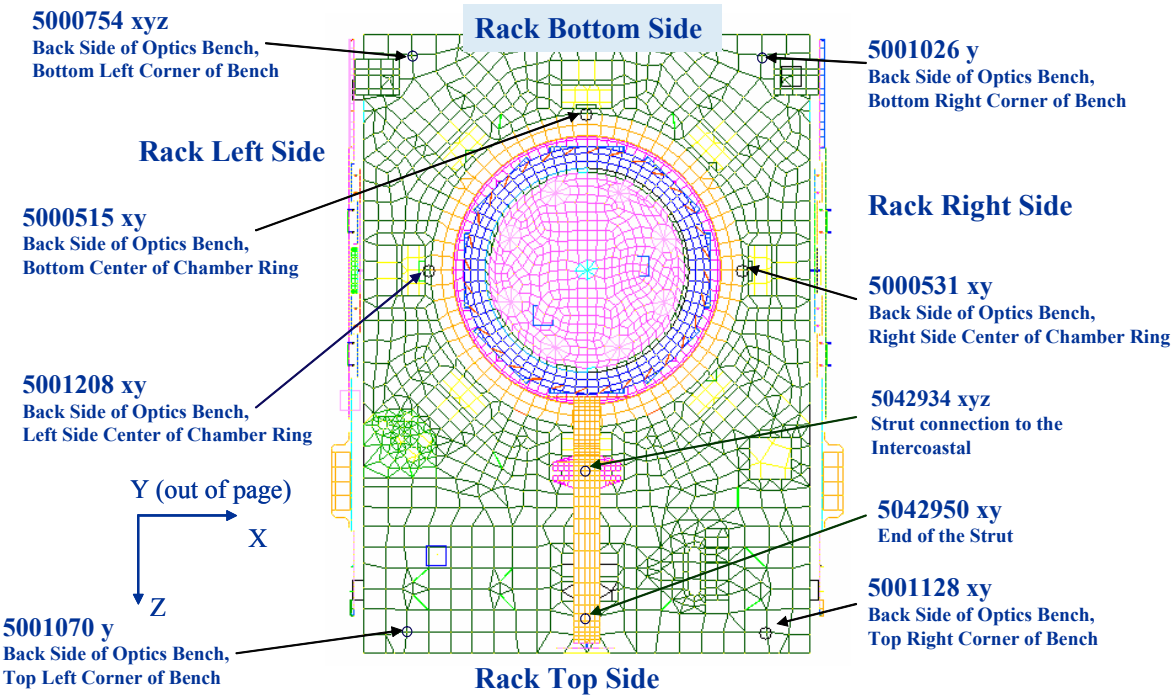

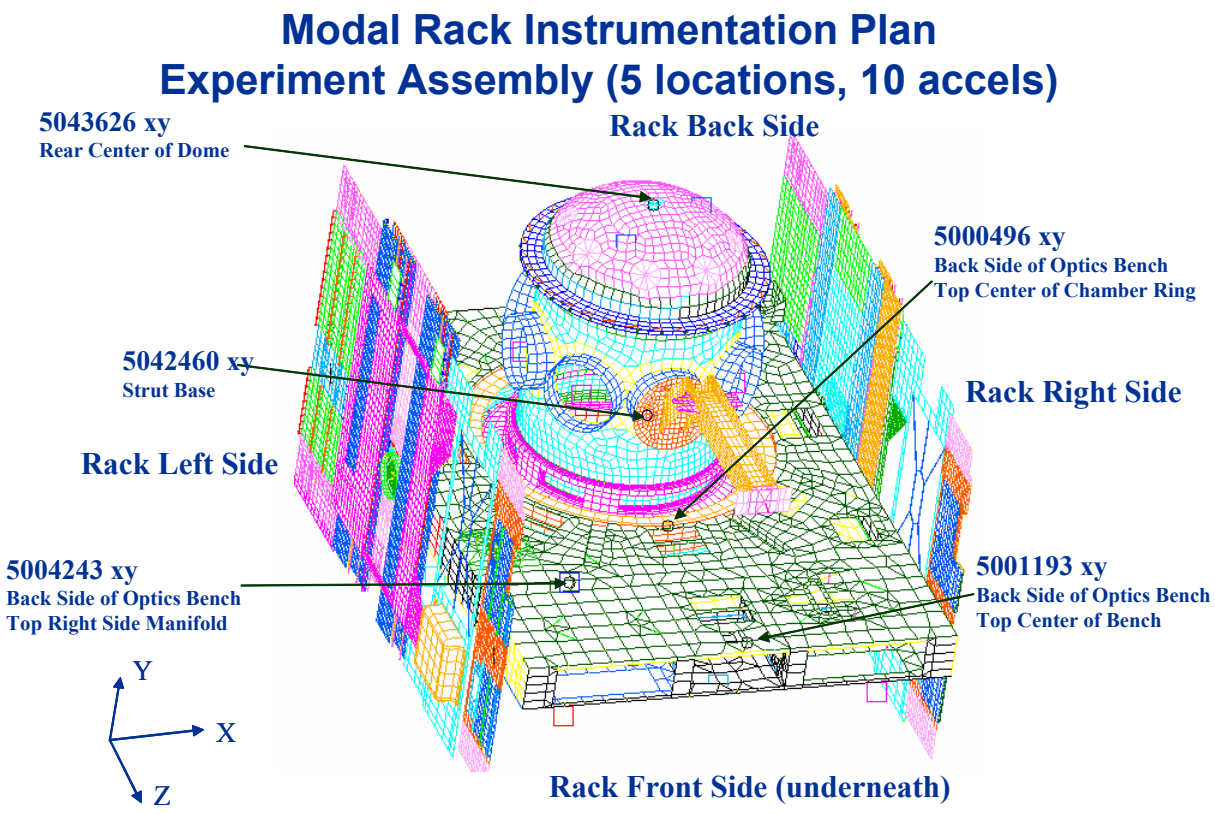
Modal Rack Instrumentation Plan
Experiment Assembly (5 locations, 10 accels)
5043626 xy
Rear Center of Dome
Rack Back Side
5000496 xy
Back Side of Optics Bench
Top Center of Chamber Ring
5042460 xy
Strut Base
Rack Right Side
Rack Left Side
5004243 xy
Back Side of Optics Bench
Top Right Side Manifold
5001193 xy
Back Side of Optics Bench
Top Center of Bench
Y
X
Z
Rack Front Side (underneath)

Modal Rack Instrumentation Plan
Experiment Assembly (1 location, 3 accels)

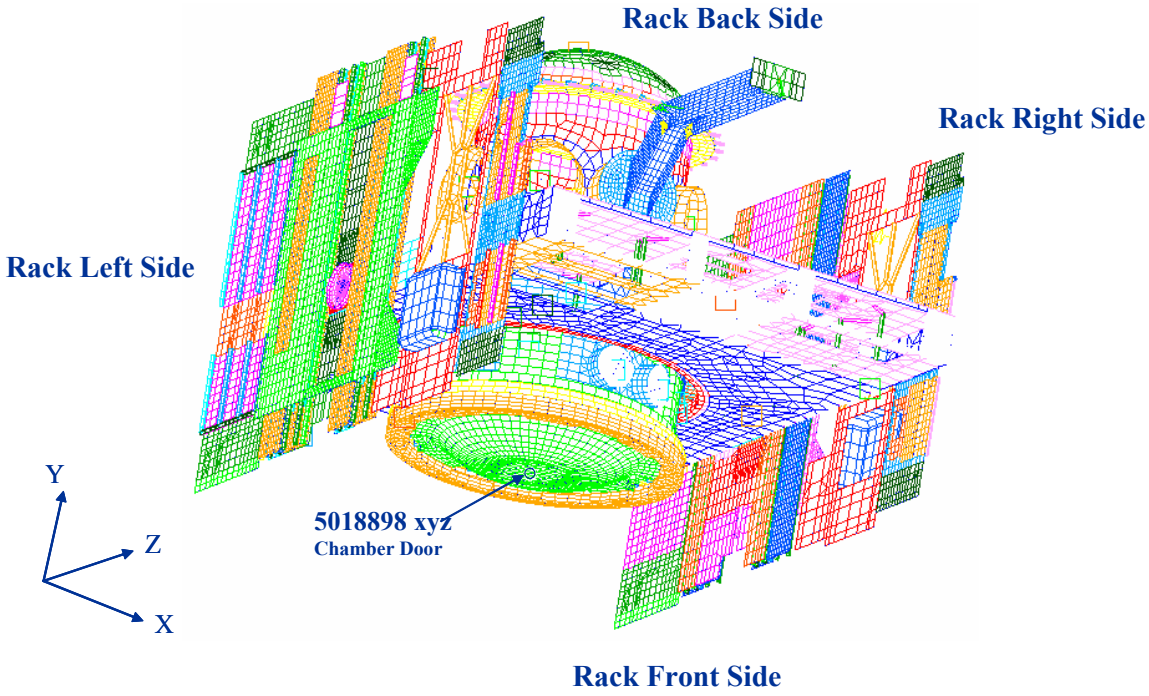

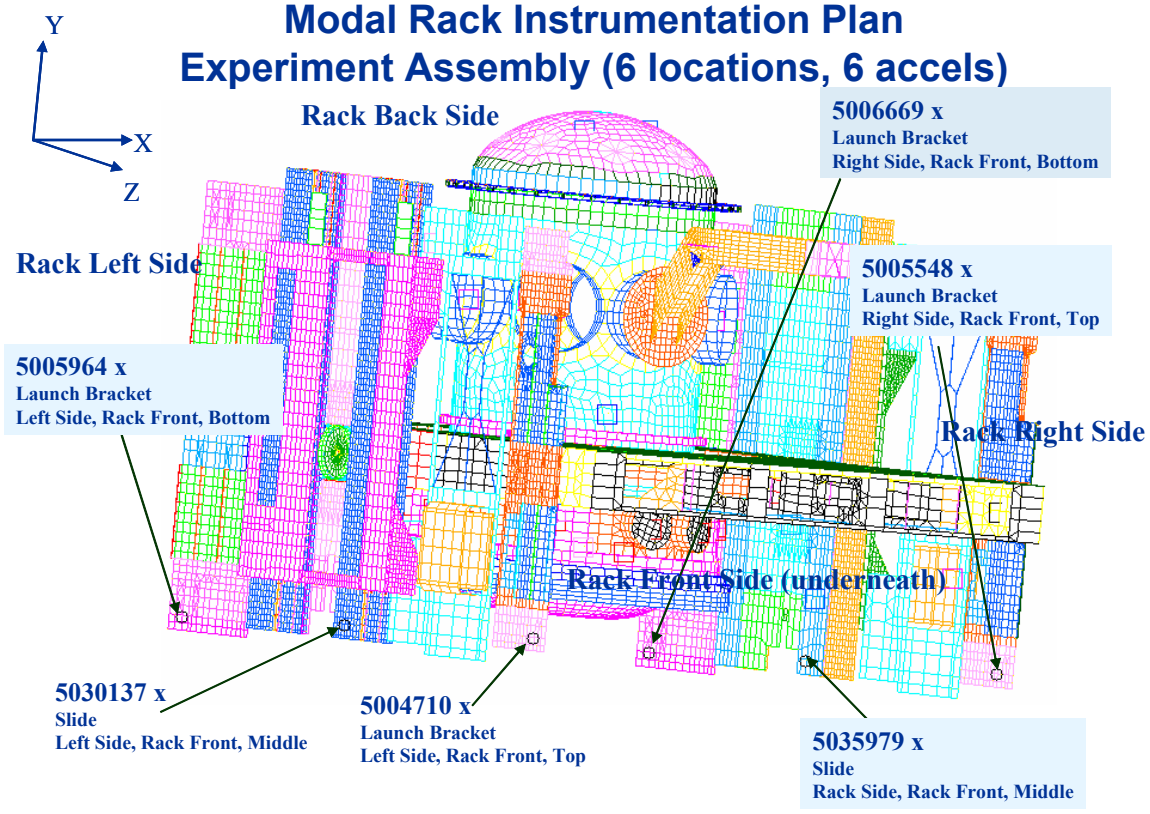
Modal Rack Instrumentation Plan
Experiment Assembly (6 locations, 6 accels)
Y
X
Z
Rack Back Side
Rack Left Side
Rack Right Side
Rack Front Side (underneath)
5006669 x
Launch Bracket
Right Side, Rack Front, Bottom
5005548 x
Launch Bracket
Right Side, Rack Front, Top
5005964 x
Launch Bracket
Left Side, Rack Front, Bottom
5030137 x
Slide
Left Side, Rack Front, Middle
5004710 x
Launch Bracket
Left Side, Rack Front, Top
5035979 x
Slide
Rack Side, Rack Front, Middle

REPORT DOCUMENTATION PAGE

Form Approved
OMB No. 0704-0188

1. AGENCY USE ONLY (*Leave blank*)	2. REPORT DATE	3. REPORT TYPE AND DATES COVERED
	May 2005	Technical Memorandum

4. TITLE AND SUBTITLE

Fluids and Combustion Facility: Combustion Integrated Rack Modal Model Correlation

5. FUNDING NUMBERS

WBS–22–770–00–12

6. AUTHOR(S)

Mark E. McNelis, Vicente J. Suarez, Timothy L. Sullivan, Kim D. Otten, and James C. Akers

7. PERFORMING ORGANIZATION NAME(S) AND ADDRESS(ES)

National Aeronautics and Space Administration
John H. Glenn Research Center at Lewis Field
Cleveland, Ohio 44135–3191

8. PERFORMING ORGANIZATION REPORT NUMBER

E–15153

9. SPONSORING/MONITORING AGENCY NAME(S) AND ADDRESS(ES)

National Aeronautics and Space Administration
Washington, DC 20546–0001

10. SPONSORING/MONITORING AGENCY REPORT NUMBER

NASA TM—2005–213795
GRC–DDV–FCF–2005–001

11. SUPPLEMENTARY NOTES

Mark E. McNelis and Vicente J. Suarez, NASA Glenn Research Center; Timothy L. Sullivan, Kim D. Otten, and James C. Akers, Analex Corporation, 1100 Apollo Drive, Brook Park, Ohio 44142. Responsible person, Mark E. McNelis, organization code DDV, 216–433–8395.

12a. DISTRIBUTION/AVAILABILITY STATEMENT

Unclassified - Unlimited
Subject Category: 39

Available electronically at http://gltrs.grc.nasa.gov

This publication is available from the NASA Center for AeroSpace Information, 301–621–0390.

12b. DISTRIBUTION CODE

13. ABSTRACT ***(Maximum 200 words)***

The Combustion Integrated Rack (CIR) is one of two racks in the Fluids and Combustion Facility on the International Space Station. The CIR is dedicated to the scientific investigation of on-orbit fire suppression, fire safety, and space system fluids management supporting NASA's Exploration of Space Initiative. The CIR hardware was modal tested and the CIR finite element model updated to satisfy the International Space Station model correlation criteria. The final cross-orthogonality results between the correlated model and test mode shapes was greater than 90 percent for all target modes.

14. SUBJECT TERMS

Structural dynamics; Modal testing

15. NUMBER OF PAGES

96

16. PRICE CODE

17. SECURITY CLASSIFICATION OF REPORT	18. SECURITY CLASSIFICATION OF THIS PAGE	19. SECURITY CLASSIFICATION OF ABSTRACT	20. LIMITATION OF ABSTRACT
Unclassified	Unclassified	Unclassified	